REVIEWS OF TOPICAL PROBLEMS

Dusty plasmas

V E Fortov, A G Khrapak, S A Khrapak, V I Molotkov, O F Petrov

Contents

Abstract. The properties of dusty plasmas — low-temperature plasmas containing charged macroparticles — are considered. The most important elementary processes in dusty plasmas and the forces acting on dust particles are investigated. The results of experimental and theoretical investigations of different states of strongly nonideal dusty plasmas — crystal-like, liquid-like, gas-like — are summarized. Waves and oscillations in dusty plasmas, as well as their damping and instability mechanisms, are studied. Some results on dusty plasma investigated under microgravity conditions are presented. New directions of experimental research and potential applications of dusty plasmas are discussed.

1. Introduction

Dusty plasmas constitute ionized gases containing charged particles of condensed matter. Other terms used for such systems are 'complex plasmas', 'colloidal plasmas', and 'plasmas with a condensed disperse phase'.

The term 'complex plasmas' is currently widely used in the scientific literature to designate dusty plasmas specially 'designed' to study the properties of the dust component. Of particular interest is the situation in which the dust particles are strongly coupled (and form liquid-like and crystal-like structures) and investigation of plasma processes at the kinetic level is possible. The main attention in our review is given to such systems. At the same time, dusty plasmas in space and the atmosphere, chemical plasmas with growing particles, etc. are hardly considered here. In light of this we will not distinguish between dusty and complex plasmas and will mostly use the term 'dusty plasma' as generally accepted.

Dust and dusty plasmas are quite natural in space. They are present in planetary rings, comet tails, and interplanetary and interstellar clouds [1 – 6]. Complex plasmas are found in the vicinity of artificial satellites and space stations [5, 6] and in thermonuclear facilities with magnetic confinement [7 – 9]. The properties of dusty plasmas are very actively investigated in the laboratory, too. Dust particles are not only deliberately introduced into a plasma but can also form and grow due to different physical processes. The widespread presence of dusty plasmas, combined with a number of their unique (relative simplicity of producing, observing, and controling the parameters, feasibility of taking measurements at a kinetic level) and unusual (openness of dusty plasma systems, inconstancy of the dust particle charge, high dissipativity, self-organization and formation of ordered structures) properties, make dusty plasmas extraordinarily attractive and interesting objects for investigations.

V E Fortov, A G Khrapak, V I Molotkov, O F Petrov. Institute for High Energy Densities, Russian Academy of Sciences,
ul. Izhorskaya 13/19, 125412 Moscow, Russian Federation
Tel. (7-095) 485 79 89
Fax (7-095) 485 79 90
E-mail: ofpetrov@ihed.ras.ru
S A Khrapak Centre for Interdisciplinary Plasma Science,
Max-Planck-Institut für Extraterrestrische Physik,
D-85741, Garching, Germany
Tel.: + 49 89 30 000 3646
E-mail: skhrapak@mpe.mpg.de
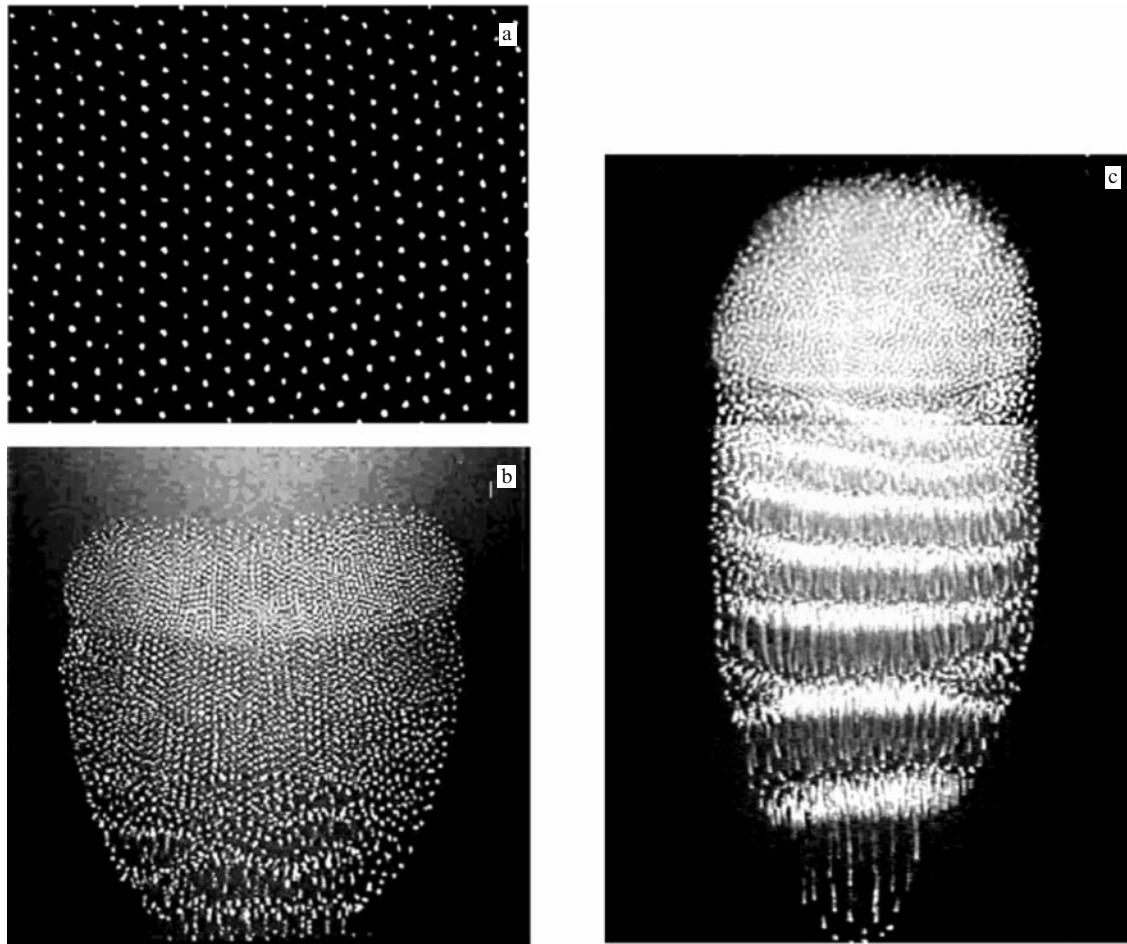
Figure 1. Typical images of the ordered structures of dust particles in rf and dc discharges. (a) A horizontal cross section of a hexagonal structure (shown is the area 6.1×4.2 mm^2 containing 392 particles 6.9 μm in diameter) formed in the sheath region of an rf discharge [17]. (b) Vertical cross section of the ordered structure in a stratified dc discharge. In the lower region of the structure, the vertical oscillation of dust particle density is present, in the central region high ordering appears, and in the periphery of the upper region the particles experience convective motion. (c) Self-excited dust acoustic wave in a dc gas discharge [18] (neutral gas pressure $p = 0.2$ Torr, wave frequency $\omega \sim 60$ s^{-1}, wave number $k \sim 60$ cm^{-1}, and propagation velocity $v_{ph} \sim 1$ cm s^{-1}).

Dust particles immersed in a plasma acquire an electric charge and constitute an additional charged component. However, the properties of dusty plasmas are much more diverse than that of usual multicomponent plasmas consisting of electrons and different types of ions. The dust particles are recombination centers for plasma electrons and ions and sometimes sources of electrons (thermo-, photo-, and secondary electron emission). This implies that the dust component can significantly influence the plasma ionization balance. In addition, the dust particle charge is not fixed, but is determined by the surrounding plasma parameters, and can vary both spatially and temporarily. Moreover, charge fluctuations are present even for constant plasma parameters because of the stochastic nature of the charging process.

Due to the large charges carried by the dust particles, the electrostatic energy of interaction between them (proportional to the product of charges of interacting particles) is high. For this reason, strong coupling in the dust subsystem can be achieved much more easily than in the electron–ion subsystem, whilst typically the dust concentration is much lower than that of electrons and ions. Hence, the appearance of short-range order and even crystallization in the dust subsystem become achievable. The first experimental realiza-

tion of the ordered (quasi-crystal-like) structures of charged microparticles was implemented by Wuerker et al. [10] in 1959 with the help of a modified Paul's trap [11]. The possibility of dust subsystem crystallization in a nonequilibrium gas discharge plasma was predicted by Ikezi [12] in 1986. Experimentally, the ordered structures of dust particles were observed almost a decade later, first near the sheath edge of rf discharges [13–16], where the strong vertical electric field can compensate for gravity and makes dust particle levitation possible. Figure 1a shows a horizontal cross section of a typical ordered (quasi-crystal-like) structure found in the sheath region of an rf discharge [17]. In the vertical direction, the particles are also ordered and arranged one beneath the other to form chain-like structures. Later on, ordered structures of macroparticles were observed in a thermal dusty plasma at atmospheric pressure [19–21], in the positive column of a dc glow discharge [22, 23], and in a nuclear-induced dusty plasma [24, 25]. Figure 1b displays an example of the ordered structure of dust particles in a dc glow discharge. In the lower region of the structure, self-excited nonlinear oscillations of dust particle density are present; most of the central region is occupied by a highly ordered regular structure, and in the upper region the particles experience convective motion [26]. Dust component crystal-

lization and phase transitions in different types of dusty plasmas constitute a wide area of current research.

The presence of the dust component is essential for the collective processes in dusty plasmas. Dust not only modifies the wave spectrum in comparison with dust-free plasma, but can also lead to the appearance of new modes and new mechanisms of damping and instability. The presence of dust introduces new characteristic spatial and temporal scales. For example, the dust plasma frequency is several orders of magnitude smaller than the ion plasma frequency, because the dust particles are extremely massive compared to ions. This leads to the emergence of a new very-low-frequency mode — the dust acoustic wave, as it is called, which represents the oscillations of particles against the quasi-equilibrium background of electrons and ions (in some sense it is analogous to the ion acoustic wave, which represents ion oscillations in gas against the equilibrium background of electrons). The characteristic frequency range of this mode is $10-100 \ s^{-1}$, which makes it particularly interesting from the experimental point of view. An illustration is presented in Fig. 1c which shows a typical pattern of dust acoustic waves. These waves were self-excited under certain conditions in a dc discharge plasma [18], revealing the existence of some mechanisms of dust acoustic wave instability.

Such properties as relative simplicity of production, observation, and control, as well as fast relaxation and response to external disturbances make dusty plasmas not only attractive objects for investigation, but also very effective instruments for studying the properties of strongly coupled plasma, fundamental properties of crystals, etc. Especially important is that the dust particles can be usually seen with the naked eye or easily visualized with the help of a simple optical technique. This allows us, in principle, to perform measurements at the kinetic level, yielding the dust particle distribution function in coordinate and momentum phase space, $f_d(\mathbf{r}, \mathbf{p}, t)$. The detailed investigation of phase transitions, particle transport, low-frequency waves, etc. at the kinetic level is thus possible. In addition, the diagnostics of dust particles and surrounding plasmas is considerably simplified.

Despite the fact that dusty plasmas in the laboratory were first discovered by Langmuir in the 1920s [27], active investigation of them began only a few decades ago, mainly in connection to such applications as rocket-fuel combustion products, solid-fuel-fired magnetohydrodynamic generators, and dusty clouds in the atmosphere [28–31]. In the late 1980s, the interest moved to such issues as dust charging, propagation of electromagnetic waves and their damping and instability, mostly in connection to space dusty plasmas [1, 32, 33]. Growth in interest in the field in the early 1990s was mostly connected with wide utilization of plasma deposition and etching technologies in microelectronics, as well as with production of thin films and nanoparticles [34–37]. This interest was caused by the fact that the presence of the dust particles in a processing plasma not only leads to the contamination of a semiconductor element surface and, hence, to the increased yield of defect elements, but can also perturb plasma in an often unpredictable way. To prevent or lower the role of these negative impacts, it is necessary to understand the processes involved in the formation and growth of dust particles in a gas discharge plasma, mechanisms of dust transport, and influence of dust on plasma parameters. Finally, in the middle 1990s, crystal-like structures of dust particles in different types of dusty plasmas were

discovered experimentally [13–16, 19–25]. These findings led to tremendous growth in the investigation of dusty plasmas, which is still in progress (we note in this context that active investigations of Wigner crystallization of ions in different types of ion traps [38], and electrons on the surface of liquid helium [39] are also being performed).

Among the present-day directions of dusty plasma investigations we can distinguish the following:

• formation of ordered structures, including crystallization and phase transitions in the dust subsystem;

• elementary processes in dusty plasmas: charging of dust for different plasma and particle parameters, interactions between the particles, external forces acting on the particles;

• linear and nonlinear waves in dusty plasmas (solitons, shock waves, Mach cones), their dynamics, damping, and instability.

Of exceptional significance are the experiments under microgravity conditions, first conducted in 1998 on-board the 'Mir' space station, and later (in the beginning of 2001) started on-board the International Space Station (the PKE-Nefedov experiment). In the absence of gravity, the influence of strong electric fields (which are necessary on the ground to levitate particles) and strong plasma anisotropies caused by these fields is substantially reduced.

Investigations into dusty plasmas are nowadays a rapidly growing field of research, which includes such aspects as fundamental problems in the physics of plasmas, hydrodynamics, kinetics of phase transitions, nonlinear physics, solid state physics, and several applications (e.g., in nano-technology, plasma technology, new materials). More and more research groups from different countries are taking up the field. The number of scientific publications appearing every year is increasing constantly. Taking this into account, the focus of the present review is first and foremost on the aspects that are required for understanding the basic properties of dusty plasmas and are most frequently needed in research. From an immense amount of material we tried to select those experimental and theoretical results which, in our opinion, illustrate the most important achievements in the investigation of dusty plasmas, reported over the last decade.

2. Elementary processes in dusty plasmas

2.1 Charging of dust particles in plasmas (theory)

In Sections 2.1.1–2.1.8, different processes leading to the charging of dust particles immersed in plasmas are considered. Expressions for the ion and electron fluxes to (from) the particle surface, caused by different processes (collection of plasma electrons and ions, secondary, thermionic and photoelectric emission of electrons from the particle surface), are given. Problems such as stationary surface potential, kinetics of charging, changing of plasma charge composition in response to the presence of the dust, as well as dust particle charge fluctuations due to the stochastic nature of the charging process, are considered. More detailed examination of charging processes can be found in Refs [40, 41]. Here we mostly focus on the processes which are important for the problems addressed in the present review. Below in this section we consider spherical dust particles as being of radius a.

2.1.1 Charging in gas discharge plasmas. In a nonequilibrium plasma of low-pressure gas discharges the ions, atoms, and

macroscopic charged particles typically remain 'cold', whilst the electron energies are relatively high. In the absence of emission processes, the charge of a dust particle is negative. This is connected to the fact that the electron and ion fluxes are directed to the surface of an uncharged particle. Similar to the theory of electric probes [42, 43] it is customary to assume that electrons and ions recombine on the particle surface, and neutral particles appearing in the process of recombination either remain on the surface or return to the plasma (in the first case, the charging can be accompanied by particle growth). Due to higher mobility of the electrons their flux exceeds considerably that of the ions, and the neutral particle begins to charge negatively. The emerging negative charge on the particle leads to the repulsion of the electrons and the attraction of the ions. The charge grows (in the absolute magnitude) until the electron and ion fluxes are balanced. On longer timescales, the charge is turned practically constant and experiences only small fluctuations around its equilibrium value (see Section 2.1.8).

The stationary surface potential of the dust particle (connected to the particle charge) is defined (with the accuracy of a coefficient on the order of unity) as $\varphi_s = -T_e/e$, where T_e is the electron temperature in energy units. Physically, this can be explained by the requirement that in the stationary state most of the electrons should not have kinetic energies sufficient to overcome the potential barrier between the particle surface and surrounding plasma.

2.1.2 Orbit motion limited approximation. For a quantitative description of the particle charging in gas discharge plasmas, probe theory is generally adopted. One of the most frequently used approaches is the orbit motion limited (OML) theory [42–44]. This approach allows one to determine the cross sections for electron and ion collection by the dust particle only from the laws of conservation of energy and angular momentum. Usually, the conditions of applicability of the OML theory are formulated as [44]

$$a \ll \lambda_D \ll l_{i(e)}, \tag{1}$$

where λ_D is the plasma screening length (the corresponding Debye radius), and $l_{i(e)}$ is the mean free path of the ions (electrons). It is also assumed that the dust particle is isolated in the sense that other dust particles do not affect the motion of electrons and ions in its vicinity.

Assuming that the electrons and the ions are collected if their trajectories cross or graze the particle surface, the corresponding velocity-dependent cross sections are given by

$$\sigma_e(v) = \begin{cases} \pi a^2 \left(1 + \dfrac{2e\varphi_s}{m_e v^2}\right), & \dfrac{2e\varphi_s}{m_e v^2} > -1, \\ 0, & \dfrac{2e\varphi_s}{m_e v^2} < -1, \end{cases} \tag{2}$$

$$\sigma_i(v) = \pi a^2 \left(1 - \frac{2e\varphi_s}{m_i v^2}\right), \tag{3}$$

where $m_{e(i)}$ is the electron (ion) mass, and v denotes the velocity of the electrons and ions relative to the dust particle. Here, the surface potential φ_s of the dust particle is negative ($\varphi_s < 0$), and the ions are singly charged. We note that within OML theory $\sigma_e(v)$ and $\sigma_i(v)$ are independent of the exact form of the electrostatic potential around the dust particle. Limitations to this approach are considered below in Section 2.1.3.

Electron and ion fluxes to the particle surface are determined by the integration of the corresponding cross sections with velocity distribution functions $f_{e(i)}(v)$:

$$I_{e(i)} = n_{e(i)} \int v \sigma_{e(i)}(v) f_{e(i)}(v) \, d^3 v, \tag{4}$$

where $n_{e(i)}$ is the electron (ion) number density. For the Maxwellian velocity distribution of plasma particles, viz.

$$f_{e(i)}(v) = (2\pi v_{Te(i)}^2)^{-3/2} \exp\left(-\frac{v^2}{2v_{Te(i)}^2}\right), \tag{5}$$

where

$$v_{Te(i)} = \sqrt{\frac{T_{e(i)}}{m_{e(i)}}} \tag{6}$$

is the electron (ion) thermal velocity, the integration in Eqn (4) performed with the use of formulas (2) and (3) gives

$$I_e = \sqrt{8\pi} \, a^2 n_e v_{Te} \exp\left(\frac{e\varphi_s}{T_e}\right), \tag{7}$$

$$I_i = \sqrt{8\pi} \, a^2 n_i v_{Ti} \left(1 - \frac{e\varphi_s}{T_i}\right). \tag{8}$$

The stationary potential of the dust particle surface (floating potential) is determined by the balance of electron and ion fluxes collected by the particle:

$$I_e = I_i. \tag{9}$$

It is convenient to introduce the following dimensionless parameters which are widely used throughout this review:

$$z = \frac{|Z_d| e^2}{a T_e}, \qquad \tau = \frac{T_e}{T_i}, \qquad \mu = \frac{m_e}{m_i}. \tag{10}$$

Here, z is the absolute magnitude of the particle charge in the units of $a T_e/e^2$, while τ and μ are the electron-to-ion temperature and mass ratios, respectively. We note that sometimes τ is used to denote the inverse ratio T_i/T_e (see, e.g., Refs [40, 41]). Typically, in gas discharge plasmas $\tau \gg 1$ ($\tau \sim 10–100$), $z \gtrsim 1$, and, of course, $\mu \ll 1$. It is also assumed that the particle charge and surface potential are connected through the expression $Z_d e = a \varphi_s$, where Z_d is the dust particle charge number (namely, charge expressed in units of the elementary charge). This connection (like for a charged sphere in vacuum) follows from a solution of the linearized problem concerning a potential distribution around a spherical macroparticle in Boltzmann plasmas, when $a \ll \lambda_D$. This is usually a good approximation, whilst, in principle, there may be some deviations due to strongly nonlinear screening and/or nonequilibrium distribution of the electrons and ions around the dust particle.

In dimensionless quantities (10), the flux balance equation (9) with expressions (7) and (8) taken into account can be rewritten in the form

$$\exp(-z) = \frac{n_i}{n_e} \left(\frac{\mu}{\tau}\right)^{1/2} (1 + z\tau). \tag{11}$$

For the isolated particle, the quasi-neutrality condition reduces to $n_i = n_e$. In this case, the dimensionless surface
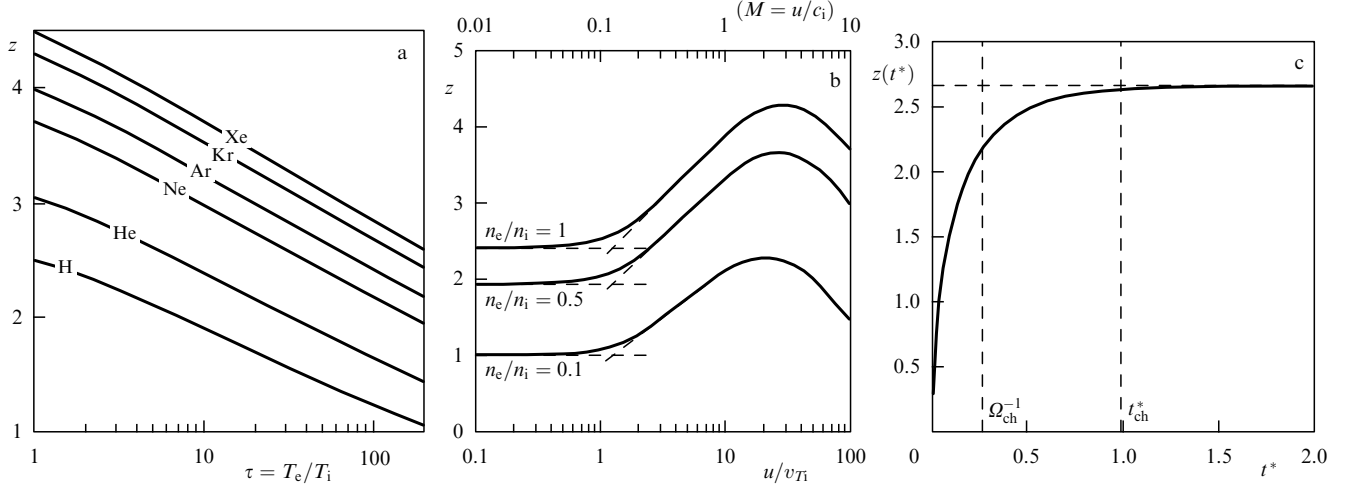
Figure 2. Dimensionless charge $z = |Z_d|e^2/aT_e$ of an isolated spherical dust particle: (a) as a function of electron-to-ion temperature ratio $\tau = T_e/T_i$ for different types of isotropic plasmas; (b) as a function of the ratio u/v_{Ti} of the ion drift to ion thermal velocity (or Mach number $M = u/c_i$, where $c_i = \sqrt{T_e/m_i}$ is the ion speed of sound) for a plasma with ion drift — the calculations were done for three values of the ratio of electron-to-ion number density and correspond to an argon plasma with $\tau = T_e/T_i = 100$, and (c) as a function of dimensionless time $t^* = (\omega_{pi}/\sqrt{2\pi})(a/\lambda_{Di})t$ for an argon plasma with $\tau = T_e/T_i = 50$ [the particle is initially uncharged, the horizontal dashed line corresponds to the stationary value of the particle charge, vertical dashed lines show two possibilities for determining the characteristic charging time (for details see text)].

potential z depends on two parameters only — the electron-to-ion temperature ratio, and the gas type (electron-to-ion mass ratio). In Fig. 2a, the values of z are presented for different gases (H, He, Ne, Ar, Kr, Xe) as functions of τ. The particle potential decreases with increasing $\tau = T_e/T_i$, and builds up with increasing gas atomic mass. For very large τ ($\tau \to \infty$) and $z \sim 1$, it follows from Eqn (11) that $z \sim 1/\sqrt{\mu\tau}$. For typical values of $\tau \sim 10-100$, the dimensionless potential ranges $z \sim 2-4$. For a particle with $a \sim 1$ μm and $T_e \sim 1$ eV, the characteristic charge number is $(1-3) \times 10^3$.

Dusty plasmas are often subject to external electric fields, which occurs, for example, near walls or electrodes of gas discharges. In this case, the ion drift relative to the stationary dust component substantially affects the particle charging. Using instead of Eqn (5) the shifted Maxwellian velocity distribution for ions, viz.

$$f_i(\mathbf{v}) = (2\pi v_{Ti}^2)^{-3/2} \exp\left[\frac{(\mathbf{v} - \mathbf{u})^2}{2v_{Ti}^2}\right] \qquad (12)$$

(where $\mathbf{u}$ is the average ion drift velocity), and the cross section (3), we get for the ion flux the following expression [5, 45, 46] (remembering that $\varphi_s < 0$):

$$I_i = \sqrt{2\pi}\, a^2 n_i v_{Ti} \left\{ \sqrt{\frac{\pi}{2}}\, \frac{1 + u^2/v_{Ti}^2 - 2e\varphi_s/T_i}{u/v_{Ti}} \mathrm{erf}\left(\frac{u}{\sqrt{2}\, v_{Ti}}\right) \right.$$
$$\left. + \exp\left(-\frac{u^2}{2v_{Ti}^2}\right) \right\}. \qquad (13)$$

Correction to expression (8) for $u \ll v_{Ti}$ is a 2nd-order infinitesimal, $\Delta I_i \sim O(u^2/v_{Ti}^2)$, whilst for $u \gg v_{Ti}$ expression (13) reduces to

$$I_i = \pi a^2 n_i u \left(1 - \frac{2e\varphi_s}{m_i u^2}\right). \qquad (14)$$

The dimensionless surface potential of the dust particle, calculated from the flux balance condition (9) with the help

of formulas (7) and (13), is shown in Fig. 2b as a function of the ion drift velocity for three values of n_e/n_i. The calculation corresponds to an argon plasma with $\tau = 100$. The figure demonstrates that the dimensionless charge is practically constant for $u \lesssim v_{Ti}$, then increases with increasing drift velocity, reaching a maximum at $u \sim c_i = \sqrt{T_e/m_i}$ (where c_i is the ion sound velocity), after which it decreases. Comparison of the exact expression (13) with approximations (8) and (14) (shown by dashed lines) indicates that some difference exists only in a narrow region near $u \sim v_{Ti}$. Numerical simulation [47] supports the applicability of the expressions presented for describing the dust particle charging in plasmas with drifting ions.

So far, we have considered the charging of an individual particle in plasmas. In reality, however, the dust concentration can be high enough. In this case, an increase in dust particle concentration leads to a decrease in their surface potential (and hence charge) in the absolute magnitude due to a reduction in the electron concentration compared to that of the ions ($n_e < n_i$). To illustrate this phenomenon, we show a simplified consideration which gives a correct qualitative picture of the physics involved. Namely, assuming that conditions (1) are satisfied we use expressions (7) and (8) for the electron and ion fluxes, respectively, taking into account the contribution of the dust component to the plasma charge composition. The latter leads to the following quasi-neutrality condition

$$n_e = n_i + Z_d n_d. \qquad (15)$$

The equilibrium surface potential is then determined [instead of formula (11)] by

$$\exp(-z) = \left(\frac{\mu}{\tau}\right)^{1/2} (1 + z\tau)(1 + P), \qquad (16)$$

where the dimensionless parameter

$$P = |Z_d| \frac{n_d}{n_e} \qquad (17)$$

determines the ratio of the charge residing on the dust component to that on the electron component (the so-called Havnes parameter) [32]. The particle charge tends to the charge of an isolated particle, when $P \ll 1$ (see Fig. 2a), whilst for $P > 1$ it is reduced considerably in the absolute magnitude. Notice that sometimes instead of expression (17) the quantity $aT_e e^{-2}(n_d/n_e)$ is used, which differs from P by the numerical factor $1/z$.

2.1.3. Applicability of the orbit motion limited approach.

In Sections 2.1.1 and 2.1.2, inequalities (1) were employed to determine the conditions of OML applicability. In this section we define more precisely the latter conditions and point out the physical mechanisms which can make the OML approach inapplicable.

First, we must remember that the expressions for electron and ion collection cross sections (2) and (3) do not depend on the exact form of the potential distribution around the dust particle. However, OML is applicable only if the potential satisfies certain conditions. The point is that the motion of the ions approaching the dust particle is determined by the *effective* interaction potential U_{eff}, which in addition to the attractive electrostatic potential $U(r)$ between positive ion and negatively charged particle contains a component associated with the centrifugal repulsion due to ion angular momentum conservation. The effective potential normalized on the ion initial kinetic energy $E = m_i v_i^2 / 2$ is given by

$$U_{eff}(r, \rho) = \frac{\rho^2}{r^2} + \frac{U(r)}{E} , \qquad (18)$$

where ρ is the impact parameter, and $U(r) < 0$. For a given ρ, the distance r_0 at which $U_{eff}(r_0, \rho) = 1$ corresponds to the distance of the closest approach between the ion and the dust particle. The ion is collected when $r_0 \leqslant a$, whilst for $r_0 > a$ it experiences elastic scattering by the particle potential, but does not reach its surface. Inserting $r = a$ and $U(a) = e\varphi_s$ into Eqn (18) we find the maximum impact parameter for ion collection:

$$\rho_c^{OML} = a \sqrt{1 - \frac{2e\varphi_s}{m_i v_i^2}} . \qquad (19)$$

Taking into account that $\sigma = \int_0^{\rho_c} 2\pi\rho \, d\rho$ we immediately get the cross section (3). However, the equation $U_{eff}(r, \rho) = 1$ does not necessarily have only one solution. It can be shown that the solution is unique only when $|U(r)|$ decreases more slowly than $1/r^2$ [48]. In reality, however, $|U(r)| \propto 1/r$ close to the particle, and $|U(r)| \propto 1/r^2$ far from it, and at intermediate distances the potential can decrease faster. In this case, the equation $U_{eff}(r, \rho) = 1$ can have multiple roots (the distance r_0 of the closest approach is given by the largest one). This means that a potential barrier for ions moving to the dust particle emerges: some ions are reflected at $r_0 > \lambda_D > a$ (see below) and, hence, cannot reach the particle surface.

As a useful example let us consider the screened Coulomb (Debye – Hückel) interaction potential between the ions and the dust particle, $U(r) = -(U_0/r) \exp(-r/\lambda_D)$, where $U_0 = e|\varphi_s| a \exp(a/\lambda_D)$. Using the normalized distance $\tilde{r} = r/\lambda_D$ it is easy to show that the behavior of the effective potential U_{eff} is governed by two dimensionless parameters: $\beta = U_0/2E\lambda_D$ and $\tilde{\rho} = \rho/\lambda_D$. Curves of the effective potential for two values of β and different values of $\tilde{\rho}$ are displayed in
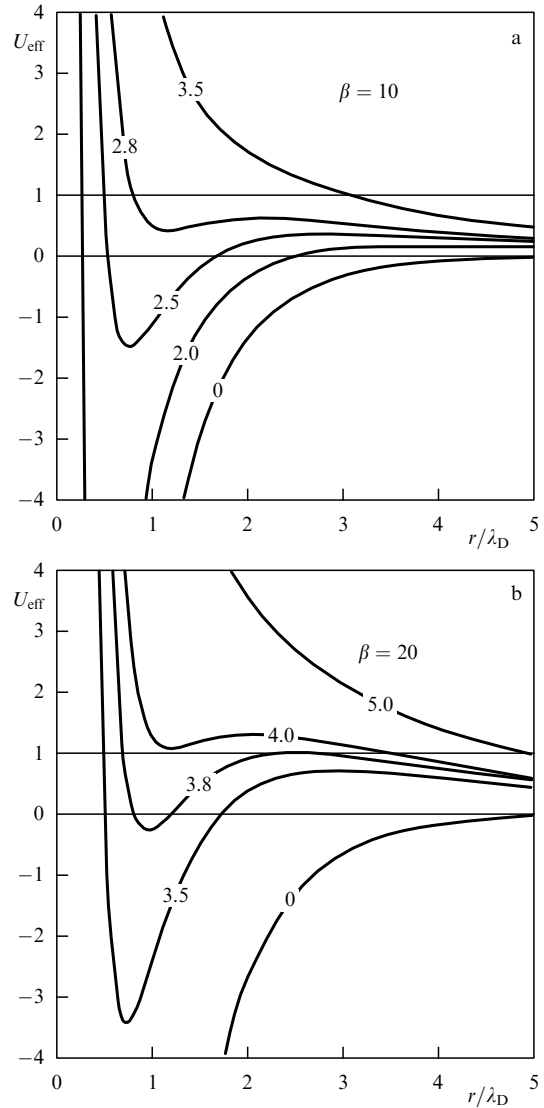
Figure 3. Curves of the effective potential for the radial ion motion in the dust particle electric field (for the screened Coulomb interaction potential) for two values of the scattering parameter β (see text) and different impact parameters ρ (indicated in the figures). The potential barrier is absent at $\beta = 10$, and present at $\beta = 20$.

Fig. 3. The potential barrier is absent at $\beta = 10$, whilst at $\beta = 20$ the existence of the barrier leads to an abrupt jump in the distance of the closest approach from $r_0/\lambda_D \sim 0.7$ to $r_0/\lambda_D \sim 2.6$ for $\rho \sim 3.8 \, \lambda_D$. It is possible to show that when the potential barrier exists, the distance of the closest approach cannot be shorter than $\sim 1.62 \, \lambda_D$ [49].

For the Debye – Hückel potential, the *necessary condition* for the existence of the potential barrier reduces to $\beta > \beta_{cr} \approx 13.2$ [50]. The barrier emerges for ions with the impact parameters $\tilde{\rho} \geqslant \tilde{\rho}_* \sim \ln\beta + 1 - 1/(2\ln\beta)$ [49]. The applicability of the OML approach is determined in this case by the condition $\rho_c^{OML} \leqslant \rho_*$; for $\rho > \rho_*$, the ions experience elastic scattering and are not collected, $r_0 > \lambda_D > a$ (see Fig. 3b). If this applicability condition is not satisfied, then OML approximation overestimates the ion flux to the dust particle surface, i.e., underestimates the absolute value of the stationary particle charge. At very large β (slow ions), OML fails because $\rho_c^{OML} \propto \sqrt{\beta}$, whilst $\rho_* \sim \ln\beta$ for $\beta \gg 1$. In particular, for the Maxwel-

lian ion velocity distribution there are *always* ions for which OML is not applicable [48]. However, the inequality $\rho_c^{OML}(v_{Ti}) \ll \rho_*(v_{Ti})$ guarantees that the corrections are small and can be ignored. Equating the impact parameters $\rho_c^{OML}(v_{Ti}) = \rho_*(v_{Ti})$ and taking into account that $\beta(v_{Ti}) = (z\tau a/\lambda_D) \exp(a/\lambda_D)$ we can determine the values of the ratio a/λ_D (for a given value of $z\tau$) for which the OML approach starts to be inapplicable. As an example we give the following numbers: when $z\tau$ increases from 50 to 500 (typical values in gas discharge plasmas), the critical value of the ratio a/λ_D decreases from ~ 0.4 to ~ 0.2; at the same time, $\beta(v_{Ti})$ increases from ~ 30 to ~ 100. We note that for a repulsive potential $U(r)$ the barrier of the effective potential does not show itself. That means that the difficulties considered are absent when describing the collection of the electrons within the OML approach.

Taking ion collisions into consideration can considerably narrow the regime of OML applicability as well. We note that in a weakly ionized gas discharge plasma the dominant type of collisions is of course that of ion – neutral collisions, which are mostly determined by the resonant charge exchange mechanism. Trajectories of the ions approaching the dust particle from the unperturbed plasma are assumed to be unaffected by collisions. This at least requires the inequality $l_i \gg \lambda_D$ to be satisfied — for distances $r \gg \lambda_D$, the dust particle does not perturb the plasma. However, this inequality does not guarantee that the OML approach is applicable. Indeed, following the work [51] let us consider how many charge exchange collisions occur within a sphere of radius ε surrounding the dust particle. If $|U(\varepsilon)|/T_n \gtrsim 1$, the majority of newly created (due to charge exchange collisions) ions having a kinetic energy determined by the neutral gas energy spectrum insufficient for returning to the unperturbed plasma, are falling on the dust particle surface. The ion flux associated with this process can be roughly estimated as $I_{i,st} = 4\pi\varepsilon^3 n_i v_{in}/3$, where $v_{in} = v_i \sigma_{in} n_n$ is the frequency of charge exchange collisions, σ_{in} is the cross section, and n_n is the number density of neutral atoms. Comparing $I_{i,st}$ with the ion flux given by OML approach (8) we find a condition allowing us to ignore the effect of ion – neutral collisions on the dust particle charging. This condition has the form $I_{i,OML} \gg I_{i,st}$ and can be much stricter than the right hand side of Eqn (1). Numerical simulation [51] shows that collisions can considerably increase the ion flux compared to that given by OML even when $l_i \gtrsim \lambda_D$. The effect considered leads to a decrease of the particle charge in the absolute magnitude. We note that the effect can be quite important in real experiments and, hence, requires detailed theoretical and experimental investigation.

Finally, the existence of extremes (minimum and maximum) in the curve of the effective potential can lead to the appearance of 'trapped ions' when charge exchange collisions are present. Trapped ions are those that move in closed orbits around the dust particle. Trapped ions can affect both the particle charging and the charge screening of the surrounding plasma. Evidently, this effect can be substantial even for the almost collisionless regime for ions, when $l_i > \lambda_D$. However, this question is not fully understood as well. Hence, we only give reference to original works [50 – 53] where the effect of trapped ions was discussed.

2.1.4 Charging in a drift – diffusion regime. When the condition $l_{i(e)} \ll \lambda_D$ is satisfied, the OML approach is no longer applicable. This situation is often called the drift – diffusion regime of charging. As before, the dust particle charge (potential) is determined by the balance of the electron and ion fluxes to its surface, which in the case considered can be written down as

$$I_i = 4\pi r^2 \left[n_i \mu_i \frac{d\varphi}{dr} + D_i \frac{dn_i}{dr} \right], \tag{20}$$

$$I_e = -4\pi r^2 \left[n_e \mu_e \frac{d\varphi}{dr} - D_e \frac{dn_e}{dr} \right], \tag{21}$$

where $\varphi(r)$ is the electrostatic potential around the dust particle, and $\mu_{i(e)}$ and $D_{i(e)}$ are the mobility and the diffusion coefficient of the ions (electrons), respectively. Equations (20) and (21) are supplemented by the Poisson equation

$$\nabla^2 \varphi = -4\pi e(n_i - n_e) \tag{22}$$

and corresponding boundary conditions. It is common to set the following boundary conditions on the collecting surface:

$$\varphi(a) = \varphi_s, \qquad \varphi(\infty) = 0;$$
$$n_i(a) = n_e(a) = 0, \qquad n_i(\infty) = n_e(\infty) = n_0. \tag{23}$$

We note that due to the fact that the ion – neutral collision cross section is usually much larger than the cross section for electron – neutral collisions, the situation in which $l_i \ll \lambda_D \ll l_e$ can be realized. In this case, the electron flux is described by the OML approach as before, and only for the ion flux should the drift – diffusion approximation be used.

A number of works were dedicated to solving the formulated or similar problems (e.g., when accounting for ionization and recombination processes in the vicinity of a collecting body, modifications of boundary conditions, etc.) starting from electric probe theory to investigation of dust particle charging in plasmas. Since this limit is still quite rarely realized in dusty plasma experiments, we give here only original references [40, 54 – 56] where some solutions have been obtained and their applicability conditions discussed.

2.1.5 Different charging mechanisms. The collection of ions and electrons from plasma is not the only possible mechanism for charging dust particles. In particular, the electrons can be emitted from the particle surface due to thermionic, photoelectric, and secondary electron emission processes. These processes are of special importance for dust charging in the working body of solid-fuel MHD generators and rocket engines [28 – 31], in the upper atmosphere [57], in space [4, 5, 58], and in some laboratory experiments, for instance, in thermal plasmas [19 – 21] or in plasma induced by UV irradiation [59], with photoelectric charging of dust particles [60], with electron beams [61], etc. Emission of electrons increases the dust particle charge and, under certain conditions, the particles can even reach a positive charge, in contrast to the situation discussed in Sections 2.1.1 – 2.1.4. Moreover, due to the emission processes, the existence of a two-component system consisting of dust particles and the electrons emitted by them is principally possible. In such a case, the equilibrium potential (charge) of the dust particle is determined by the balance of the fluxes that are collected by the particle surface and emitted from it, and the quasineutrality condition takes the form

$$Z_d n_d = n_e. \tag{24}$$

Such a system serves as the simplest model for investigating different processes associated with emission charging of dust particles [28, 29, 62]. Let us briefly consider each of the emission processes listed above.

Thermionic emission. The flux of the emitted thermal electrons increases with increasing the dust particle surface temperature and depends on the sign of the particle charge. This is because the emitted electrons should not only be capable of escaping from the particle surface but also possess enough energy to overcome the potential barrier (for a positively charged particle) between the surface and quasineutral plasma. For an equilibrium plasma characterized by a temperature T, it is common to use the following expressions for the flux of thermoelectrons [30]:

$$I_{\mathrm{th}} = \frac{(4\pi a T)^2 m_{\mathrm{e}}}{h^3} \exp\left(-\frac{W}{T}\right)$$
$$\times \begin{cases} 1, & \varphi_{\mathrm{s}} < 0, \\ \left(1 + \frac{e\varphi_{\mathrm{s}}}{T}\right) \exp\left(-\frac{e\varphi_{\mathrm{s}}}{T}\right), & \varphi_{\mathrm{s}} > 0. \end{cases} \quad (25)$$

Values of the work function W of thermoelectrons for different metals and semiconductors lie typically within the ranges from 2 to 5 eV. In the case of dielectric particles, where free electrons appear due to ionization, thermionic emission cannot play a significant role because the particles usually melt before the thermionic emission makes substantial contribution to the electron flux. In the case of negatively charged particles, the electric field is directed in such a way that it accelerates the electrons from the particle surface. In this case, some increase in emission current can be expected due to the work function reduction by the effect of the field (Schottky effect). As usual, the equilibrium particle charge ($\sim \varphi_{\mathrm{s}}$) can be found from the balance of the plasma particle fluxes to/from its surface.

Photoelectric emission. Dust particles can be positively charged due to photoelectric emission, when irradiated in a buffer gas by a flux of photons with energies exceeding the work function of photoelectrons from the particle surface [63, 64]. The characteristic value of the work functions for most of the materials does not exceed 6 eV, and hence photons with energies $\leqslant 12$ eV can charge dust particles without ionizing a buffer gas. The flux of emitted electrons depends on the properties of the irradiation source, particle material, and the sign of the particle charge in the following way [44, 65]:

$$I_{\mathrm{pe}} = 4\pi a^2 Y J \begin{cases} 1, & \varphi_{\mathrm{s}} < 0, \\ \exp\left(-\frac{e\varphi_{\mathrm{s}}}{T_{\mathrm{pe}}}\right), & \varphi_{\mathrm{s}} > 0, \end{cases} \quad (26)$$

where J is the photon flux density, and Y is the quantum yield for the particle material. It is also assumed that radiation is isotropic, the efficiency of radiation absorption is close to unity, which occurs when the particle size is larger than the radiation wavelength, and the photoelectrons possess Maxwellian velocity distribution with the temperature T_{pe}. The last of these lies in most cases within the ranges from 1 to 2 eV. It is noteworthy that quantum yield strongly depends not only on the particle material, but also on the direction of incident radiation. The quantum yield is very low just above the threshold, and for the most interesting regime of a vacuum ultraviolet it can reach a value of one photoelectron per several photons. Therefore, the photoelectric emission

mechanism of particle charging can be especially important in space.

Secondary electron emission. The flux I_{se} of secondary electrons is connected to that of primary electrons, I_{e}, through the secondary emission coefficient δ which determines the number of emitted electrons per incident electron: $I_{\mathrm{se}} = \delta I_{\mathrm{e}}$. The coefficient δ depends both on the energy E of primary electrons and on the dust particle material. The dependence $\delta(E)$ turns out to be practically universal for different materials, if δ is normalized on the maximum yield δ_{m} of electrons, and E is normalized on the value E_{m} of energy at which this maximum is reached. The corresponding expressions for the case of monoenergetic electrons can be found in Refs [5, 44]. The values of the parameters δ_{m} and E_{m} for some materials given in Ref. [5] lie within the ranges: $\delta_{\mathrm{m}} \sim (1-4)$, and $E_{\mathrm{m}} \sim (0.2-0.4)$ keV. For the case of Maxwellian-distributed electrons, the expression for δ was given, for instance, in Ref. [44]. Note that the number of secondary electrons, which can reach the surface of the material and escape from it, decreases exponentially from the surface to the bulk of the material. This means that the yield of secondary electrons is mostly associated with the thin near-surface layer.

2.1.6 Kinetics of dust particle charging. The kinetic equation for dust particle charging in plasmas is written as follows

$$\frac{\mathrm{d}Z_{\mathrm{d}}}{\mathrm{d}t} = \sum_j I_j = I, \quad (27)$$

where the summation is made over all the fluxes I_j of charged particles collected or emitted by the dust particle, taken with the corresponding sign. The stationary dust particle charge is determined from the condition $\mathrm{d}Z_{\mathrm{d}}/\mathrm{d}t = 0$. Let us consider particle charging in the absence of emission processes. In so doing, we use the standard equations (7) and (8) for the electron and ion fluxes to the negatively charged spherical isolated particle, derived within the OML approach. Introducing dimensionless time

$$t^* \rightarrow \frac{\omega_{\mathrm{pi}}}{\sqrt{2\pi}} \left(\frac{a}{\lambda_{\mathrm{Di}}}\right) t,$$

where $\lambda_{\mathrm{Di}} = \sqrt{T_{\mathrm{i}}/(4\pi e^2 n_{\mathrm{i}})}$ is the ionic Debye radius, and $\omega_{\mathrm{pi}} = v_{T\mathrm{i}}/\lambda_{\mathrm{Di}}$ is the ion plasma frequency, we get instead of Eqn (27) the following equation

$$\frac{\mathrm{d}z}{\mathrm{d}t^*} = \frac{1}{\sqrt{\mu\tau}} \left[\exp\left(-z\right) - \left(\frac{\mu}{\tau}\right)^{1/2} (1 + \tau z)\right]. \quad (28)$$

Combined with the initial condition $z(t^* = 0) = 0$, this equation allows us to determine the stationary value of the particle charge $z = z(\tau, \mu)$ for $t^* \rightarrow \infty$, and the characteristic time of charging, $t^*_{\mathrm{ch}}(\tau, \mu)$, from the uncharged state. Notice that the condition of charge stationarity: $\mathrm{d}Z_{\mathrm{d}}/\mathrm{d}t^* = 0$ coincides with equation (11) for $n_{\mathrm{e}} = n_{\mathrm{i}}$. In Fig. 2c, the solution to equation (28) with the initial condition $z(t^* = 0) = 0$ is shown for an argon plasma at $\tau = 50$. The characteristic charging time can be determined as, for example, $t^*_{\mathrm{ch}} = |Z_{\mathrm{d}}|/I_0$, where $I_0 = I_{\mathrm{e}0} = I_{\mathrm{i}0}$ are the electron and ion fluxes in a stationary state. However, it is useful to introduce the following definition which is extensively utilized in describing different processes in dusty plasmas. Let us define the charging frequency Ω_{ch} (inverse charging time) as the relaxation frequency for a small charge deviation from the

stationary value:

$$\Omega_{\mathrm{ch}} = \frac{\mathrm{d}I}{\mathrm{d}Z_{\mathrm{d}}}\bigg|_{Z_{\mathrm{d}0}}, \tag{29}$$

where the derivative should be evaluated for the stationary value of the particle charge. In the case considered we get, using Eqns (7) and (8), the following expression

$$\Omega_{\mathrm{ch}} = I_0 \, \frac{e^2}{aT_{\mathrm{e}}} \, \frac{1 + \tau + z\tau}{1 + z\tau} \, . \tag{30}$$

The values of $\Omega_{\mathrm{ch}}^{-1}$ and t_{ch}^* are shown by the vertical dashed lines in Fig. 2c.

The thermionic and photoelectric charging mechanisms are considered in Refs [62, 66] for the simplest system consisting of dust particles and electrons emitted from their surfaces.

We note that dust particle charging is usually a fast process with the characteristic time scale $t_{\mathrm{ch}}^{-1} \sim \omega_{\mathrm{pi}}(a/\lambda_{\mathrm{Di}})$. Therefore, the real time for the charge to achieve its stationary value can be determined by other processes proceeding in the system. For example, when cold particles are injected into a hot plasma, in which the thermionic emission plays a considerable role, then the charging time may, in principle, correspond to the time that is required for the particle surface to reach the temperature of the surrounding plasma.

2.1.7 Charge composition of dusty plasmas. The presence of dust particles in plasmas often leads to considerable changes in plasma charge composition. The point is that the dust particles are the ionization and recombination centers for the plasma electrons and ions. Particles that emit electrons and are turned positively charged may increase the electron concentration in the plasmas. Conversely, when the particles absorb electrons from the plasma they become negatively charged and reduce the number of free electrons. The quasi-neutrality condition in dusty plasma, which is expressed by equation (15), allows us to formulate the condition indicating when the presence of a dust component drastically influences the charge composition of the plasma. This condition is given by the inequality $|Z_{\mathrm{d}}|n_{\mathrm{d}}/n_{\mathrm{e}} \equiv P \geqslant 1$. In the absence of emission processes, electrons and ions recombine on the dust particles. The frequency of plasma loss is determined then by the formula

$$v_{L\mathrm{e(i)}} = I_{\mathrm{e(i)}} \, \frac{n_{\mathrm{d}}}{n_{\mathrm{e(i)}}} \, , \tag{31}$$

where $I_{\mathrm{e(i)}}$ is the flux of electrons (ions) absorbed by the dust particle surface. For considerable dust concentrations, the frequency of electron and ion losses on the particles can exceed the recombination frequency in the dust-free plasma (volume recombination and/or plasma losses in the walls of a discharge camera). In this case, the existence conditions for the plasma can change, because an increase in the recombination frequency should be compensated for by a corresponding increase in the ionization frequency [67]. When the particles emit electrons, they serve as ionization sources as well. The particle contribution to the ionization is characterized by the frequency $v_{I\mathrm{e(i)}}$ equal to the flux of emitted electrons (ions). In the limiting case, emitting particles put in a nonionized gas completely determine the charge composition of the plasma,

playing the roles of sources and sinks for the electrons. The two-component system of dust particles and the electrons emitted by them is characterized then by the quasi-neutrality condition (24).

2.1.8 Dust particle charge fluctuations. In the equations (7), (8), (25), and (26) for the electron and ion fluxes, as well as in the charging kinetic equation (27), the discreteness of electrostatic charges is ignored. In other words, the particle charge is treated as a continuous variable. However, the charging currents represent in reality sequences of events bound to electron and ion absorption or emission by the dust particle surface. These sequences and time intervals between the successive acts of absorption and emission are random. As a result, the particle charge can fluctuate around its average value.

Several studies in recent years addressed the problem of small charge fluctuations that arise from the random nature of the charging process [62, 68 – 72]. In particular, the case of laboratory gas discharge plasma, where dust is charged by collecting electrons and ions, was mainly considered within the framework of the OML approach. Nevertheless, in the work [62], several different charging mechanisms, including thermionic and photoelectronic emission processes, were also considered. The key results of these investigations can be formulated as follows. Independently of the charging mechanism, random charge fluctuation can often be described as a stationary, Gaussian and Markovian process (or the Ornstein – Uhlenbeck process [73]). This process was originally adopted to describe the stochastic behavior of the *velocity* of a Brownian particle. In our case, it describes the behavior of the randomly fluctuating deviation of a particle charge from its average value: $Z_1(t) = Z_{\mathrm{d}}(t) - Z_0$, where $Z_0 = \langle Z_{\mathrm{d}}(t) \rangle$ is the average particle charge determined by flux equality condition (9). Let us summarize the main properties of charge fluctuations:

(1) charge fluctuation amplitude has zero average:

$$\langle Z_1(t) \rangle = 0 \, ; \tag{32}$$

(2) its temporal autocorrelation function has an exponential form

$$\langle Z_1(t) Z_1(t') \rangle = \langle Z_1^2 \rangle \exp\left(-\Omega_{\mathrm{ch}}|t - t'|\right), \tag{33}$$

where Ω_{ch} is the charging frequency given by Eqn (29);

(3) the average of the amplitude squared of charge fluctuation is proportional (similar to many random processes) to the absolute magnitude of the average charge:

$$\langle Z_1^2 \rangle = \gamma |Z_0| \, , \tag{34}$$

where γ is a coefficient of proportionality. The analytical expressions for γ can be found in Ref. [62] for several different charging mechanisms. Within the OML approach for electron and ion collection, one finds

$$\gamma = \frac{1 + z\tau}{z(1 + \tau + z\tau)} \, . \tag{35}$$

For typical dusty plasma parameters in gas discharges $\tau \sim 10^2$ and $z \sim 3$ giving $\gamma \sim 0.3$;

(4) the process defined as $Y(t) = \int_0^t Z_1(x)\,\mathrm{d}x$ for $t \geqslant 0$ is Gaussian but neither stationary nor Markovian. With the

help of formula (33), the following equation

$$\langle Y(t)^2 \rangle = \frac{2\langle Z_1^2 \rangle}{\Omega_{\rm ch}^2} \left[\Omega_{\rm ch} t + \exp\left(-\Omega_{\rm ch} t\right) - 1 \right] \qquad (36)$$

can be obtained. Usually, it is enough to use these properties for investigating the influence of charge fluctuations on dynamic processes in dusty plasmas. In particular, the following works can be mentioned: dust particle 'heating' (in terms of the kinetic energy) in an external electric field due to charge fluctuations was investigated in Refs [72, 74 – 76]; instabilities of dust particle oscillations due to charge fluctuations were considered in Refs [77, 78], and dust diffusion across a magnetic field due to random charge fluctuations was studied in Ref. [79] with application to astrophysical plasma.

2.1.9 Experimental determination of dust particle charge.
In Sections 2.1.1 – 2.1.8 most attention was given to theoretical concepts of dust particle charging in plasmas. Experimental examination of dust particle charges is of extreme importance, especially in cases where the plasma parameters are unknown or cannot be determined with sufficient accuracy. In this section we point out several original papers describing experimental determination of particle charges under various conditions. In the work [61], the charging of particles of various materials and diameters from 30 to 120 μm by thermal and monoenergetic suprathermal electrons was experimentally investigated. For conditions in which the charging was dominated by suprathermal electrons, the particles were charged to the potential proportional to the electron energy and the charge magnitude proportional to the particle radius, in agreement with theoretical models. When electron energy reached a threshold value (different for various materials), from which the secondary electron emission became important, a sharp decrease in the particle potential and charge was found. In the work [60], photoelectric emission charging of dust particles with diameters of ~ 100 μm was studied. Conducting particles acquired a positive floating potential and charge both increasing linearly with the decreasing work function of photoelectrons. Behavior of dust particles charged by solar radiation in microgravity conditions on-board the orbital station 'Mir' was investigated in Refs [59, 80, 81]. An analysis of particle dynamics after UV irradiation, reported in Ref. [59], revealed that the particles with mean radius 37.5 μm were charged to approximately $10^4 e$. In the work [82], probe measurements were performed in order to investigate the influence of dust concentration on particle charge. In accordance with the theoretical predictions, a significant reduction in the charge was found when dust concentration increased. Measurements of the particle charge in a dc discharge plasma were performed in Ref. [83]. In this work, aperiodic oscillations of an isolated particle excited by a focused laser beam were studied. A nonlinear dependence of the particle charge on the particle size was evidenced. Other methods of charge determination based on an analysis of interparticle collisions and particle oscillations will be considered in Sections 2.4 and 4.1, respectively.

2.2 Electrostatic potential around a dust particle
Distribution of the electrostatic potential $\varphi(r)$ around an isolated spherical dust particle of charge $Z_{\rm d}$ in an isotropic plasma satisfies the Poisson equation (22) with the boundary conditions $\varphi(\infty) = 0$ and $\varphi(a) = \varphi_{\rm s}$. The potential is connected to the particle charge through the relationship

$$\frac{{\rm d}\varphi}{{\rm d}r}\bigg|_{r=a} = -\frac{Z_{\rm d} e}{a^2} \,. \qquad (37)$$

In a plasma with a Boltzmann distribution of electrons and ions, where the condition $|e\varphi_{\rm s}/T_{\rm e(i)}| < 1$ is satisfied, the right hand side of Eqn (22) can be linearized, which yields

$$\varphi(r) = \varphi_{\rm s}\, \frac{a}{r} \exp\left(-\frac{r-a}{\lambda_{\rm D}}\right), \qquad (38)$$

where $\lambda_{\rm D}^{-2} = \lambda_{\rm De}^{-2} + \lambda_{\rm Di}^{-2}$ in the case under consideration. The surface potential is connected to the charge through the formula $\varphi_{\rm s} = Z_{\rm d} e/a(1 + a/\lambda_{\rm D})$. For the potential distribution in the case $a \ll \lambda_{\rm D}$, we can use the following expression

$$\varphi(r) = \frac{Z_{\rm d} e}{r} \exp\left(-\frac{r}{\lambda_{\rm D}}\right). \qquad (39)$$

The potential (39) is the screened Coulomb potential which is often applied to describe the electrostatic interaction between the particles in dusty plasmas. In different physical systems this form of the potential is also known as the Debye – Hückel or Yukawa potential. If the surface potential is not small compared to the temperatures of electrons and/or ions, then at sufficiently large distances from the particle surface one can still use Eqn (39) in which, however, the surface potential $\varphi_{\rm s}$ should be replaced by some effective potential $\varphi_{\rm eff}$, with $|\varphi_{\rm eff}| < |\varphi_{\rm s}|$. The effective potential can be calculated numerically for known plasma parameters [84, 85].

The equilibrium case considered above is uncommon for dusty plasmas. In particular, if the charging is determined by electron and ion collection as well as their recombination on the particle surface, then plasma is continuously absorbed on the particles. This means that some external ionization sources, which continuously supply energy to the plasma, are required for its occurrence. Hence, the system considered is open. In this case, the equilibrium (Boltzmann) distributions of electrons and ions around the particle are disrupted — the electron and ion fluxes directed from the particle surface to the plasma are absent. Thus, formula (39) is, strictly speaking, inapplicable independently of whether the Boltzmann distributions can be expanded or not in terms of the potential (in dusty plasma this expansion is usually not possible because typically $|e\varphi_{\rm s}/T_{\rm e}| \gtrsim 1$, and $|e\varphi_{\rm s}/T_{\rm i}| \gg 1$). Let us consider first the asymptotic behavior of the potential at large (compared to the Debye radius) distances. To calculate the electrostatic potential around a relatively small $(a \ll \lambda_{\rm D})$ dust particle within the framework of the OML approach, we follow Ref. [3] and represent the ion velocity distribution function in the form

$$f_{\rm i}(\mathbf{v}) = \begin{cases} f_0(v), & \theta > \theta_* \,, \\ 0, & \theta \leqslant \theta_* \,, \end{cases} \qquad (40)$$

where $f_0(v)$ is a Maxwellian distribution function, and θ is the angle between $\mathbf{v}$ and $\mathbf{r}$ vectors. The angle θ_* defines the solid angle in the velocity space where the ions (moving away from the particle) are absent due to absorption. At large distances from the particle, the angle θ_* is small and can be determined using the OML approach:

$$\sin^2 \theta_* \approx \frac{a^2}{r^2}\left(1 + \frac{2e|\varphi_{\rm s}|}{m_{\rm i} v^2}\right). \qquad (41)$$

Assuming $\varphi_s \approx Z_d e/a$ we arrive at the following asymptotic behavior of the electrostatic potential around the particle (see, e.g., Refs [3, 86, 87]):

$$\frac{e\varphi(r)}{T_e} \approx -\frac{1 + 2z\tau}{4(1 + \tau)} \frac{a^2}{r^2} , \qquad (42)$$

which holds at sufficiently large distances from the particles, when $r \gg a\sqrt{z\tau}$ and $r > \lambda_D \ln(\lambda_D/a)$. The first of these inequalities ensures that θ_* is small, while the second means that the screened Coulomb potential (39) is small compared to the asymptotic value (42). We note that the dependence $\varphi(r) \propto r^{-2}$ at large distances from an absorbing body in plasmas is well known from probe theory (see, e.g., Refs [42, 86]). In typical gas discharge plasmas $\tau \gg 1$ and $z \sim 1$, so that Eqn (42) can be considerably simplified:

$$\varphi(r) = \frac{Z_d e a}{2r^2} . \qquad (43)$$

At smaller distances from the particle, the electrostatic potential can also differ from the screened Coulomb potential [86]. The question of how significant this difference might be is not fully understood: there exist only several numerical calculations for a limited set of plasma parameters. In particular, in Refs [67, 88] the electrostatic potential around a spherical particle in an isotropic plasma was calculated numerically from a self-consistent solution for the Poisson – Vlasov equation in a collisionless regime for the ions and electrons. The main results of these works can be formulated as follows: for not too large distances from a relatively small ($a \ll \lambda_D$) particle, the electrostatic potential can be approximated with a reasonable accuracy by the potential of the form (39) with the screening length λ_L close to the ionic Debye radius: $\lambda_L \sim \lambda_D \sim \lambda_{Di}$; for larger particles, formula (39) is still applicable, but with the screening length increasing with the particle size and reaching values close to the electron Debye length λ_{De} or even larger. For still larger distances, the potential asymptotically tends to the r^{-2} dependence in accordance with expression (43).

Finally, as shown in Ref. [53], under certain conditions the existence of trapped ions can lead to even better agreement between the potential calculated in a self-consistent way and the screened Coulomb potential for distances up to several Debye radii [at larger distances $\varphi(r) \sim r^{-2}$, as discussed above].

So far, we have assumed that the plasma is isotropic. Often, especially in laboratory experiments, ions are drifting with a nonzero velocity $\mathbf{u}$ relative to the dust particles at rest. A test particle immersed in such a plasma creates a perturbed region of flow downstream from the particle — a wake. The electrostatic potential created by a point-like charge at rest is defined in the general case (see Ref. [89]) as

$$\varphi(\mathbf{r}) = \frac{Z_d e}{2\pi^2} \int d\mathbf{k} \, \frac{\exp(i\mathbf{k}\mathbf{r})}{k_i k_j \varepsilon_{ij}(\mathbf{k}, 0)} , \qquad (44)$$

where $\varepsilon_{ij}(\mathbf{k}, \omega)$ is the permittivity tensor of a plasma, and $\mathbf{k}$ is the wave vector. Using a certain model for $k_i k_j \varepsilon_{ij}(\mathbf{k}, \omega)$ one can, in principle, calculate the distribution $\varphi(\mathbf{r})$ (at least for some limiting cases), which is anisotropic in this case. This was done in Refs [90 – 96]. The potential distribution can also be obtained from numerical modeling (see, for example, Refs [95, 97 – 102]). Physically, generation of electrostatic wakes in dusty plasmas is analogous to the generation of electromagnetic waves by a particle at rest, which is placed in a moving medium [103, 104]. When dealing with supersonic ion drift velocities $(T_e/m_i)^{1/2}$, which are evident in the sheath region of rf discharges, the analogy with the Vavilov – Cherenkov effect can be useful. The qualitative description of the effect under consideration is the following. In the directions upstream from and perpendicular to the ion flow, the potential has the form of a screened Coulomb potential; downstream from the flow (within a certain solid angle) potential has a periodically oscillating character with decay. As shown by numerical modeling, the shape of the wake potential is sensitive to ion collisions (ion – neutral collisions) [105] and the electron-to-ion temperature ratio which governs Landau damping [106]. In typical situations, these mechanisms can effectively reduce wake structure to one oscillation; at larger distances, the wake structure is smeared. The shape of the wake potential depends on the value of the Mach number $M = u/c_i$, however, the wake itself appears both in supersonic and subsonic regimes of the ion drift. In this context, we mention the work [98] where some examples of the wake structures calculated numerically for different plasma conditions are presented. The effects of finite particle size and asymmetry of the charge distribution over its surface are considered in Refs [107, 108]. The wake effect is usually invoked for explaining the vertical ordering of the dust particles (chain formation) in ground-based experiments: due to the opposite sign of the potential in the wake, there may appear an attractive force between the particles (of the same sign of charge) situated along the ion flow.

Recently, another effect was also pointed out, which might play some role in the vertical ordering of dust particles along the ion flow. This effect is connected with a distortion of the ion velocity field by the upstream particle and the appearance of a horizontal component of the force, caused by the ion momentum transfer in absorbing and Coulomb collisions with the downstream particle [98, 101]. This force — the ion drag force — brings the downstream particle back to the axis with the origin at the upstream particle position and parallel to the ion flow. Numerical modeling of the ion velocity field in the wake showed that for certain conditions the force associated with the perturbation of ion velocities prevails over the electrostatic one [101]. We note once again that both effects considered are sensitive to ion – neutral collisions. First, the collisions reduce the ion directed velocity in an external electric field (and, hence, plasma anisotropy). Second, they limit the perturbed plasma region (both the potential and the ion velocity field) around a probe particle to a length scale on the order of the ion free path. Therefore, the mechanisms considered can be effective only at sufficiently low pressures.

Note that in this section we were dealing with the potential distribution around an 'isolated' particle. Such a consideration is justified when the dust component does not play the role of a real plasma component and the interparticle separation significantly exceeds the Debye radius. In the opposite situation, the dust component can also contribute to the plasma screening of a test charge. Equation (22) should also be modified to take into account the charge variation in response to the plasma perturbation. We will not consider this situation here; the details can be found in the recent review by Morfill et al. [41].

2.3 Main forces acting on dust particles in plasmas
The main forces acting on dust particles in plasmas can be conveniently divided into two groups: the first one includes

the forces which do not depend on the particle charge (force of gravity, neutral drag force, thermophoretic force), while the second one includes forces which depend directly on the particle charge (electrostatic force and the ion drag force).

2.3.1 Force of gravity. The gravitational force is determined by the expression

$$F_g = m_d g , \qquad (45)$$

where g is the gravitational acceleration. The gravitational force is proportional to the particle volume, viz. $F_g \sim a^3$.

2.3.2 Neutral drag force. When the particle is moving, it experiences a force of resistance from the surrounding medium. In the case of weakly ionized plasma, the main contribution to this resistance force comes from the neutral component. This resistance force — the neutral drag force — is in most cases proportional to the particle velocity, because the latter is usually much smaller than the thermal velocity of neutral atoms or molecules. One should distinguish between two regimes depending on the value of the Knudsen number Kn, which is the ratio of the atomic or molecular free path to the particle size: $\mathrm{Kn} = l_n/a$. It is common to call the regime for which $\mathrm{Kn} \ll 1$ as the hydrodynamic regime. In this limit, the resistance force is given by the Stokes expression [109]

$$F_n = -6\pi \eta a u , \qquad (46)$$

where η is the neutral gas viscosity, and u is the particle velocity relative to the neutral gas. The minus sign means that the force is directed opposite to the vector of relative velocity. In the opposite limiting case of $\mathrm{Kn} \gg 1$, which is often called a free molecular regime, and for sufficiently small relative velocities ($u \ll v_{Tn}$), the neutral drag force can be written as [110, 111]

$$F_n = -\frac{8\sqrt{2\pi}}{3} \gamma a^2 n_n T_n \frac{u}{v_{Tn}} , \qquad (47)$$

where n_n and T_n are the concentration and temperature of neutrals, respectively, and γ is a coefficient on the order of unity that depends on the exact processes proceeding on the particle surface. For example, $\gamma = 1$ for the case of complete collection or specular reflection of neutrals from the particle surface at collisions, and $\gamma = 1 + \pi/8$ for the case of diffuse scattering with full accommodation. For high relative velocities ($u \gg v_{Tn}$), the neutral drag force is proportional to the velocity squared (see, for example, Refs [112, 113]):

$$F_n = -\pi a^2 n_n m_n u^2 , \qquad (48)$$

where m_n is the mass of neutrals. It should be noted that these expressions were originally derived for uncharged particles in a neutral gas. In this way, the polarization interaction, which is associated with a nonuniform electric field in the vicinity of the dust particle, was not taken into account. However, the radius of the polarization interaction turns out to be much smaller than the particle size, so that in most cases the corrections can be ignored.

For most dusty plasmas, formula (47) is applicable. We note that it can be rewritten in the form $F_n = -m_d v_{dn} u$, where v_{dn} stands for the effective momentum transfer frequency of dust – neutral collisions.

2.3.3 Thermophoretic force. If a temperature gradient is present in a neutral gas, then the particle experiences a force directed oppositely to this gradient, i.e., in the direction of lower temperatures. This is associated with the fact that the larger momentum is transferred from the neutrals coming from the higher temperature region. In the case of full accommodation, this force (called the thermophoretic force) can be expressed as [114]

$$F_{th} = -\frac{4\sqrt{2\pi}}{15} \frac{a^2}{v_{Tn}} \varkappa_n \nabla T_n , \qquad (49)$$

where $\varkappa_n$ is the thermal conductivity coefficient of gas. The simplest estimation of this coefficient gives $\varkappa_n \approx C\bar{v}/\sigma_{tr}$ [57], where C is a numerical factor on the order of unity, so that $C = 5/6$ for atoms, and $C = 7/6 \, (9/6)$ for diatomic molecules with unexcited (excited) vibrational states, respectively; $\bar{v} = \sqrt{8T_n/\pi m_n}$, and σ_{tr} is the transport scattering cross section for gas atoms or molecules.

Inserting the value of $C = 5/6$ for the atomic gas into Eqn (49) we get

$$F_{th} \approx -\frac{16}{9} \frac{a^2}{\sigma_{tr}} \nabla T_n . \qquad (50)$$

This estimate shows that the thermophoretic force depends on the particle radius, gas type (through σ_{tr}), and temperature gradient, but does not depend on the neutral gas pressure and temperature. For particles of about 1 μm radius and mass density ~ 1 g cm^{-3} in an argon plasma, the thermophoretic force is comparable to the force of gravity at temperature gradients $\nabla T_n \sim 10$ K cm^{-1}. Note that the expression (49) was derived for an unbounded system. If the dust particle is situated near the electrode or the walls of a discharge camera, then one should take into account corrections associated with the accommodation of neutrals when they collide with the electrode or wall surfaces. These corrections basically change the numerical factor in formula (49) [115]. Experimental investigation of the effect of thermophoretic force on the behavior of dust particles in gas discharge plasmas was performed in Refs [116–118]. In these works, it is shown that the thermophoretic force can be used for particle levitation and controlled action on the ordered structures of dust particles in the quasi-neutral bulk of a plasma.

2.3.4 Electrostatic force. If an electric field E is present in plasmas, it acts on a charged particle. For conducting particles, the electrostatic force is given by [119]

$$\mathbf{F}_e = Z_d e \mathbf{E} \left[1 + \frac{(a/\lambda_D)^2}{3(1 + a/\lambda_D)} \right] . \qquad (51)$$

An effective electric field can be introduced as follows:

$$\mathbf{E}_{eff} = \mathbf{E} \left[1 + \frac{(a/\lambda_D)^2}{3(1 + a/\lambda_D)} \right] ,$$

then $\mathbf{F}_e = Z_d e \mathbf{E}_{eff}$. An increase in E_{eff} compared to E is connected to plasma polarization in the vicinity of the dust particle, which is induced by the external electric field. Plasma polarization induces a dipole moment $\mathbf{p} \approx a^3 \mathbf{E}_{eff}$ on the dust particle directed along the field. If the electric field is nonuniform, then such a dipole experiences a force

$$\mathbf{F}_{dp} = (\mathbf{p}\nabla)\mathbf{E} . \qquad (52)$$

In typical dusty plasmas the inequality $a \ll \lambda_D$ is valid, so that the electrostatic force is $\mathbf{F}_e \approx Z_d e \mathbf{E}$, and the dipole moment is $\mathbf{p} \approx a^3 \mathbf{E}$, as for a conducting sphere in a vacuum. The dipole moment is usually very small and one can typically ignore the force $\mathbf{F}_{dp}$, in contrast to $\mathbf{F}_e$. Let us mention Refs [120, 121] where the action of electrostatic force on the dust particle in a nonuniform plasma with ion flows was calculated. It was shown that there appears an additional component of the force proportional to the gradient of the plasma charge density or to the gradient of the corresponding Debye radius (which is dependent on the ion flow velocity), and acting in the direction of decreasing Debye length. In typical dusty plasma conditions ($a \ll \lambda_D$), this component is smaller than F_e by approximately a factor of a/λ_D.

2.3.5 Ion drag force. If there exists a drift of ions (electrons) relative to the dust particle, there appears a force associated with the momentum transfer from the plasma to the dust particle. Due to the larger ion mass, the effect associated with the ions typically dominates. The movements of ions relative to dust particles can be associated with the presence of an external electric field or with the (thermal) motion of the particles relative to the stationary background of ions. The force considered is usually called the ion drag force. The ion drag force is connected with two processes: momentum transfer from the ions that are collected by the particle, and momentum transfer from the ions that are elastically scattered in the electric field of the particle.

The fact that the ion drag force can be important for various processes in dusty plasmas was ascertained even before the active laboratory investigation of dusty plasmas started [122–124]. Presently, it is considered to be established that ion drag affects (or even determines) location and configuration of the dust structures in laboratory plasma facilities [124], is responsible for dust structures (e.g., clusters) rotation in the presence of a magnetic field [125–127], affects the properties of low-frequency waves in dusty plasmas [128, 129], causes the formation of a 'void' (a region free of dust particles) in the central part of an rf discharge in experiments under microgravity conditions [130–134], and governs the diffusion and mobility of weakly interacting Brownian particles in strongly ionized plasmas [135, 136]. All this indicates the importance of a correct estimation of the ion drag force and its dependence on plasma parameters. However, a self-consistent model describing all possible situations has not yet been constructed. The complications here are caused by the necessity of taking into account ion–neutral collisions in the vicinity of the dust particle, the effect of neighboring particles, necessity of knowing the exact distribution of the electrostatic potential around the particle, and other problems which cannot be considered to be fully solved. Rather, there exist several approaches which can be utilized under certain conditions.

So far, the results have been obtained only for pair-collision approximations, i.e., for the case of collisionless ions with $l_i \gg r_{int}$, and 'isolated' dust particles with $\Delta \gg r_{int}$, where r_{int} is the characteristic radius of interaction between the ion and the dust particle, and Δ is the mean interparticle distance. This situation will be considered below. The general expression for the ion drag force is written as (see, for example, Ref. [110])

$$\mathbf{F}_I = m_i n_i \int \mathbf{v} f_i(\mathbf{v}) \, \sigma_i^{tr}(v) v \, d\mathbf{v}, \tag{53}$$

where $f_i(\mathbf{v})$ is the ion velocity distribution function, and $\sigma_i^{tr}(v)$ is the momentum transfer cross section for ion collisions with the dust particle. In weakly ionized plasmas, it is often reasonable to use a shifted Maxwellian distribution (12) for ion velocities. For subthermal ion drifts, it can be expanded as follows

$$f_i(\mathbf{v}) \simeq f_{i0}(v) \left[1 + \frac{\mathbf{uv}}{v_{Ti}^2} \right]. \tag{54}$$

Here, u is the drift velocity of ions relative to the dust particle ($u < v_{Ti}$), and $f_{i0}(v)$ is the isotropic Maxwellian function (5) for ions. Thus, to calculate the ion drag force it is necessary to determine the momentum transfer cross section $\sigma_i^{tr}(v)$ for ion–particle collisions.

First, let us study the case of a point-like particle. In this case, the momentum transfer cross section is defined in the following way [137]:

$$\sigma_i^{tr}(v) = \int_0^\infty \left[1 - \cos \chi(\rho, v) \right] 2\pi \rho \, d\rho. \tag{55}$$

Here, ρ is the impact parameter, χ is the scattering angle, and $\chi(\rho, v) = |\pi - 2\varphi_0(\rho, v)|$, where

$$\varphi_0 = \int_{r_0}^\infty \frac{\rho \, dr}{r^2 \sqrt{1 - U_{eff}(r, \rho, v)}}, \tag{56}$$

and the effective potential U_{eff} is determined from Eqn (18). The momentum transfer cross section for ion collisions with a massive dust particle of charge Z_d can be obtained either by self-consistent calculation of the potential distribution around a sufficiently small particle ($a \ll \lambda_D$) and subsequent integration in expressions (55) and (56), or by assuming a certain form of the interaction potential $U(r)$ *a priori* with subsequent evaluation of the same integrals.

The results of different calculations of the momentum transfer cross section are presented in Fig. 4a. It is useful to express the dependence of the cross section on the ion velocity through the dimensionless scattering parameter β introduced in Section 2.1. In the case considered, it can be written down as

$$\beta(v) \approx \frac{|Z_d| e^2}{m_i v^2 \lambda_D},$$

where v denotes the relative velocity over which the averaging should be performed. A self-consistent determination of the cross section with preliminary numerical calculation of the potential distribution around a small dust particle was reported in Ref. [50]. Numerical computations for the attractive screened Coulomb potential of interaction were performed in Refs [49, 138, 139]. As can be seen from Fig. 4a, these numerical results demonstrate good agreement, which should be attributed to the fact that for $a \ll \lambda_D$ the potential distribution calculated self-consistently can be quite well approximated by the screened Coulomb potential within a few screening lengths from the particle [88]; longer distances do not contribute considerably to the momentum transfer.

The standard theory of Coulomb collisions of charged particles in plasmas, which is based on pure Coulomb interaction potential with cutoff at impact parameters exceeding the plasma screening length, gives the following
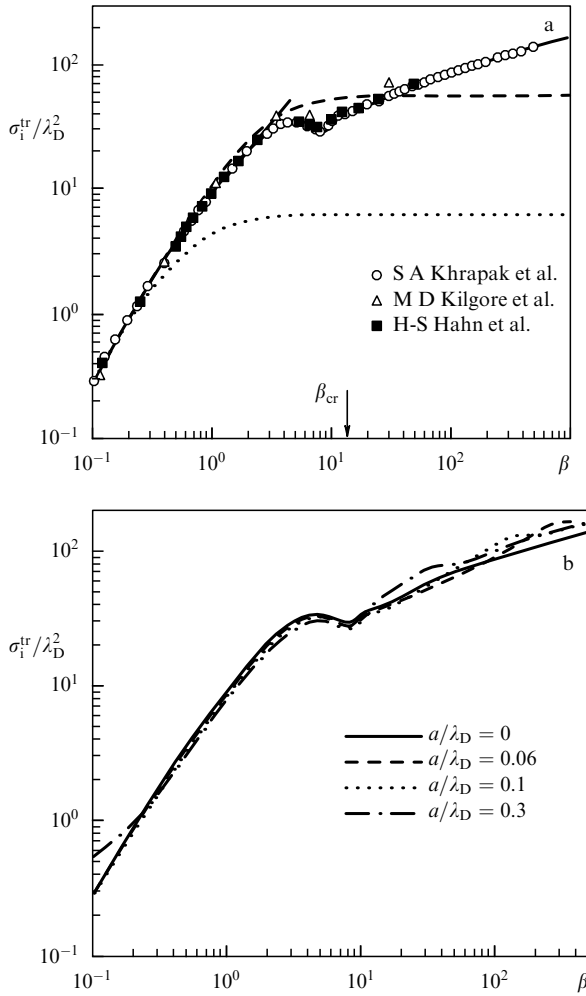
Figure 4. Momentum transfer cross section (normalized on the square of screening length λ_{D}^2) versus the scattering parameter β: (a) for a point-like particle; the symbols correspond to the results of numerical calculations [138] — ■, [50] — △, [49, 139] — ○; dotted line corresponds to the standard Coulomb scattering theory [Eqn (57)]; dashed line corresponds to the approximation (58) proposed in Ref. [50]; solid curves correspond to the analytical expressions proposed in Ref. [133] ($\beta < 5$) and Ref. [49] ($\beta > \beta_{\mathrm{cr}}$), and the arrow indicates the value of $\beta = \beta_{\mathrm{cr}} \approx 13.2$; (b) for a finite size particle; the numerical results are shown for different values of a/λ_{D}, indicated in the figure.

result for the momentum transfer cross section:

$$\frac{\sigma_{\mathrm{i}}^{\mathrm{tr}}}{\lambda_{\mathrm{D}}^2} = 4\pi\beta^2 \Lambda_{\mathrm{c}} \,, \qquad (57)$$

where $\Lambda_{\mathrm{c}} = \ln\left(1 + 1/\beta^2\right)/2$ is the Coulomb logarithm [110]. Figure 4a shows that the standard Coulomb scattering theory significantly underestimates the cross section above $\beta \sim 1$, i.e., for sufficiently slow ions. This is not surprising, because the theory of Coulomb collisions can be grounded only for $\beta \ll 1$. In this case, the interaction radius — the Coulomb radius $r_{\mathrm{c}} = |Z_{\mathrm{d}}|e^2/(mv^2)$ — is small compared to the screening length λ_{D}. The ratio of the momentum transfer from collisions with $r_{\mathrm{c}} < \rho < \lambda_{\mathrm{D}}$ to that with $\rho < r_{\mathrm{c}}$ is approximately equal to the Coulomb logarithm $\Lambda_{\mathrm{c}} \approx \ln(1/\beta) \gg 1$. The relative contribution from collisions with $\rho > \lambda_{\mathrm{D}}$ is small ($\sim \Lambda_{\mathrm{c}}^{-1}$) because of the screening [139]. Therefore, the momentum transfer is mostly associated with the scattering in the bare Coulomb potential (for $r \ll \lambda_{\mathrm{D}}$, the

screening can be neglected), and the Coulomb scattering theory adequately (with logarithmic accuracy) determines the momentum transfer cross section for $\beta \ll 1$. We note that dominant contribution to the momentum transfer in this case is due to small-angle scattering (the deflection is strong only if $\rho < r_{\mathrm{c}}$).

In a common electron–ion plasma, the condition $\beta \ll 1$ is usually very well satisfied [49, 133], excluding the case of a strongly nonideal plasma, for which the pair-collision approximation considered here is meaningless anyway. However, for dusty plasmas the particle charge is large ($|Z_{\mathrm{d}}| \gg 1$) and the scattering parameter for ion–particle collisions is not necessarily small. For a typical particle size of 1 μm, the scattering parameter is on the order of $\beta \sim 10$. In this case, the interaction range exceeds the screening length, it is not possible to neglect impact parameters larger than the screening length, and the main contribution to the momentum transfer is due to large-angle scattering. The theory of Coulomb scattering fails under these conditions (see Fig. 4a). Therefore, all the calculations of the ion drag force, which use expression (57) [113, 122–124], are also incorrect in this case.

In the work [50], a fit of the obtained numerical data to the analytical form of Eqn (57) was performed. The following analytical expression was proposed:

$$\frac{\sigma_{\mathrm{i}}^{\mathrm{tr}}}{\lambda_{\mathrm{D}}^2} = C_1 \beta^2 \ln\left(1 + \frac{C_2}{\beta^2}\right) \qquad (58)$$

with $C_1 \approx 3.748$ and $C_2 \approx 15.33$ determined from the best agreement of Eqn (58) with the calculated results. As follows from Fig. 4a, this approximation lies much closer to the numerical data compared to the standard result (57). However, this fit is physically ungrounded and, as a consequence, demonstrates an improper asymptotic behavior for large enough β ($\beta > \beta_{\mathrm{cr}}$).

Analytical expressions for the momentum transfer cross section were recently obtained in Refs [49, 133] for an attractive screened Coulomb interaction potential. In these works, different approaches were used. This is connected to the fact that at $\beta = \beta_{\mathrm{cr}} \approx 13.2$ the behavior of ion trajectories in the vicinity of the dust particle changes qualitatively due to the appearance of the barrier in the effective potential (see Section 2.1.3).

In the work [133], it was proposed for the case $\beta < \beta_{\mathrm{cr}}$ to take into account the ions (with impact parameters $\rho > \lambda_{\mathrm{D}}$) approaching the particle surface closer than the screening length ($r_0 \leqslant \lambda_{\mathrm{D}}$). This basically leads to the following modification of the Coulomb logarithm

$$\tilde{\Lambda}_{\mathrm{c}} = \ln \frac{1 + \beta}{\beta + a/\lambda_{\mathrm{D}}} \,. \qquad (59)$$

In the limit of point-like particles, $\tilde{\Lambda}_{\mathrm{c}} = \ln(1 + 1/\beta)$ and when $\beta \ll 1$ expression (59) coincides with the result of the standard Coulomb scattering theory. However, for $\beta \gtrsim 1$ there is considerable difference. Figure 4a shows that the approach proposed precisely describes the numerical results up to $\beta \approx 5$.

The case of $\beta > \beta_{\mathrm{cr}}$ was considered in Ref. [49] and the authors arrived at the following analytical expression for the cross section

$$\sigma_{\mathrm{i}}^{\mathrm{tr}} = A\pi\rho_*^2(\beta) + B\lambda_{\mathrm{D}}^2\left(1 + 2\ln^{-1}\beta\right), \qquad (60)$$

where $A \approx 0.81$, $B \approx 6.4$, and

$$\rho_*(\beta) \approx \lambda_D \left(\ln \beta + 1 - \frac{1}{2\ln \beta} \right).$$

Figure 4a demonstrates good agreement between Eqn (60) and numerical results.

When taking into account the finite size of the dust particles, then in addition to the parameter β describing the scattering from a point-like particle, there appears a second parameter a/λ_D. The physics of the ion momentum transfer changes as follows: the ions with $\rho < \rho_c$ experience inelastic collisions with the particle (collection), while the ions with $\rho > \rho_c$ are scattered in the electric field of the particle. The total momentum transfer cross section for the case of a finite-sized particle is the sum of collection (absorption) and scattering cross sections: $\sigma_i^{tr} = \sigma_i^c + \sigma_i^s$. Assuming that at absorbing collisions the ions transfer their initial momentum (i.e., ignoring the possible physical processes on the particle surface), we find that the collection formally corresponds to the scattering angle $\chi = \pi/2$, yielding

$$\sigma_i^c = \int_0^{\rho_c} 2\pi\rho \, d\rho = \pi\rho_c^2 \, .$$

The scattering part σ_i^s of the cross section is given now by Eqn (55), with the lower (zero) limit of integration replaced by ρ_c. When OML approach is valid, the impact parameter corresponding to collection, $\rho_c = \rho_c^{OML}$, is determined by formula (19), and the collection cross section is given by expression (3). If $\rho_c^{OML} > \rho_*$, then OML is no longer applicable. In this case, for $a < \lambda_D$ we have $\rho_c = \rho_*$ and $\sigma_i^c = \pi\rho_*^2$.

The influence of the finite particle size on the total momentum transfer cross section is discussed in detail in Refs [49, 139]. Figure 4b shows the dependence of the total cross section $\sigma_i^{tr}(\beta)$ for several values of a/λ_D. The main result is that the cross section for a finite-sized particle does not differ dramatically from that of a point-like particle even in the region $\beta \gg 1$, where the main contribution to the momentum transfer is due to ion collection [49].

When the dependence of the momentum transfer cross section on β (i.e., on the velocity) is known, it is possible to calculate the ion drag force F_I by performing integration in formula (53). For subthermal drifts one should also use formula (54). When $\beta(v_{Ti}) \lesssim 5$, one can use the expression

$$F_I = -\frac{8\sqrt{2\pi}}{3} a^2 n_i m_i v_{Ti} u \left(1 + \frac{1}{2} z\tau + \frac{1}{4} z^2\tau^2 \Pi \right) \quad (61)$$

derived in Ref. [133]. Here, Π is the modified Coulomb logarithm integrated with the ion velocity distribution function:

$$\Pi = 2 \int_0^\infty \exp(-x) \ln \frac{2\lambda_D/a + z\tau}{2x + z\tau} \, dx \, .$$

The last term in parentheses in Eqn (61) corresponds to elastic scattering and is dominant. In Ref. [49], the estimate

$$F_I \sim -\pi\rho_*^2(v_{Ti}) \, n_i m_i v_{Ti} u \quad (62)$$

was submitted for $\beta(v_{Ti}) > \beta_{cr}$. Note that in this case $F_I \propto T_i^{3/2} m_i^{1/2}$ but depends only logarithmically on a, n_i, and τ.

In the case of highly anisotropic plasma, $u \gg v_{Ti}$, the integration in expression (53) can be simplified with the substitution $f_i(\mathbf{v}) \sim \delta(\mathbf{v} - \mathbf{u})$ into the corresponding integrand. Notice that in this limiting case the value of β is substantially lower than in an isotropic plasma, first due to $u \gg v_{Ti}$ and, second, due to the fact that the Debye length is determined by electrons rather than by ions: $\lambda_{De} \gg \lambda_{Di}$. Hence, the cross section (57) with the modified Coulomb logarithm (59) is applicable for estimations of F_I. Moreover, in the case $\beta(u) \ll 1$, the modification is even unnecessary as discussed above. Neglecting the weak logarithmic dependences we get $F_I \sim u^{-2}$ for this case, i.e., the ion drag force decreases with the relative velocity. Finally, in the limiting case of very high relative velocity only the geometrical particle size matters, and then [113]

$$F_I = -\pi a^2 m_i n_i u^2 \, , \quad (63)$$

i.e., F_I increases again with the relative velocity. The qualitative description of this nonmonotone behavior of F_I as a function of the relative velocity was given by Goree et al. [131].

Let us briefly discuss the question concerning which value of λ_D should be used in the expressions encounted in this section. In the case of isotropic plasma, λ_D is the linearized Debye radius:

$$\lambda_D \sim (\lambda_{De}^{-2} + \lambda_{Di}^{-2})^{-1/2} \, ,$$

which is close to λ_{Di} for $T_e \gg T_i$. Only for relatively large particles ($a \gtrsim \lambda_{Di}$) does an approximation of numerically calculated potential by the Debye–Hückel form yield a larger value for the effective screening length (see Section 2.2). In highly anisotropic plasmas, $u \gg v_{Ti}$, ions hardly screen the particle charge, and one may possibly assume that $\lambda_D \sim \lambda_{De}$, while in this case the potential distribution itself (and correspondingly the screening length) is anisotropic, i.e., depends on the direction (see, e.g., Ref. [106]).

We discuss this apparently simple question because in recent experiments on determination of the ion drag force [141, 142] the authors postulated $\lambda_D = \lambda_{De}$, despite the experiments having been performed in a central part of an rf discharge, where the ambipolar electric field is weak and the ion drift is (sub)thermal. The correct choice of the screening length in this case would be $\lambda_D \sim \lambda_{Di}$. Apparently, the authors of works [141, 142] were forced to make this incorrect assumption because in interpreting their experimental results they were using the standard theory of Coulomb scattering. Meanwhile, the dusty plasma parameters in Refs [141, 142] corresponded to the condition $\beta > 1$, where this theory underestimates considerably the scattering cross section (see Fig. 4a). Substitution $\lambda_D \to \lambda_{De}$ in the Coulomb logarithm of formula (57) allows us to enhance the cross section considerably because the argument of the Coulomb logarithm for ion–dust collisions is close to unity when $\beta > 1$. This artificial enhancement of the cross section allows the authors to achieve some qualitative agreement with the experimental results [141, 142]. However, as follows from the arguments given above, this agreement is based on an unfounded physical assumption. The employment of the results obtained for the case $\beta > 1$ and considered above [expressions (59) and (60)] would be more consistent. In this way, good agreement with the experiment can be obtained without

using any unphysical assumptions. More details on this issue can be found in comment [143].

Finally, we point out a few problems which require further elaboration. These are, first and foremost, the influence of the exact potential distribution around the dust particle on the ion drag force, consistently taking ion–neutral collisions into consideration, and an investigation of the situation in which the characteristic radius of ion–particle interaction exceeds the interparticle distance.

2.4 Interaction between dust particles in plasmas

The potential of interaction between dust particles differs from the Coulomb interaction potential between charged particles in a vacuum. As will be shown below, the potential of interaction between the dust particles is, generally speaking, determined not only by electrostatic interactions between the particles. Variability of the particle charges as well as a number of collective effects, some of them discussed below, are responsible for these differences. 'Collective interactions' can also lead to the attraction of similarly charged particles, which can occur for a certain critical dust concentration (for a detailed consideration see Ref. [40]). For lower dust concentrations, the interparticle interaction, screening, and charging can be calculated in the approximation of 'isolated' particles. In this case, the electrostatic interaction between the particles is assessed when the electrostatic potential distribution $\varphi(r)$ in a plasma surrounding a test particle is known. The absolute value of the electrostatic force acting on a particle with a fixed charge Z_d and located at a distance r from the test particle can be presented in the form $F_{de} = -dU_{el}(r)/dr$, where

$$U_{el}(r) = Z_d e \varphi(r). \tag{64}$$

Thus, it is necessary to know the distribution $\varphi(r)$ of the potential in plasmas. As was previously shown in Section 2.2, the potential of an isolated spherical particle in an isotropic plasma is purely Coulombic at small distances $r \ll \lambda_D$; for $r \sim \lambda_D$, the screening is important and the Debye–Hückel form can be often used; finally, at distances exceeding several screening lengths the potential has an inverse power-law asymptotics. Hence, up to the distances considerably exceeding λ_D it is reasonable to use a screened Coulomb type of the potential

$$U_{el}(r) = \frac{Z_d^2 e^2}{r} \exp\left(-\frac{r}{\lambda_D}\right). \tag{65}$$

For larger distances $r > \lambda_D \ln(\lambda_D/a) \approx (3-5)\lambda_D$, a long-range repulsion takes place, which is associated with the plasma velocity anisotropy in the vicinity of a collecting particle. According to expressions (43) and (64), the asymptotic behavior of the interaction potential is given by

$$U_{el} \approx \frac{Z_d^2 e^2 a}{2r^2}. \tag{66}$$

Estimate (66) holds for distances not exceeding the free path of ions in collisions with dust particles or neutrals, and correspondingly the range of applicability of formula (66) is narrow enough.

Different additional mechanisms governing attraction and repulsion between the dust particles can exist as a consequence of the openness of dusty plasma systems, the openness caused by continuous exchange of energy and matter between the particles and surrounding plasmas. Shortly after the first experimental discovery of dusty plasma crystallization, the possibility of the attraction between the two particles of like charge signs was pointed out [144]. In this work, the attraction was attributed to a decrease in particle charges when the distance between them is decreasing. Later on, it was shown that this result is incorrect due to the incompleteness of the energy analysis, and it was also indicated that the formation of dusty plasma crystals does not necessarily mean the existence of attraction between the dust particles, because in most of the experiments the particles are confined by external forces [145]. Nevertheless, the work [144] stimulated the investigation of supplementary (to electrostatic) mechanisms of interparticle interaction. Some of them are considered below.

The continuous flow of plasma electrons and ions on the surface of a dust particle leads to a drag experienced by neighboring particles. This can result in an effective attractive force between the particles, which is called the ion shadowing force. The magnitude of this force is mainly determined by the ion component due to larger ion masses. Such an attractive mechanism was first considered by Ignatov [146] and Tsytovich and co-workers [3, 147], and later on in works [87, 98]. Note that the ion shadowing force basically represents the ion drag force in the ion flow directed to the surface of a test particle. Strictly speaking, the ion shadowing force is not pairwise, since the interaction between several particles (more than two) depends on their mutual arrangement.

Additional attraction or repulsion mechanisms can be associated not only with the ion component but also with neutrals, if, once scattered from the particle surface, they leave the surface with an energy spectrum different from that determined by the temperature of neutrals. This can happen if the particle surface temperature T_s is different from the neutral gas temperature T_n and full or partial accommodation takes place. The temperature of the particle surface is governed by the balance of various processes, such as radiative cooling, exchange of energy with neutrals, and recombination of electrons and ions on the surface [148]. In the case $T_s \neq T_n$, there exist net fluxes of energy and momentum between gas and particles. Hence, if two particles are located sufficiently close to each other, an anisotropy in momentum fluxes on the particles will also exert a shadowing force between them, which in this case is associated with the neutral component. This effect was first considered by Tsytovich et al. [149].

For both neutral and ion shadowing effects, the corresponding potentials U_{ns} and U_{is} scale similarly with distance, namely, $U_{ns}(r) \sim U_{is}(r) \propto 1/r$. Hence, at large distances the shadowing interaction will overcome the long-range electrostatic repulsion (66). The existence of attraction makes the formation of dust molecules (an association of two or more particles coupled by long-range attraction) possible. The theoretical examination of the conditions of molecular formation can be found in Refs [3, 87]. For conditions of an isotropic plasma, however, the formation of dust molecules has not yet been experimentally established. This can be first of all connected to the fact that rather large particles are needed for the substantial shadowing effect. In ground-based experiments, such particles can levitate only in the sheath regions of discharges, where the electric field is strong enough to balance for gravity. In these regions, the effects of plasma anisotropy are of primary importance. The ions moving

towards the cathode with superthermal velocities contribute here practically nothing to screening. In addition, as discussed in Section 2.2, the focusing of ions occurs downstream from the particle — the so-called wake is formed. This leads to differences in the interaction in the planes parallel and perpendicular to the ion flow. Along the flow, the electrostatic potential has a damped periodic structure in which attraction between particles is possible.

2.4.1 Experimental determination of the interaction potential.
Determination of the interaction potential constitutes a delicate experimental problem. Only a few such experiments have been performed [150–153]. An elegant method based on an analysis of elastic collisions between the two particles was proposed by Konopka et al. [150, 151]. In another method, laser radiation is used to manipulate particles [152, 153]. Let us describe these methods separately.

In the collision method [151], particles of radius $a \approx 4.5\ \mu m$ and an argon plasma at pressure $p = 2.7$ Pa were utilized. The particles are introduced into an rf discharge through a small hole in the glass window built into the upper electrode and are levitated above the lower electrode, where the electric field compensates for gravitational force. To confine the particles horizontally, a ring is placed on the lower electrode, which introduces a horizontal parabolic confining potential. The manipulation of the particles and activation of elastic collisions between them is performed with the use of a horizontal electric probe introduced into the discharge chamber. During the collision, the particle trajectories are determined by the confining potential and the interparticle interaction potential which is a function of interparticle spacing. An analysis of recorded trajectories of the dust particles during collisions yields the coordinates and velocities of both the particles during collision. Then, the form of the interaction potential can be reconstructed from the equation of motion. Application of this method [151, 154] showed that for low discharge powers and pressures the interaction potential coincided with the screened Coulomb potential (39) within experimental uncertainties. This is illustrated in Fig. 5. The role of other interaction mechanisms is insignificant for the given plasma conditions, which, however, does not exclude the possibility of their existence [87]. The measurements also allow the determination of the particle effective charge and plasma screening length because these two parameters determine the form of the Coulomb screened potential. A detailed discussion of these experiments, assumptions made in their theoretical interpretation, and some proposals for using this technique in experimental investigations can be found in Ref. [41].

A method based on laser manipulation of the dust particles was employed to study interaction between the particles in the direction of the ion flow [152]. Its modification for two particles was described in the work [153], which is discussed in some detail below. The essence of the experiment was the following. Two particles of different masses are used: the first one having a radius $a \approx 1.7\ \mu m$, and the second one being a cluster of two such particles sticking together. The particles are introduced into a plasma of an rf discharge in helium at a pressure of $p \sim 50-200$ Pa. Because of the different charge-to-mass ratios, the particles are levitated at different vertical equilibrium positions in the anisotropic sheath region above the lower electrode — more massive particles levitate closer to the electrode. Due to an inhomogeneous electric field, the force balance (determined by the
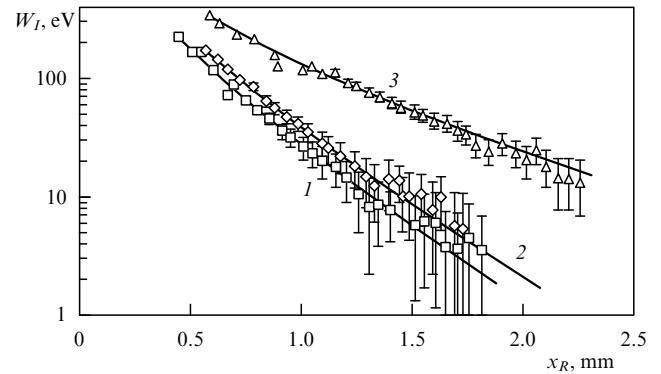
Figure 5. Potential energy W_I of interaction between two particles versus the distance x_R between them [151]. Measurements were taken at $p = 2.7$ Pa and different rf peak-to-peak voltages U_p. Symbols correspond to experimental results, solid lines show their fit to a screened Coulomb potential $U(r) = Q_{eff}^2 \exp(-r/\lambda)/r$ leading to the following effective particle charge Q_{eff} and a screening length λ (T_e is the measured electron temperature): $1 - |Q_{eff}| = 13900e$, $\lambda = 0.34$ mm, $T_e = 2.0$ eV, $U_p = 233$ V; $2 - |Q_{eff}| = 16500e$, $\lambda = 0.40$ mm, $T_e = 2.2$ eV, $U_p = 145$ V, and $3 - |Q_{eff}| = 16800e$, $\lambda = 0.90$ mm, $T_e = 2.8$ eV, $U_p = 64$ V. Note that the screening length determined from the experiment is closer to the Debye radius for electrons than for ions. This is in qualitative agreement with the conception that the ion velocity is close to the ion sound velocity $c_i = \sqrt{T_e/m_i}$ in the (collisionless) sheath and ions do not contribute to the particle charge screening. (The figure is kindly provided by U Konopka.)

electrostatic and gravity forces) fixes their vertical positions. Both particles, meanwhile, are free to move in the horizontal plane. The first observation was the following. For sufficiently low pressures, the particles tend to form a bound state, in which the lower particle is vertically aligned to the upper one. Note that similar structures (vertically aligned chains) are quite common for many experimental investigations of multilayer dust crystal formation in gravity conditions. With increasing pressure, the bound state can be destroyed, and the particle separation in the horizontal plane is limited only by a very weak horizontal confinement due to a specially concave electrode. The existence of these states indicates some mechanisms of attraction and repulsion between the particles, which change each other in response to changes in plasma parameters. It is also found that the effect exhibits hysteresis (dependent on the pressure).

Next, to prove that the aligned bound state is due to attraction between the particles rather than its being forced by an external confinement, the particles were manipulated by laser radiation. The laser beam is focused either on the upper or the lower particle, causing its motion. It was found that when the upper particle is pushed by the laser beam, then the lower particle follows its motion and the bound state is not destroyed. This behavior proves that the lower particle is subject to an attractive horizontal force mediated by the upper particle. If the lower particle is pushed by the laser beam, then the upper particle's response is much weaker and the bound state can be easily destroyed. Hence, the interaction between the particles is asymmetric. It is clear that the attraction between the particles situated along the ion flow can be attributed to the wake effect. However, the question of whether it has an electrostatic nature or is associated with momentum transfer from the ions scattered by the upper particle [101] still needs to be investigated.

2.5. Formation and growth of dust particles

In the laboratory conditions, the dust particles are usually introduced into a plasma deliberately. On the other hand, they may, in principle, be self-formed in plasmas. There are several possible sources of the dust particles. First is condensation leading to the appearance of solid particles or droplets. This process is typical for expanding plasmas, e.g., adiabatic plasma expansion in a vacuum or expansion of plasma in the channel of an MHD generator [28, 29]. In chemically reacting mixtures, the dust particles may appear due to chemical reactions [155]. Finally, erosion of electrodes and walls of a discharge chamber also leads to the appearance of macroparticles [36]. In plasmas, the particles may grow. One of the reasons is the surface recombination of ions, which leads to a permanent sedimentation of the material on the particle surface. The agglomeration of dust particles may also become valid.

In the work [155], one of the possible scenario of particle's formation and growth was considered. It includes four stages: first, primary clusters are formed; once they have grown to a critical size, heterogeneous condensation occurs; at the next stage, the processes of coagulation and agglomeration are dominant, and at the last stage, the condensation of monomers on the isolated multiply charged particles turns to be most important.

On the whole, the processes of dust particle formation and growth in plasmas are not fully understood and require further investigation. The importance of this problem is largely connected to the needs of plasma technologies in, for example, the production of nanoparticles and thin films, and material processing.

3. Strongly coupled dusty plasmas and phase transitions

3.1 Theoretical approaches

3.1.1 Strong coupling of dusty plasmas. The conditions which can be realized in dusty plasmas are quite diverse and depend on relations among their characteristic parameters. One of the fundamental characteristics of a many-particle interacting system is the coupling parameter Γ defined as the ratio of the potential energy of interaction between neighboring particles to their kinetic energy. For the Coulomb interaction between charged particles one finds

$$\Gamma = \frac{Z^2 e^2}{T \Delta} \, , \tag{67}$$

where $\Delta = n^{-1/3}$ characterizes the average interparticle spacing, and T characterizes their kinetic energy. For the plasma electrons and ions one obtains

$$\Gamma_{e(i)} = \frac{e^2 n_{e(i)}^{1/3}}{T_{e(i)}} \tag{68}$$

(ions are assumed to be singly charged). The system is commonly called strongly coupled when $\Gamma \gtrsim 1$. It is well known that charges in plasmas are screened. Hence, in dusty plasmas, in addition to the average interparticle spacings, the Debye screening radii of each species and the dust particle radii appear as characteristic scales of length. In conditions typical of dusty plasma experiments, the number of electrons (ions) $N_{e(i)}^D$ in the electron (ion) Debye sphere is large:

$N_{e(i)}^D = n_{e(i)} \lambda_{De(i)}^3 \gg 1$, and hence electron and ion species are ideal, because $\Gamma_{e(i)} \sim (N_{e(i)}^D)^{-2/3} \ll 1$.

The situation with the dust component is qualitatively different. As before, for $N_d^D \gg 1$, the dust subsystem is ideal; in this case, the dust appears as an additional plasma component which introduces new spatial and temporal scales in the system. The dust particles contribute to screening, the effective screening length now being

$$\lambda_D^{-2} = \lambda_{De}^{-2} + \lambda_{Di}^{-2} + \lambda_{Dd}^{-2}$$

(the particles charges are fixed here). In the opposite case of $N_d^D \ll 1$, the dust subsystem is not always strongly coupled, because the screening can be determined only by electrons and ions. The interparticle distance can be shorter than the dust Debye radius, but the particles are not necessarily strongly interacting, being screened by the electron–ion background.

Most theories developed thus far to describe the properties of dusty plasmas employ the following model: negatively charged particles are confined within the plasma volume due to some confining force (usually of electrostatic character) and interact between themselves via the isotropic screened Coulomb (Debye–Hückel or Yukawa) repulsive potential

$$U(r) = \frac{Z_d^2 e^2}{r} \exp\left(-\frac{r}{\lambda_D}\right), \tag{69}$$

where the screening is governed by plasma electrons and ions. This model gives a simplified picture of dusty plasma behavior and is unsuited to some experiments, especially when plasma anisotropy plays a considerable role. Moreover, this model does not take into account variations of particle charges, long-range interactions, the exact form of the confining potential, etc. However, it has proved useful in providing qualitative results which are supported by experiments, and hence it may be considered as the base on which one can construct more realistic models intended to represent actual dusty plasmas under various conditions.

3.1.2 Phase diagram of Debye–Hückel systems. Besides complex plasmas, particles interacting with a Debye–Hückel potential have been extensively studied in different physical systems ranging from elementary particles to colloidal suspensions. Not surprisingly, their phase diagrams have received considerable attention. Various numerical methods [usually Monte Carlo (MC) or molecular dynamics (MD) simulations] have been employed [156–159].

In the case considered, the static properties of the system are completely determined by two independent dimensionless parameters. The first one measures the effective system temperature and is defined as $\tilde{T} = T/m_d \omega_E^2 \Delta^2$, where ω_E is the Einstein frequency of the crystalline structure oscillations. Since ω_E depends on crystal structure, the fcc Einstein frequency is commonly used for definiteness. The other is the so-called structure (lattice) parameter

$$\varkappa = \frac{\Delta}{\lambda_D} \, . \tag{70}$$

This choice of parameters comes historically from the theories of colloidal solutions. On the other hand, the ordering parameter commonly used for complex plasmas is the Coulomb coupling parameter in the form (67), namely

$\Gamma_d = Z_d^2 e^2 / \Delta T_d$. This is because early investigations of plasma crystallization focused on one-component plasmas (OCP), which can be considered as a limiting case for $\lambda_D \to \infty$ or $\varkappa \to 0$ of the Debye–Hückel model [38, 160–162]. The reduced temperature and the Coulomb coupling parameter are related by the formula

$$\tilde{T} = \frac{\omega_{pd}^2}{4\pi\Gamma_d\omega_E^2} \, ,$$

where $\omega_{pd} = (4\pi Z_d^2 e^2 n_d / m_d)^{1/2}$ is the dust plasma frequency. The ratio ω_E / ω_{pd} is a known function of $\varkappa$ [157, 163]. In Fig. 6a, the phase diagram of the Debye–Hückel system, summarizing available numerical results, is drawn in the $(\varkappa, \Gamma_d)$-plane. Three phases were found, depending on the values of coupling and structure parameters. For very strong coupling, $\Gamma_d > \Gamma_M$, where Γ_M denotes the value of Γ_d in the melting curve, there are solid fcc and bcc phases and a liquid phase for $\Gamma_d < \Gamma_M$. The bcc phase is stable at small $\varkappa$, while fcc is stable at larger $\varkappa$. The 'triple point' is at $\varkappa \approx 6.90$ and $\Gamma_d \approx 3.47 \times 10^3$ [159].

Of particular interest for plasma crystallization experiments is the form of the melting (crystallization) curve $\Gamma_M = \Gamma_M(\varkappa)$ [12, 157–159, 163, 164, 167]. Results with OCP systems ($\varkappa = 0$) indicate that the crystallization proceeds at $\Gamma_d = \Gamma_{OCP} \approx 106$ (or ≈ 172 if the Wigner–Seitz radius $(4\pi n_d / 3)^{-1/3}$ is used as the length unit instead of Δ) [160, 168, 169]. The corresponding reduced temperature is $\tilde{T}_M \approx 0.0022$. Several assumptions have been made in the literature concerning the analytical dependence of Γ_M on $\varkappa$. Starting from the OCP limit, Ikezi [12] assumed that one simply has to take screening into account through $U(\Delta)/T = \Gamma_{OCP}$, so that according to formula (69) one arrives at

$$\Gamma_M = \Gamma_{OCP} \exp{(\varkappa)}. \tag{71}$$

Another simple argument is the following. The dimensionless temperature is proportional to the mean square of the particle oscillation amplitude in the quasi-harmonic approximation and, according to the Lindemann criterion, should be approximately constant along the melting curve. As the numerical values of the Einstein frequencies for the bcc and fcc lattices differ by less than 1% in the region where the bcc lattice is stable, one may assume that

$$\tilde{T}_M \approx \tilde{T}_{OCP}. \tag{72}$$

To reach a better agreement with the calculated results, the authors of Ref. [158] used a linear fit to their numerical data instead of relationship (72). They resorted to the expression

$$\tilde{T}_M \approx \tilde{T}_{OCP}(1 + 0.1\varkappa). \tag{73}$$

Finally, in Ref. [167] it was proposed that the characteristic dust lattice wave (DLW) frequency (see Section 4) be used instead of ω_E in the determination of $\tilde{T}$. Using the Lindemann criterion with this normalization, the dependence of Γ_M on $\varkappa$ becomes

$$\Gamma_M = \Gamma_{OCP} \frac{\exp{(\varkappa)}}{1 + \varkappa + \varkappa^2/2} \, . \tag{74}$$

The arguments used in deriving expressions (71)–(74) are not sufficiently rigorous. They can, therefore, be considered only as phenomenological melting conditions.
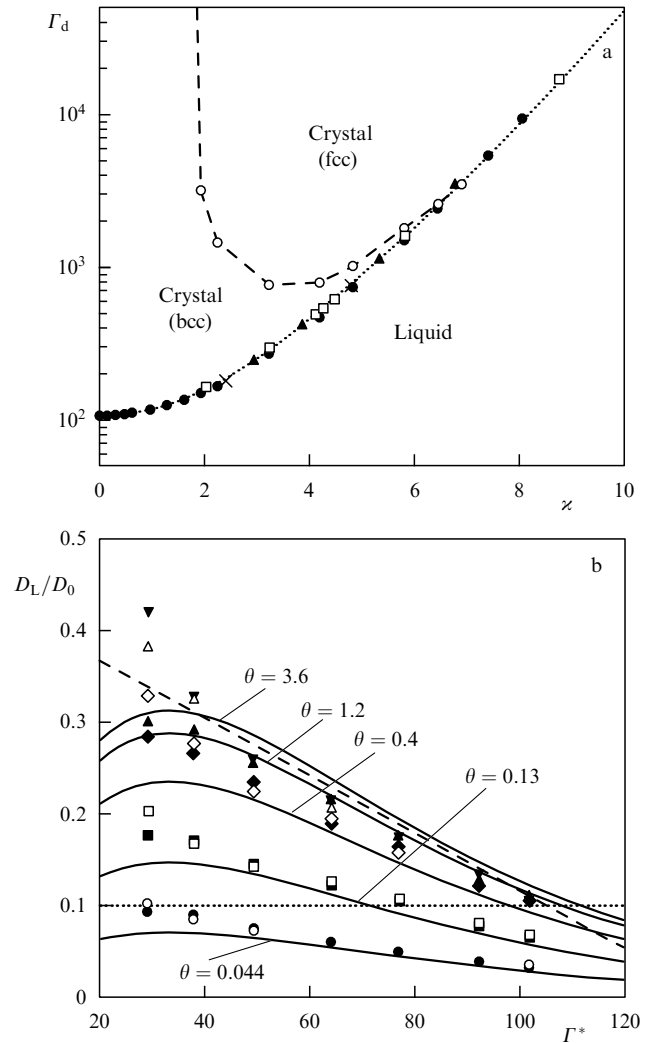
Figure 6. (a) Phase diagram of Debye–Hückel systems, obtained from numerical modeling. Open circles correspond to the bcc–fcc phase boundary [159]. The fluid–solid phase boundary is marked by triangles [164], squares [158], and solid circles [159]. The crosses correspond to jumps in the diffusion constant, observed in the simulations of dissipative Debye–Hückel systems [165, 166]. The dashed line is the fit to the numerical data judged by eye. (b) The ratio D_L/D_0 for strongly interacting Debye–Hückel systems as a function of the effective coupling parameter Γ_d^*. The results of numerical simulations [165, 166] for different values of the dynamic parameter θ are shown. Solid symbols correspond to $\varkappa = 2.42$, and open symbols correspond to $\varkappa = 4.84$. The values of θ are 0.044 (circles), 0.13 (squares), 0.4 (diamonds), 1.2 (triangles), and 3.6 (inverted triangles) [only for $\varkappa = 2.42$]. The dashed line corresponds to the approximation applicable for $\theta \gg \theta_{cr}$. The solid lines represent analytical expression (78) for different values of the dynamic parameter (indicated in the figure). The horizontal dotted straight line corresponds to $D_L/D_0 = 0.1$.

Note that although all the expressions (71)–(74) give the same (correct) result at $\varkappa = 0$, they demonstrate different dependences of Γ_M on $\varkappa$. As shown in Ref. [166], expression (71), widely used in the literature, is in poor agreement with simulation results. Expression (72) provides somewhat better agreement. Expressions (73) and (74) yield the best agreement. Good agreement of formula (73) with the results of numerical simulations is not surprising — it is reached by using a linear fit to the numerical results. On the other hand, the functional form of Eqn (74) is simple and ensures better agreement with numerical experiments in the regime mostly

relevant to complex plasmas experiments, namely $\varkappa < 5$. Thus, it is convenient to introduce a *modified coupling parameter*

$$\Gamma^* = \Gamma_{\mathrm{d}} \left(1 + \varkappa + \frac{\varkappa^2}{2} \right) \exp\left(-\varkappa \right) , \qquad (75)$$

of which the value $\Gamma_{\mathrm{M}}^* \approx 106$ uniquely determines the location of the melting (crystallization) curve in the phase diagram.

3.1.3 Crystallization criteria.
From a practical point of view, a simple criterion is often required, which allows us to judge whether the system under consideration is in a crystalline or liquid state. Different phenomenological criteria for the crystallization (melting) of systems of interacting particles exist, which are often independent of the exact form of interaction potential between the particles. Some of them are convenient for dusty plasmas. Best known is the Lindemann criterion [170], according to which melting of the crystalline structure occurs when the ratio of the root-mean-square particle displacement to the mean interparticle distance reaches a value of ~ 0.15. Notice that this value can somewhat vary for various physical systems, mainly due to different procedures used to determine the average interparticle spacing. Another criterion is the value of the first maximum of the structural factor in the liquid state [171], which reaches a value of ~ 2.85 in the crystallization curve. There also exists a simple crystallization criterion expressed in terms of the pair correlation function, the ratio of the minimum to the maximum of which should be approximately equal to 0.2 under crystallization. A simple dynamic crystallization criterion, similar in spirit to the Lindemann criterion, was proposed by Löwen et al. [172]. According to this criterion, crystallization occurs when the diffusion constant reduces to a value of ~ 0.1 compared to the diffusion constant for noninteracting particles. Later on, it was noted that this criterion holds for both 2D and 3D systems [173].

3.1.4 Dynamics of Debye – Hückel systems.
The motion of dust particles in a dusty plasma with not too low a pressure can be considered as Brownian motion — modified, however, by interaction between the particles themselves. The question to be answered is, therefore, to what extent this interaction affects the particle dynamics. The dynamical properties of the dust component are fully determined by three dimensionless parameters, as can be clearly seen by normalizing the equations of motion of particles to a dimensionless form [165]. These are the parameters Γ_{d} and $\varkappa$, introduced in Section 3.1.2, while the third one is an appropriate measure of system dissipativity. Following the work [166] let us define this parameter in the form

$$\theta = \frac{\nu_{\mathrm{dn}}}{\omega_{\mathrm{d}}} \qquad (76)$$

and call it the *dynamic parameter*. Here, ν_{dn} stands for the damping rate associated with particle – neutral collisions (the neutral component typically determines dissipation because the degree of plasma ionization is very low in experiments, $\alpha \sim 10^{-6} - 10^{-7}$), and ω_{d} is some characteristic frequency associated with the charged dust component. In principle, the dust-plasma frequency or the Einstein frequency may be used for normalization. However, as will be clear from the following, it is most convenient to use for this purpose the dust lattice wave frequency.

One of the most fundamental quantities characterizing the dynamic behavior of the system is the single-particle diffusion coefficient. For 3D diffusion it is determined as

$$D(t) = \frac{\left\langle \left[\mathbf{r}(t) - \mathbf{r}(0) \right]^2 \right\rangle}{6t} , \qquad (77)$$

where $\mathbf{r}(t)$ is the particle trajectory, and $\langle \ldots \rangle$ denotes ensemble averaging. The diffusion constant is then $D_L = \lim_{t \to \infty} D(t)$. The limit $t \to \infty$ is understood in the sense that the time t is longer than any other microscopic time in the system ($\nu_{\mathrm{dn}}^{-1}, \omega_{\mathrm{d}}^{-1}$), but shorter than the characteristic diffusion time to a distance on the order of the system size or timescale for significant changes of dusty plasma parameters in the experiment. Due to the interaction between the particles, the value of D_L is smaller than the bare Brownian diffusion constant for noninteracting particles: $D_0 = T_{\mathrm{d}} / m_{\mathrm{d}} \nu_{\mathrm{dn}}$, where T_{d} is the temperature characterizing the chaotic (thermal) velocities $\nu_{T\mathrm{d}} = \sqrt{T_{\mathrm{d}} / m_{\mathrm{d}}}$ of the dust particles. In the limiting case of a crystalline structure, D_L tends to zero, as the displacement of particles located at the lattice sites is limited. Therefore, the ratio D_L / D_0 for dissipative systems appears as a natural quantity reflecting the nature and strength of the interaction potential.

Diffusion in Debye – Hückel systems has been studied using numerical modeling in Refs [157, 163, 165, 166, 172, 174, 175]. The problem of self-diffusion in nondissipative systems ($\theta = 0$) was considered in Refs [157, 163, 174]. In the context of colloidal solutions, in which dissipation is many orders of magnitude higher than in dusty plasmas, the diffusion was considered in Refs [172, 175]. In particular, the problems of subdiffusive behavior of the time-dependent diffusion coefficient (77) [175] and the value of the diffusion constant at the liquid – solid phase boundary [172] were addressed.

A systematic study of diffusion in dissipative Debye – Hückel systems by means of Brownian dynamics simulations for parameters typical of isotropic gas discharge plasmas was performed in Refs [165, 166, 176]. In these works, interaction with the medium is modelled by the Langevin force consisting of two terms: one of which describes systematic friction, while the other is the random force describing the stochastic action of the medium. The friction is usually due to the neutral component, while the random component of the force is either associated with individual collisions with neutral atoms or molecules, or can have another origin: plasma electric field microfluctuations, charge fluctuations, etc. Independently of its nature, the random component can be in the first approximation described as a delta-correlated Gaussian white noise whose amplitude determines the dust temperature T_{d}. The equations of motion incorporating the interaction between the particles and the particle interaction with the medium are solved numerically in 3D with periodic boundary conditions. The diffusion coefficient is determined by appropriate averaging over particle trajectories.

The main results are summarized in Fig. 6b, which shows the behavior of the ratio D_L / D_0 as a function of the modified coupling parameter Γ^*. As the coupling increases, the ratio D_L / D_0 decreases and at some point it experiences an abrupt jump, decreasing by several orders of magnitude in the very narrow range $102 \leqslant \Gamma^* \leqslant 106$. This jump takes place at $\Gamma^* \approx \Gamma_{\mathrm{M}}^*$, thus indicating the first-order phase transition (crystallization). In addition, Fig. 6b demonstrates that the ratio D_L / D_0 is completely determined by the parameters Γ^*

and θ, and it is not separately dependent on $\varkappa$. Moreover, if the dissipation is sufficiently high, $\theta > \theta_{cr}$, then the ratio D_L/D_0 becomes practically independent of θ as well. On the other hand, for $\theta \ll \theta_{cr}$, numerical results tend towards those obtained for nondissipative systems in Ref. [163]. In the intermediate case, the ratio D_L/D_0 depends on θ, as indicated above. The phenomenological expression describing this dependence was proposed in Ref. [176], and it has the form

$$\frac{D_L}{D_0} = \frac{\theta \Gamma^* \exp\left(-3\Gamma^*/\Gamma_M^*\right)}{6(1 + 2\pi\theta)} . \tag{78}$$

This empirical expression demonstrates reasonable agreement with numerical data for $\Gamma^* \gtrsim 30$, as follows from Fig. 6b. Using this expression we can also submit an estimate: $\theta_{cr} \sim 1/2\pi \approx 0.2$. Finally, the dynamic criterion of crystallization, requiring that $D_L/D_0 \approx 0.1$ in the liquid phase near the crystallization curve, turns to be applicable to strongly dissipative systems, but is not confirmed for weakly dissipative systems ($\theta \ll \theta_{cr}$).

The above-described results can, in principle, be used for dusty plasma diagnostics. However, the direct application of the results of 3D modeling of Debye–Hückel systems to the analysis of experiments on dusty plasmas under microgravity conditions and of laboratory experiments with fine powders is largely limited due to a number of reasons (e.g., plasma anisotropy, long-range interactions including shadowing effects, the effect of external forces and/or boundary conditions, particle charge variations, etc.).

3.2 Experimental investigation of phase transitions in dusty plasmas

3.2.1 Dusty plasma crystals in an rf discharge.
Since the discovery of dusty plasma crystals in 1994, the investigation of phase transitions in different types of dusty plasmas has been actively performed in dozens of laboratories. Phase transitions in the dust component are studied in capacitive and inductive discharges, glow dc discharge, thermal plasmas of combustion products of different fuels, as well as nuclear- and photo-induced plasmas. Below in this section we will discuss those experiments in which strong coupling of the dust component, leading to phase transitions to ordered states, is revealed in the most striking way.

Dusty plasma crystals were discovered in a capacitively coupled low-pressure rf discharge in inert gases almost simultaneously in several laboratories [13–16]. The schematic of a typical experimental setup [151] is shown in Fig. 7. The experimental apparatus includes a lower electrode 5–10 cm in diameter capacitively coupled to an rf generator ($f = 13.56$ MHz) and an upper grounded electrode. The electrodes are placed into a vacuum chamber. Micron-sized dust particles fill a container and can be introduced into the discharge through a metallic grid. The electrode separation is typically 3–10 cm. The particle visualization is performed with the use of laser illumination. The laser beam is transformed into a sheet approximately 100 μm thick using a lens and illuminates the particles in the horizontal or vertical plane. The particles introduced into the plasma become (highly) charged negatively and levitate in the sheath above the lower electrode, which, on the average, acts as a cathode over a period of applied rf voltage. To confine the particles horizontally, a metallic ring with an inner diameter of 3–6 cm and a height of 1–3 mm is placed on the lower electrode. Sometimes, instead of a ring, a special curved electrode is
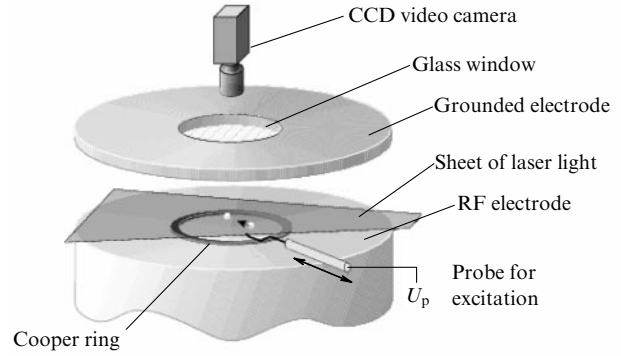
Figure 7. Schematic of experimental setup used to investigate the formation of ordered structures in an rf discharge.

used. The light scattered by the particles is recorded by a video camera.

Dust particles (of not too large a size) usually levitate in the sheath above the lower electrode due to the balance of the main forces, which include electrostatic force (directed upwards for a negatively charged particle), force of gravity (directed downwards), and the ion drag force (also directed downwards — in the direction of the time-averaged electric field). Under certain conditions, the particles form an ordered structure consisting of several fairly extended horizontal layers. The number of particles in such a structure can reach $\sim 10^3 - 10^5$, while the number of layers can vary from one to a few dozen [177]. Figure 1a illustrates an image of the horizontal cross section of the ordered structure (fragment of one layer) consisting of monodispersed polymer ($\rho = 1.5$ g cm^{-3}) particles ~ 6.9 μm in diameter [17]. The structure displayed is highly ordered and exhibits a hexagonal lattice. The particles are usually settled strictly below each other in different horizontal layers, forming a cubic lattice between layers. Such an arrangement can be a consequence of ion focusing downstream from the particles — the wake effect (see Section 2.2).

It is difficult to obtain real three-dimensional structures in ground-based experiments in rf discharges. In these conditions, dusty plasma crystals have substantially a two-dimensional, or more exactly so-called $2\frac{1}{2}$-dimensional, character. This is directly connected to the action of gravity. To support particles against gravity, strong electric fields are required. Such strong fields can be established only in plasma sheaths which are characterized by a high degree of anisotropy and suprathermal (or even supersonic) ion flows. External forces acting on the dust particles are comparable to the interparticle forces. Hence, the dust systems are strongly compressed, inhomogeneous, and anisotropic in the vertical direction. In these conditions, comparison with theoretical results obtained for 3D Debye–Hückel systems is incorrect.

For reference, we summarize typical plasma and particle parameters in these experiments. Particle diameters usually lie in the range from 1 to 30 μm. Neutral (typically inert) gas pressure ranges from 0.01 to 1 Torr. Plasma concentration in the bulk of a discharge is $n_e \sim n_i \sim 10^8 - 10^{10}$ cm^{-3}, the electron temperature is $T_e \sim 1 - 5$ eV, and ions are typically assumed to be in equilibrium with neutrals (usually at room temperature), so that $T_i \sim T_n \sim 0.03$ eV. Let us also emphasize some properties of sheaths where the particles levitate. The sheath is a region of a positive space charge, so

that the ion concentration exceeds that of electrons even in the absence of dust. The ion velocity at the edge of the collisionless sheath satisfies the Bohm criterion $u \geqslant c_i = \sqrt{T_e/m_i}$, where c_i is the ion-sound wave velocity. For the collisional sheath, the ion directed velocity can be lower than the velocity of sound, but the ions are still typically suprathermal: $u \gg v_{Ti}$. The characteristic spatial scale of the particle charge screening in this case is given by the electron Debye radius λ_{De}, because fast ions do not contribute considerably to screening. Finally, it should be recalled that the potential of interaction between the particles is highly anisotropic. In the direction perpendicular to the ion flow, the interparticle interaction is determined as before by a screened Coulomb potential (with a screening length close to λ_{De}), while in the direction parallel to the flow the effects caused by ion focusing downstream from the particles become important (see Section 2.4).

Structural properties of strongly coupled dusty plasmas were investigated in Refs [13–16, 177–179]. Crystalline structures such as bcc, fcc, and hcp, as well as their coexistence, were found for certain plasma and particle parameters.

For the quantitative analysis of the ordered structures of particles observed in the experiment, it is common to use the following three characteristics [178]: the pair correlation function $g(r)$, the bound-orientational correlation function $g_6(r)$, and the structure factor $S(k)$. The pair correlation function $g(r)$ represents the probability of finding two particles separated by a distance r. For the case of an ideal crystal, $g(r)$ is a series of δ-functions (peaks) whose positions and heights depend on crystal structure type (for the gas state $g(r) \equiv 1$). The pair correlation function measures the translational order in the structure of interacting particles. The bound-orientational correlation function for two-dimensional systems is defined in terms of the nearest-neighbor bond angles with respect to an arbitrary axis. For a perfect hexagonal structure $g_6(r) \equiv 1$, while for other phases $g_6(r)$ decays with distance. The bond-orientational correlation function measures orientational order in the structure. Finally, the static structure factor measures order in the structure, similar to $g(r)$. It is defined as

$$S(k) = \frac{1}{N} \left\langle \sum_{i,j} \exp\left[i\mathbf{k}(\mathbf{r}_i - \mathbf{r}_j)\right] \right\rangle,$$

where $\mathbf{r}_i$ and $\mathbf{r}_j$ are the positions of particles i and j, and $\langle \ldots \rangle$ denotes ensemble averaging. Note that the structure factor is connected to the pair correlation function via the Fourier transform (see, e.g., Ref. [160]):

$$S(k) = 1 + n_d \int d\mathbf{r} \left[g(r) - 1\right] \exp\left(-i\mathbf{k}\mathbf{r}\right).$$

These characteristics are applied for the analysis of static properties of the highly ordered dust particle structure in Ref. [178]. In the same work, a comparison between the obtained quantitative results and predictions of the 2D melting theory developed by Kosterlitz, Thouless, Halperin, Nelson, and Young (KTHNY theory) is drawn.

As already noted in the Introduction, dusty plasmas possess a number of unique properties which make these systems extremely attractive for investigation of different collective processes, including phase transitions. In particular, relatively short temporal scales for relaxation and response to external perturbations, as well as simplicity in observation, allow us not only to study static structure characteristics, but also to investigate the dynamics of phase transitions in detail [154, 180–182]. Usually, phase transitions from crystal-like to liquid-like or gas-like states are experimentally investigated. Melting of a crystalline lattice can be initiated either by a decrease in the neutral gas pressure or by an increase in the discharge power. This can be attributed to the fact that the plasma parameters change under these conditions in such a way that the coupling in the system decreases. The decrease in coupling is first of all connected, at least in experiments with the lowering of the neutral pressure, with a significant increase in the kinetic energy of the dust particles. For example, the initial temperature which was close to the neutral gas temperature ($T_d \sim T_n \sim 0.03$ eV) in highly ordered crystal-like structures increased with the lowering of pressure and structure melting up to ~ 5 eV [180] or even ~ 50 eV [181] at minimal pressures examined in these works. This 'anomalous heating' of the dust component in plasmas indicates some source of energy which is effectively transferred into the kinetic energy of the dust particles. Dissipation of the kinetic energy in turn is determined by collisions with neutrals. With a decrease in pressure the dissipation goes down, which leads to the 'heating' of the particles. Several possible mechanisms of anomalous heating were considered in the literature: stochastic fluctuation of the particle charge and energy gain in an external electric field [17, 72, 74–76]; heating due to ion focusing and its attendant anisotropy in the interaction of particles from different lattice planes [183]; spatial particle charge variations caused by plasma nonuniformity [184], and current-driven instability of liquid-like dusty plasma due to ion drift [185]. However, the exact origin of the heating has still not been established. Hence, further detailed experimental investigation and comparison of the results with different theoretical models are required.

Let us discuss in more details the process of dusty plasma crystal melting induced by reducing pressure. We focus mainly on the results of a classical experiment [180] in which the melting of a 'flat' plasma crystal (with a thickness of only a few lattice planes) formed by monodispersed melamine–formaldehyde particles 6.9 μm in diameter was investigated. The melting in this experiment was initiated by the continuous lowering of pressure in krypton plasma from $p = 42$ Pa, at which the stable ordered state of dust particles with thermal energy $T_d \sim T_n$ existed, to $p = 22$ Pa, for which the system lost any order and formed a 'gaseous' state. The pair correlation function, bond-orientational correlation function, and kinetic energy of the dust system were measured while lowering the pressure.

From these analyses, the four 'states' during the melting transition were identified. The first, the 'crystalline' state, is characterized by the conservation of the crystalline lattice in the horizontal plane and chain formation in the vertical direction as the pressure weakly reduced from the initial value. The particles in the lattice experience thermal oscillations ($T_d \sim T_n$) and highly occasional large-amplitude nonthermal oscillations — mostly in the vicinity of lattice defects. The second, the 'flow and floe' state, is characterized by the coexistence of islands of ordered crystalline structure (floes) and systematic directed particle motion (flows). In this state, the translational and orientational orders decrease significantly and occasional vertical particle migrations to other lattice planes are possible. Particle thermal motion still
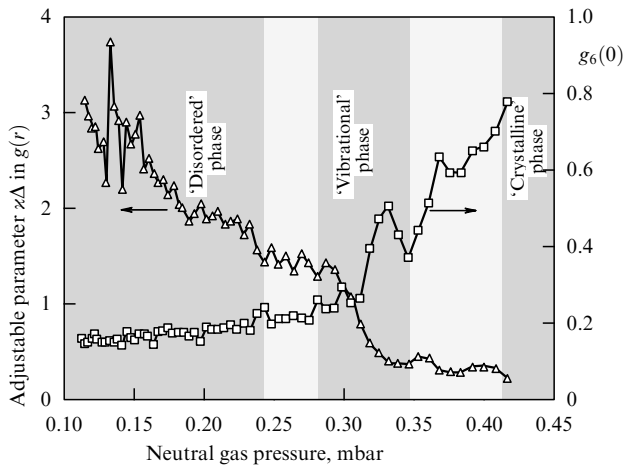
Figure 8. The evolution of translational ($\triangle$) and orientational ($\square$) order parameters during the phase transition as a function of neutral gas pressure [180]. Three regions are shaded: the 'crystalline' phase at ~ 0.42 mbar; the 'vibrational' phase at ~ 0.32 mbar, and the 'disordered' phase at ~ 0.24 mbar. The intermediate 'flow and floe' state (right light-colored region) occurs at ~ 0.36 mbar.
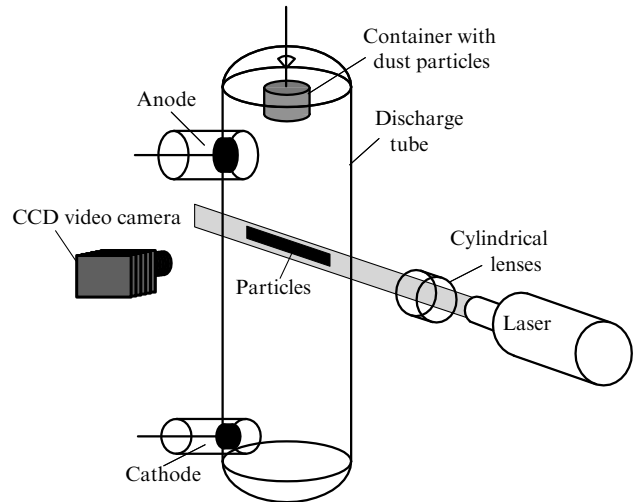

Figure 9. Schematic of the experimental setup for studying the formation of ordered structures in a dc gas discharge.

corresponds to room temperature, $v_{Td} \sim 0.2$ mm s^{-1}, while directed flow velocities are typically half of this. The third, the 'vibrational' state, is characterized by some increase in orientational order and diminishing flow regions. However, isotropic particle vibrations with increasing amplitudes appear. Kinetic energy and vertical migrations of particles increase and the translational order continues to decrease. Finally, in the fourth, the 'disordered' state, there is not any translational or orientational order. The particles migrate freely both in the horizontal and vertical planes. The particle kinetic energies are hundreds of times greater than the neutral temperature ($T_d \sim 4.4$ eV).

Figure 8 shows the quantitative results for correlation functions $g(r)$ and $g_6(r)$ during melting. Three regions are shaded: 'crystalline', 'disordered' and 'vibrational'. In the last region, the correlation function $g_6(0)$ characterizing orientational order has a local maximum. The left light-colored region, which corresponds to the monotone decrease in translational order, separates the 'disordered' state from the region of local increase in the orientational order in the 'vibrational' state.

In concluding, we note once again that, strictly speaking, theoretical concepts of 2D and 3D melting are not applicable to describing these experiments because the systems are essentially $2\frac{1}{2}$-dimensional. From this point of view, the experimental investigation of a monolayer crystal melting, as well as experiments on phase transitions in 3D systems under microgravity conditions, might be valuable.

3.2.2 Ordered structures of dust particles in a dc discharge. A dc gas discharge can also be used for the formation of ordered structures in dusty plasmas [22, 67, 81, 186]. The sketch of the typical experimental setup is given in Fig. 9. A discharge is typically created in a vertically positioned cylindrical tube. The particles introduced into the plasma can levitate in the regions where the external forces are balanced. They are illuminated by a laser light and their positions are registered by a video camera. Typical conditions in the discharge are the following: a pressure in the range $0.1-5$ Torr, and a discharge current of $\sim 0.1-10$ mA.

The ordered structures are usually observed in standing striations of the positive column of the glow discharge but can also be observed in an electric double layer formed in the transition region from the narrow cathode part of the positive column to the wide anode part, or in specially organized multielectrode system having three or more electrodes at different potentials, etc. — that is, in the regions where the electric field can be strong enough to levitate the particles. For these regions, some properties considered in Section 3.2.1 in the context of an rf discharge (e.g., plasma anisotropy, ion drift) are also relevant.

Most of the experiments were performed in standing striations of glow discharges. In the positive column of a low-pressure discharge, loss of electron energy in elastic collisions is small and the electron distribution function is formed under the action of the electric field and inelastic collisions. This can lead to the appearance of striations — that is, regions of spatial periodicity of the plasma parameters with the characteristic scale of an order of a few centimeters [187 – 189]. The electron concentration, their energy distribution, and the electric field are highly nonuniform along the striation length. The electric field is relatively strong (around $10-15$ V cm^{-1} at a maximum) at the head of striation — that is, a region occupying $25-30\%$ of the total striation length, and relatively weak (around 1 V cm^{-1}) outside this region. The maximum value of the electron concentration is shifted relative to the maximum strength of the electric field in the direction of the anode. The electron energy distribution is substantially bimodal, with the head of the striation being dominated by the second maximum whose center lies near the excitation energy of neutral gas atoms. Due to the high floating potential of the walls of the discharge tube, the striations exhibit a substantially two-dimensional character: the center – wall potential difference at the head of the striation reaches $20-30$ V. Thus, an electrostatic trap is formed at the head of each striation, which in the case of vertical orientation is capable of confining particles with high enough charge and low enough mass from falling into the cathode positioned lower, while the strong radial field prevents particle sedimentation on the tube walls.

The process of structure formation proceeds routinely as follows: after being injected into the plasma of the positive
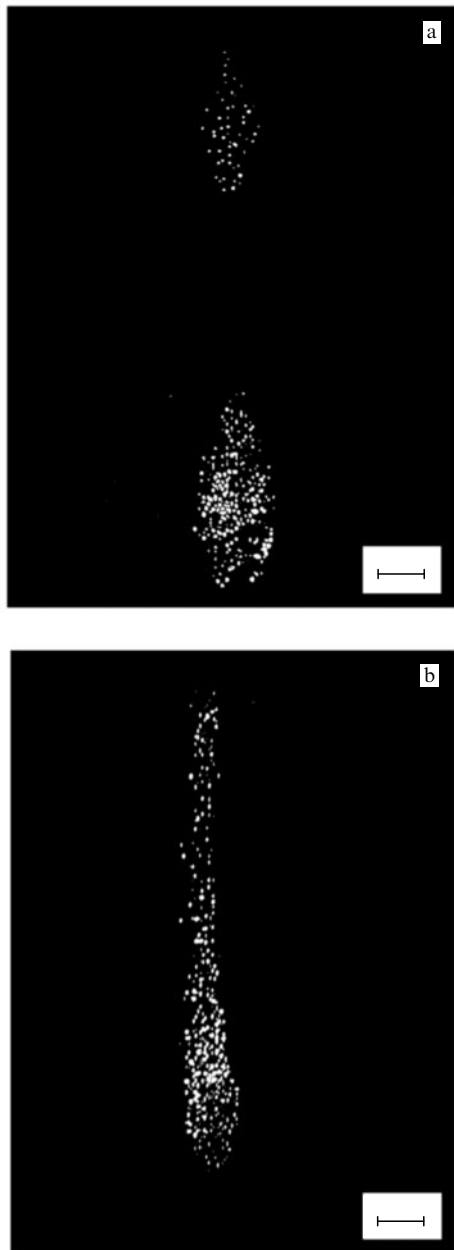
Figure 10. Video images of structures comprising charged microspheres of borosilicate glass: (a) in two neighboring striations (pressure around 0.5 Torr, discharge current of 0.5 mA); (b) after their coalescence (pressure around 0.4 Torr, discharge current of 0.4 mA). The scale of length in the figure corresponds to 3 mm.

column, the charged particles fall past their equilibrium position and then, over the course of several seconds, emerge and form a regular structure which is preserved sufficiently long (until the end of observation) provided that the discharge parameters are unchanged. The simultaneous existence of ordered structures in several neighboring striations can be observed. Figure 10a demonstrates an image of two dust structures formed by hollow thin-walled microspheres made of borosilicate glass with a diameter of $50 – 63$ µm in two neighboring striations. Figure 10b shows their coalescence into one rather extended formation, occurring due to varying the discharge parameters [67]. This figure indicates the possibility of forming structures much more extended in the vertical direction than in rf discharges. In fact, the three-

dimensional quasi-crystalline dusty structures were obtained in the work [67] for the first time.

In dc discharges, the transition of quasi-crystalline structures to fluid and gaseous states is also observed, similar to dusty plasma in rf discharges. This occurs either by lowering the pressure or increasing the discharge current. For example, for the structure comprising Al_2O_3 particles of diameter $3 – 5$ µm at a pressure of 0.3 Torr and a current of 0.4 mA (estimated electron number density $n_e = 10^8$ cm^{-3}, and temperature $T_e \sim 4$ eV), the correlation function reveals long-range order with four well-pronounced peaks (see Ref. [67]). When the discharge current is increased by almost one order of magnitude to 3.9 mA ($n_e = 8 \times 10^8$ cm^{-3}), the structure 'melts' and the correlation function reveals only short-range order. We note that during this 'phase transition' the interparticle distance, equal to 250 µm, remains approximately constant.

Similar to dusty crystals in rf discharge plasmas, the effect of 'anomalous heating' of particles was observed in dc plasmas. Under certain conditions, the particles acquired very high kinetic energies of up to 50 eV [186]. This heating causes dust crystal melting, observed when the plasma parameters are changed.

Under certain discharge conditions, an increase in the number of small-sized particles gives rise to the formation of complex structures where different regions coexist (see Fig. 1b): the high ordering region ('plasma crystals'), and regions of convective and oscillatory motion of particles ('dusty plasma liquids'). Usually, in the lower part of the structure, the particles oscillate in the vertical direction (dust density waves) at a frequency of $25 – 30$ Hz and a wavelength of about 1 mm, the mean interparticle distance being 200 µm. Such self-excited oscillations can correspond to the instability of the dust acoustic wave, the possible mechanisms of which are considered in Section 4. Most of the central region of the structure is occupied by a crystal-like structure with a pronounced chain-like configuration. At the periphery of the upper part of the structure, the particles undergo convective motion whose intensity decreases towards the center of the structure. This complex picture is apparently associated with a peculiar distribution of plasma parameters and forces acting on the dust particles within a striation.

3.2.3 Ordered structures in a thermal plasma. Thermal plasma constitutes a low-temperature plasma characterized by equal temperatures of the electron, ion, and neutral components. The existence of liquid or solid small-sized particles in such a plasma can significantly affect its electrophysical properties. Effects associated with the presence of particles were already observed in early experiments focused on studying plasma of hydrocarbon flames (see, e.g., Ref. [29]).

Experimental investigations of the ordered dust structure formation in a thermal plasma were performed in a quasi-laminar weakly ionized plasma flow at temperatures of $1700 – 2200$ K and atmospheric pressure [19, 190 – 192]. A plasma source formed an extended and uniform volume (about 30 cm^3) of quasi-neutral thermal plasma, where the particles of CeO_2 were introduced. The main plasma components are the charged particles, electrons, and singly charged Na^+ ions. The electron density varies from 10^9 to 10^{12} cm^{-3}. The dust particles are charged by background electron and ion fluxes and via thermionic emission. Due to the dominant role of the latter mechanism, the particle charge

is positive and equal to $10^2 - 10^3$ elementary charges. Here, in contrast to gas discharges in laboratory conditions, the plasma is isotropic and quite uniform because gravity does not play any important role.

The relatively large volume and uniformity of the plasma allow us to measure gas and particle properties by different probe and optical methods to find the characteristic plasma parameters. Different probe methods were employed to measure the densities of alkali metal ions and electrons. The gas temperature and the concentration of alkali atoms were measured by the generalized reversal technique and full absorption technique, respectively. In order to determine the mean (Sauter) diameter D_{32} and the particle concentration $n_{\rm d}$ in the plasma flow, the aperture transparency method was used. The spatial dust structure is analyzed using the pair correlation function $g(r)$ measured with a time-of-flight laser counter. The measurement volume of the counter is formed by focusing an argon laser ($\lambda = 0.488$ μm) beam in a certain region of the plasma flow. The radiation scattered by individual particles as they traverse the measurement volume is transduced to electric signals by a photodetector. The received signals are then processed in order to calculate the pair correlation function $g(r)$.

The results of measuring spatial dust structures were compared with experimental data obtained for an aerosol flow at room temperature. In the last case, only air with CeO_2 particles was injected into the inner region of the burner. Such a system models a plasma with a random (chaotic) spatial distribution of dust particles — a 'gaseous plasma'.

Comparison of the pair correlation functions for CeO_2 particles with diameter $D_{32} \approx 1.8$ μm in aerosol flow at temperature $T_g \approx 300$ K and in a plasma at temperature $T_g = 2170$ K and particle concentration $n_{\rm d} = 2.0 \times 10^6$ cm^{-3} showed [21] that they are almost identical. This means that a weakly ordered 'gaseous' structure is produced. At a lower temperature $T_g = 1700$ K and significantly higher particle number density $n_{\rm d} = 5.0 \times 10^7$ cm^{-3}, the pair correlation function $g(r)$ demonstrates short-range order which is characteristic of a liquid-like structure [21]. In such a plasma, the measurements give for the ion number density $n_{\rm i} \sim 10^9$ cm^{-3}, which is about one order of magnitude lower than the electron number density $n_{\rm e} \sim 5 \times 10^{10}$ cm^{-3}. The particle charge evaluated from the quasi-neutrality condition $Z_{\rm d} n_{\rm d} = n_{\rm e}$ is positive and equals approximately 10^3 elementary charges with an accuracy of a factor of 2. Then the ratio of the average interparticle separation to the electron Debye length is $\varkappa \sim 2$, and the modified coupling parameter lies in the range $\Gamma^* \sim 50-200$. These values are close to the crystallization conditions for the isotropic three-dimensional Debye – Hückel model (see Section 3.1.2). The fact that the structures found in the experiment are relatively weakly ordered is explained by a significant nonstationarity of the system: the time interval between particle injection into the plasma and correlation function measurements is not enough for the ordered structures to form completely. This evidence was supported by MD simulation of the dynamics of the

ordered dust-particle structure formation in conditions of experiment [193, 194].

In Ref. [195], experiments on determining the parameters of a plasma with a condensed disperse phase (CDP) of combustion products of synthetic solid fuels with various compositions are reported. In most of the experiments, the coupling parameter Γ was smaller than unity and ordering of CDP particles was absent. The main reason preventing the formation of ordered structures is the existence of a substantial amount of alkali-metal impurities in fuels. This leads to an increase in the degree of plasma ionization and, hence, to a decrease in the plasma screening length (Debye radius). The ordered structures of CDP particles were only observed for samples of aluminium-coated solid fuels with a low content of alkali metals. In this case, the coupling parameter reached values of $10-30$, corresponding to structures with a liquid-like order. An analysis of the experimental pair correlation functions revealed a short-range order for sufficiently high particle concentrations.

3.2.4 Ordered structures in nuclear-induced plasmas. Nuclear-induced plasma is produced by nuclear-reaction products which, passing through a medium, create ion–electron pairs, as well as excited atoms and molecules in their tracks. In terms of physical characteristics, the nuclear-induced plasma of inert gases differs significantly from thermal and gas discharge plasmas. At the relatively low intensities of a radioactive source, typical of laboratory conditions, this plasma has a distinct track structure. The tracks are randomly distributed in space.

The experiments were performed in an ionization chamber which is placed in a hermetical transparent cell [196]. Either β-particles (decay products of ^{141}Ce) or α-particles and fission fragments (decay products of ^{252}Cf) were used as ionizing particles [196, 197]. The energies of reaction products, their free paths in air and dust particle material, as well as the number of secondary electrons emitted in collisions of the ionizing particle with a dust particle are given in Table 1.
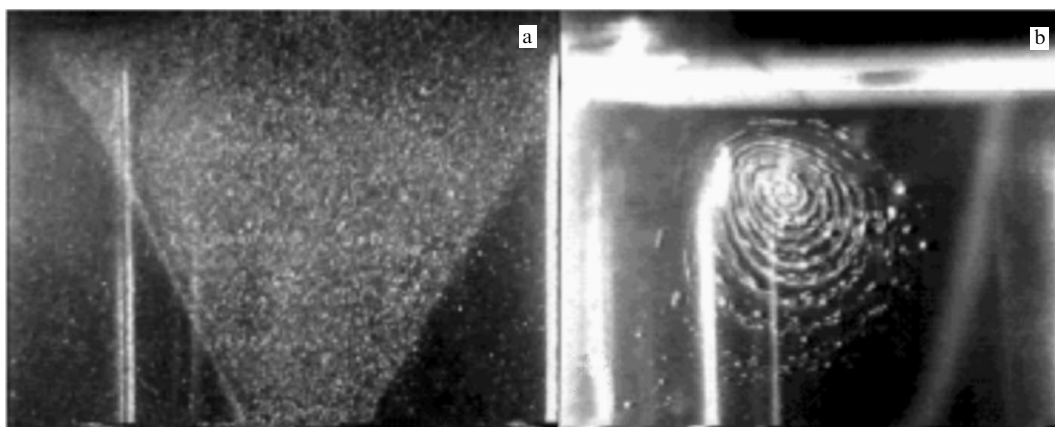
In a plasma of atmospheric air at an external electric field strength of 20 V cm^{-1}, the levitating particles form liquid-like structures — the pair correlation function has one maximum. At stronger electric fields, the dust particles move in closed trajectories which form a torus with the axis aligned with that of the cylindrical chamber.

In an inert gas, sufficiently dense dust clouds with sharp boundaries exist, and the dust particles form a liquid-like structure inside these clouds (Fig. 11a). In a nonuniform electric field, the particles form a rotating dust structure in which agglomeration of small particles into coarse fragments proceeds in the course of time (Fig. 11b) [198].

In the experiments, particles of Zn and CeO_2 were used. The particle radius was estimated experimentally from the particle steady-state falling velocity after the removal of the electric field and was found to be 1.4 μm. The electric charge was inferred from the equilibrium condition for slowly

Table 1. Major characteristics of ionizing particles.

Ionizing particle	Average initial energy, keV	Total range in solid matter (CeO_2), μm	Total range in air ($p = 1$ atm), cm	Number of secondary electrons per particle
β-particle	138	58	5.6	≈ 5
Average fission fragment	9×10^4	5.5	2.3	≈ 250
α-particle	6×10^3	20	4.7	≈ 10

Figure 11. (a) Dust structures of micron-sized Zn particles in a nuclear-induced plasma in neon at a pressure of 0.75 atm and an electric field strength of 30 V cm^{-1}; (b) rotating dust structures of micron-sized Zn particles in neon. The agglomeration of particles is visible.

moving levitating particles. The particle charge depended on the particle radius and lay in the range from 400 to 1000 elementary charges.

For the theoretical calculation of the charge on a spherical particle in the nuclear-induced plasma, nontraditional approaches are used because this plasma is spatially and temporally inhomogeneous. The charging process is considered after the track plasma has separated into two clouds: one of electrons, and the other of ions. When the electron or the ion cloud meets a dust particle on its drift to the corresponding electrode, then this particle acquires some charge from the cloud. A statistical treatment of these charging events constitutes the essence of the mathematical model posed for calculating the particle charge. The electron current to the particle is determined by the electron collection cross section in the collisionless limit. To obtain the ion current, the diffusion approximation is used. In the simulation, the code first generates the event of creation, the direction of emission from the source, and the type of ionizing particle (alpha-particle or a fission fragment) [25]. The simulation shows that the particle charge fluctuates with time. On the one hand, the dust particle acquires a charge in the electron attachment process; on the other hand, its charge decreases substantially in the less frequent events of interaction with the ions. The contribution from alpha-particles leads to a complicated dependence of the charge on time. The characteristic timescale for changing the charge is $10^{-3} - 10^{-2}$ s. This time is short enough, and hence the particle interaction with external fields can be expressed in terms of effective constant charge. A time-averaged charge calculated from this model is in most cases close to the values obtained for levitating particles from the balance between gravity and electrostatic forces. The charge fluctuations with amplitudes comparable to the charge itself can be one of the reasons preventing the formation of highly ordered structures of dust particles.

When a particle gets into the track region, the cascade electrons having a mean energy of ~ 100 eV could cause charges which are sufficient for dust system crystallization. To investigate the charging process, a numerical model based on a system of equations describing two-dimensional space-time track evolution has been developed. The system of equations included the kinetic equation for electrons, the continuity equation for heavy components (ions, atoms, etc.),

the Poisson equation, and equations describing chains of plasma-chemical reactions. It follows from the calculations that a particle can collect no more than 10 electrons from one track. This means that the influence of many tracks is required in order to produce the large charge on the particle.

In order for the charging rate in the track regions to prevail over that due to drift flows, the ionizing flux of a value of approximately 10^{13} cm^{-2} s^{-1} is required. Such a flux can be obtained in the beam of a charged particle accelerator. Experiments using a circular continuous beam with an aperture of 15 mm, current of 1 μA, and proton energy of 2 MeV were performed. In the absence of an external electric field, the stratification (i.e., formation of regions free of dust particles) of the dust component in neon was observed.

3.3 Dust clusters in plasmas
Dust clusters in plasmas constitute the ordered systems of a finite number of dust particles interacting via the pairwise repulsive Debye – Hückel potential and confined by external forces (e.g., of electrostatic nature). Such systems are sometimes also called Coulomb or Yukawa clusters. The difference between dust clusters and dust crystals is conditional: both systems in fact consist of a finite number of particles. The term 'dust clusters' is usually reserved for systems with the number of particles $N \lesssim 10^2 - 10^3$, while for larger formations the term 'dust crystals' can be used. More precise definition of clusters would be the ratio of the number of particles in the outer shell to the total number of particles in the system. For crystals, this ratio should be small. Similar systems are met, for instance, in usual singly charged plasmas in Penning or Paul traps [38, 199], where the vacuum chamber is filled with the ions, as well as in colloidal solutions [200]. The distinctions between systems are due to different types of interaction potential and different forms of confining potential.

Historically, clusters consisting of repulsive particles in an external confining potential were first investigated with the use of numerical modeling (mostly by Monte Carlo and molecular dynamics methods). Taking into account the possibility of applying the simulation results to dust clusters, we mention here the works [201 – 206]. Most simulations were performed for two-dimensional clusters in an external harmonic (parabolic) potential. Such a configuration is usually realized in ground-based experiments with dusty
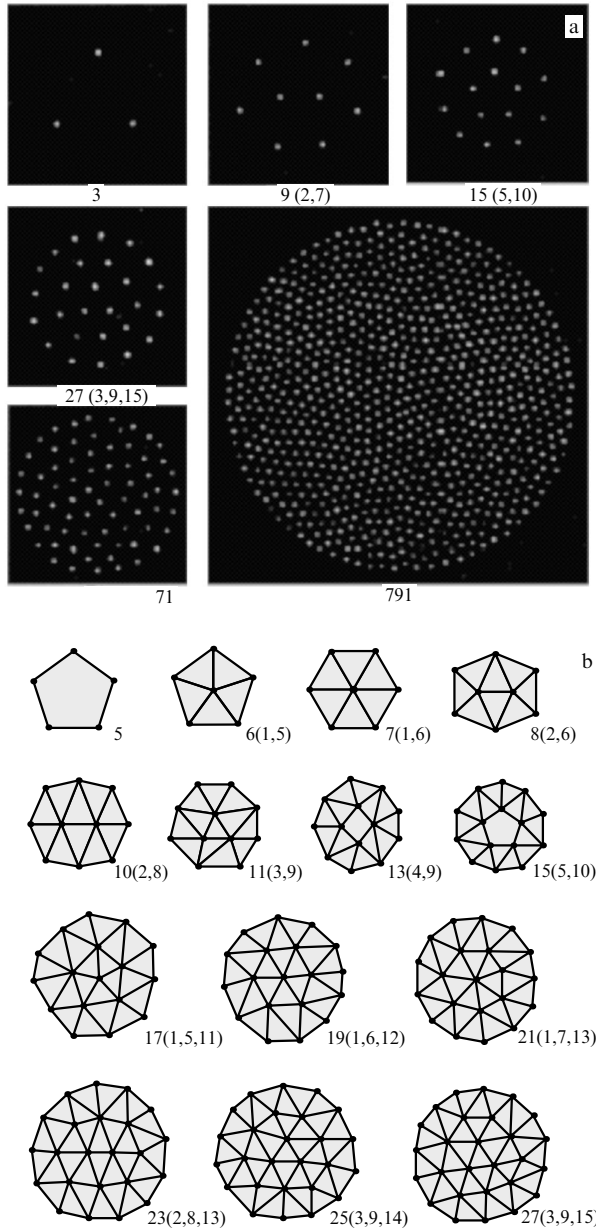
Figure 12. Video images of experimentally found [207] (a) typical dust cluster structures consisting of different numbers of particles (the scales are not the same for the pictures; typical interparticle spacing is between 0.3 and 0.7 mm); (b) typical shell configurations of several dust clusters composed of different numbers of particles. (The figure is kindly provided by Lin I.)

plasma in gas discharges (see Section 3.2.1). The simulations show that for a relatively small number of particles in the cluster the 'shell structure' is formed with the number of particles N_j in the jth shell ($\sum_j N_j = N$). At zero temperature, the unique equilibrium configuration $(N_1, N_2, N_3, \ldots)$ exists for a given particle number N. Such configurations form an analog to the Mendeleyev's Periodic Table, the structure of which depends on the shape of the interaction potential, confining potential, and their relative strengths. At finite temperatures, metastable states with energies close to the ground state can also be realized.

The first experimental investigation of dust clusters was reported in Ref. [207]. The experiment was performed in the sheath of an rf discharge. A hollow coaxial cylinder of 3 cm in diameter and 1.5 cm in height was put on the bottom electrode to confine the dust particles. Clusters with a number of particles from a few up to 791 were investigated. The photo images of the typical cluster structures with different numbers of particles are exemplified in Fig. 12a. Figure 12b shows a series of typical shell configurations observed for dust clusters. For a large number of particles, the inner particles form a quasi-uniform hexagonal structure, while near the outer boundary particles form several circular shells. The mean interparticle separation increases up to about 10% from the center to the cluster boundary.

In Refs [127, 208], the rotation of dust clusters around their symmetry axis was effected. In the first of the cited works, the cluster rotation was caused by the light pressure of the laser beam; not only could the cluster rotate as a whole, but also intershell rotation could be excited. In the second work, the cluster rotation was initiated by the presence of the magnetic field parallel to the cluster axis of symmetry. The magnetic field distorts the ion trajectories, with the result that the collisions of ions with the dust particles cause the cluster rotation.

In the work [209], the oscillations of particles in clusters consisting of 3, 4, and 7 particles were investigated. The application of the results obtained to dusty plasma diagnostics was also discussed (determination of the particle charge and plasma screening length). In this context we also mention the work [210] in which the stability conditions and analytical expressions for the frequencies of the basic modes were found for the simplest clusters consisting of 2, 3, and 4 particles and an arbitrary form of interaction potential between them.

4. Oscillations, waves, and instabilities in dusty plasmas

In this section, the wave processes in dusty plasmas are described. In selecting the material, priority was given to phenomena for which both theoretical and experimental results exist and those used for dusty plasma diagnostics in the laboratory. Our main attention is concentrated on linear waves in dusty plasmas without magnetic fields, although there also exists extensive literature on nonlinear waves and waves in the presence of magnetic fields. We focus on the effects which are directly associated with the presence of the dust component. Often they have no analogs in the usual multicomponent plasmas. In Section 4.1, the problem of individual particle oscillations in sheaths of gas discharges is investigated. An introduction to the theory of linear waves in dusty plasmas is given in Section 4.2, and some mechanisms of their instability and damping are also considered. In Section 4.3, some experimental results are discussed, including generation of waves as a tool for dusty plasma diagnostics.

4.1 Oscillations of individual particles in a sheath region of gas discharges

In most of the ground-based experiments, negatively charged dust particles can only levitate in the regions of sufficiently strong electric fields, where the electric force compensates for gravity. This occurs, for example, in the sheath of an rf discharge, where the electric field averaged over the oscillation period is directed along gravity force [due to the large mass, neither the dust particles nor the ions respond to the rf field ($f \sim 14$ MHz)]. This is also true in regard to the cathode sheath of a dc discharge. The electric field in these regions

increases almost linearly towards the electrode [211] and reaches sufficiently high values on its surface. Variations in the particle charge are connected to ion acceleration under the action of the electric field and to an increase in the ratio $n_i/n_e > 1$ as the electrode is approached (see Fig. 2b). Usually, the charge first somewhat decreases (increases in the absolute magnitude), reaches a minimum, and then increases and can even reach positive values close to the electrode. Examples of numerical calculations of the dependence of the particle surface potential on the distance from the electrode in collisionless and collisional sheaths of rf and dc discharges can be found in Ref. [113] for a set of plasma parameters. For not too heavy particles, there usually exists a stable particle equilibrium position in the sheath. Let us assign the vertical coordinate $z = 0$ to this position. The force balance condition gives

$$m_d g + Z_{d0} E_0 = 0, \qquad (79)$$

where $Z_{d0} = Z_d(0)$ and $E_0 = E(0)$. For small displacements of a particle around its equilibrium position (linear oscillations), the potential energy can be expressed in the form $W(z) \approx m_d \Omega_v^2 z^2/2$, where

$$\Omega_v = -\frac{\partial}{\partial z}\left[\frac{Z_d(z)E(z)}{m_d}\right]_{z=0} \qquad (80)$$

characterizes the frequency of vertical oscillations. As follows from relationship (80), Ω_v depends on the derivative of the electrostatic force at the equilibrium position and on the particle mass. Due to the relatively large mass of the dust particles, the value of Ω_v is not very high and typically lies in the range $1 - 100$ s^{-1}. Hence, it is convenient to use low-frequency excitations for determining the resonance frequency of particle vertical oscillations, which can be expressed through the plasma and particle parameters.

As a simplest example we refer to a harmonic excitation of particle oscillations. The equation for small amplitude oscillations is written as

$$\ddot{z} + v_{dn}\dot{z} + \Omega_v^2 z = \frac{F_{ex}(t)}{m_d}, \qquad (81)$$

where $F_{ex} = f_0 \cos \omega t$, and f_0 is the amplitude of an external force. Equation (81) constitutes an equation of forced oscillations in the presence of friction (see, e.g., Ref. [137]). Its solution for stationary oscillations has the form $z(t) = A(\omega)\cos(\omega t + \delta)$, where $A(\omega)$ is the amplitude of forced oscillations, viz.

$$A(\omega) = \frac{f_0}{m_d\sqrt{(\Omega_v^2 - \omega^2)^2 + v_{dn}^2 \omega^2}}, \qquad (82)$$

δ is the phase shift, and $\tan \delta = v_{dn}\omega/(\omega^2 - \Omega_v^2)$. The amplitude grows when ω approaches Ω_v and reaches the maximum at $\omega = (\Omega_v^2 - v_{dn}^2/2)^{1/2}$. The value of ω corresponding to the maximum of the amplitude for $v_{dn} \ll \Omega_v$ is different from Ω_v only by a second-order correction. Hence, changing ω and measuring the oscillation amplitude (82), it is possible to determine Ω_v and v_{dn}. Such measurements were performed for the first time in Ref. [16] and were later used to determine the particle charge in Refs [212–216]. Excitation is caused either by applying an additional low-frequency signal to the electrode (in a modified variant — to a small probe inserted in a plasma in the vicinity of the levitated particle) or by affecting the particle with the aid of laser radiation [215].
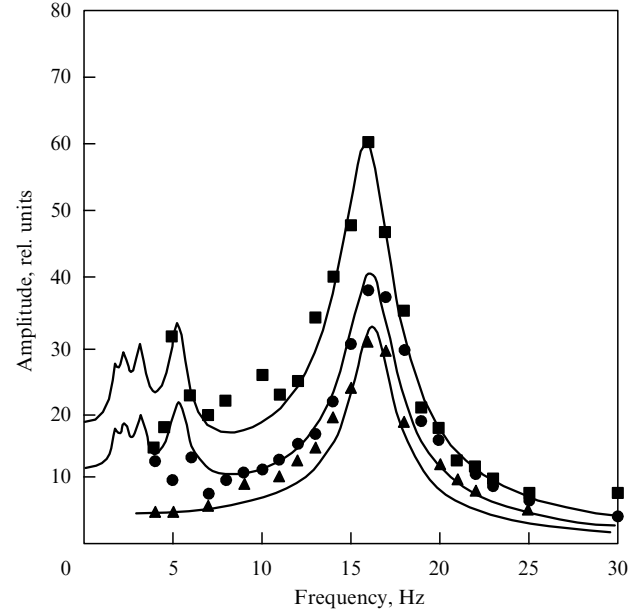
Figure 13. The dependence of the amplitude of dust particle vertical oscillations in the sheath of an rf discharge on the excitation frequency [213]. Symbols correspond to experimental findings, and curves — to theoretical results. Different excitation methods were used: electrode excitation with sine wave (▲), electrode excitation with rectangular voltage wave (●), excitation with radiation pressure from a chopped laser beam, analogous to rectangular wave (■). All the methods yield the same resonance frequency of ~ 17 Hz, from the value of which the particle charge can be evaluated. (The figure is kindly provided by A Piel.)

The exciting force is not necessarily harmonic, but this does not influence the essential properties of oscillations. Typical experimental findings are presented in Fig. 13.

The main difficulty in estimating the particle charge from experimental results is to establish the connection between Ω_v and Z_d. It is often supposed that the dependence of the particle charge on the vertical coordinate is much weaker than that of the electric field, i.e., in the first approximation it is believed that $Z_d \approx Z_{d0} = \text{const}$, and therefore $\Omega_v^2 \approx -Z_{d0}E'(0)/m_d$. The value of the derivative E' is often practically constant over the sheath and is linked through the Poisson equation with the electron and ion number densities:

$$E'(z) = 4\pi e[n_i(z) - n_e(z)].$$

The concentrations n_i and n_e are determined by extrapolating the results of probe measurements in the bulk plasma into the sheath region, using different theoretical models. Probe measurements in the sheath are not practical because of difficulties in their interpretation. Therefore, the described method is not very accurate. However, it is widely used in experiments because of its simplicity and the absence of other methods exhibiting essentially higher accuracy.

By increasing the amplitude of the excitation force it is possible to excite nonlinear oscillations. The experiments and their theoretical interpretation are described in Refs [217, 218]. An example of a numerical model, which takes into account the dependences of particle charge, electric field, and external force amplitude on the vertical coordinate, as well as the location of an excitation source with respect to the dust particle and force balance in the sheath, is given in Ref. [219]. The characteristic property of nonlinear oscillations is the hysteretic dependence of their amplitude on the excitation

frequency. We also note that excitation of nonlinear oscillations allows us, in principle, to investigate the electric field and/or dust particle charge distributions along the sheath.

Vertical oscillations of particles in the sheath regions of gas discharges can be caused not only by the application of an external force, but also can be self-excited due to effects specific to dusty plasmas. For example, a drastic increase in the amplitude of vertical oscillations was examined experimentally under certain conditions (e.g., with lowering pressure) in the sheath of rf and dc discharges [220, 221]. Different theoretical aspects of vertical oscillations were considered in Refs [72, 74, 78, 222]. Below, we will ignore the simplest effect associated with the particle Brownian motion which is caused by the stochastic character of particle collisions with neutral atoms. This effect is always present and is additive to other effects. Its value (oscillation amplitude) is typically quite small from a practical point of view.

One of the effects leading to vertical oscillations is associated with random particle charge variations caused by the stochastic nature of particle charging [72, 74, 75]. To describe this effect, the right-hand side of Eqn (81) should be presented in the form $F_{ex} = eE_0 \, \delta Z_d$, where δZ_d is the random deviation of the particle charge from its average value, which is a random function of time. The oscillation amplitude will also be a random function of time. However, using the properties of random charge fluctuations (32)–(35), it is possible to derive its root-mean-square value. It can be easily shown that for typical conditions $\Omega_{ch} \gg \Omega_v \gg v_{dn}$, the mean square amplitude of oscillations associated with the random charge variations can be estimated as

$$\langle \Delta z^2 \rangle \approx \frac{g^2 \gamma^2}{|Z_d| \Omega_{ch} \Omega_v^2 v_{dn}} , \qquad (83)$$

and increases with decreasing neutral gas pressure. Notice also that since $\Omega_{ch} \propto a$, $v_{dn} \propto a^{-1}$, $|Z_d| \propto a$, and in the first approximation $\Omega_v \propto |Z_d|/m_d \propto a^{-2}$, we have $\langle \Delta z^2 \rangle \propto a^3$, i.e., the mean square oscillation amplitude is proportional to the particle mass.

Another effect, which is also associated with the variability of the particle charge, results from the finite charging time. The qualitative theory of this effect was proposed in Ref. [220] to describe the following experimental evidence. When decreasing the neutral pressure and/or plasma density below some critical value (for the pressure p, the corresponding value is ~ 3 mTorr), self-excitation of oscillations (their amplitude grows with time) of the dust particles levitating in the sheath region of a dc discharge occurs. The time scale of the amplitude growth is ~ 10 s. In the final state either saturation takes place (the amplitude reaches a constant value determined, e.g., by nonlinear effects) or, if the amplitude is too large, the particle leaves the plasma reaching the electrode surface. This behavior testifies to the existence of an instability mechanism for vertical oscillations, which is effective under low neutral gas pressures. A physical interpretation of the phenomenon was proposed by Nunomura et al. [220]. According to the authors, due to the finite charging time, the charge of the oscillating particle experiences some delay with respect to its 'equilibrium' value $Z_d^{(eq)}(z)$ corresponding to infinitely slow particle motion. The particle motion is not merely potential in this case. If in the equilibrium position $Z_d'(0) < 0$, then for a particle moving along the electric field (downwards) the absolute value of the charge $|Z_d(z)|$ is smaller than the equilibrium value $|Z_d^{(eq)}(z)|$.

When the particle is moving in the opposite direction (upwards), the inverse inequality is satisfied. Thus, over the oscillation period the particle acquires energy from the electric field. The oscillations become unstable when the energy gain is higher than the energy dissipation due to friction.

Quantitative interpretation of this mechanism was formulated in Ref. [78]. The right-hand side of Eqn (83) can be written in the considered case as $F_{ex} = eE_0 \, \delta Z_d$, where $\delta Z_d = Z_d(z, t) - Z_d^{(eq)}(z)$, with the equilibrium value $Z_d^{(eq)}(z) = Z_{d0} + z Z_d'(0)$. The dynamics of charging is given by Eqn (27) which in this case takes the form

$$\frac{\partial \delta Z_d}{\partial t} + \dot{z} \frac{\partial Z_d}{\partial z} = -\Omega_{ch} \, \delta Z_d . \qquad (84)$$

Assuming harmonic oscillations, namely $z, \delta Z_d \propto \exp(-i\omega t)$, we get from equation (81), with the help of equation (84), the following relationship

$$(\omega_{ch} - i\omega)(\omega^2 + iv_{dn}\omega - \Omega_v^2) = -i\omega \, \frac{eE_0}{m_d} Z_d'(0) . \qquad (85)$$

When the conditions $\Omega_{ch} \gg \Omega_v \gg v_{dn}$ are satisfied, we have for weakly unstable (weakly damped) oscillations, $|\mathrm{Re}\,\omega| \gg |\mathrm{Im}\,\omega|$, the dependences

$$\mathrm{Re}\,\omega \approx \Omega_v , \qquad 2\,\mathrm{Im}\,\omega \approx -v_{dn} - \frac{eE_0}{m_d \Omega_{ch}} Z_d'(0) . \qquad (86)$$

The condition $\mathrm{Im}\,\omega > 0$ corresponds to the unstable solution. Hence, the necessary condition of the instability is $Z_d'(0) < 0$, while the sufficient condition is formulated as

$$\left| \frac{Z_d'(0)}{Z_{d0}} \right| > \frac{v_{dn} \Omega_{ch}}{g}$$

(here the force balance condition is used). This instability mechanism was proposed to explain the increase in the amplitude of vertical oscillations with decreasing pressure in experiment [220]. Some other possible instability mechanisms were proposed in the experimental work [221] dealing with the investigation of instabilities of vertical oscillations in the sheath of an rf discharge.

4.2 Linear waves and instabilities in weakly coupled dusty plasmas

Almost simultaneously with the experimental discovery of crystallization in complex plasmas, new low-frequency waves (dust acoustic waves) and instabilities leading to self-excitation of such traveling waves were observed [18, 222–225]. This stimulated interest in the theoretical investigation of wave processes in dusty plasmas. The most consistent approach to this problem, requiring solution of the kinetic equations for dusty plasmas, faces a number of difficulties associated with the appearance of a new degree of freedom (the dust particle charge) and the necessity of correctly evaluating collision integrals for different types of elastic and inelastic collisions. Attempts to construct a kinetic theory were undertaken in the works [226–230]. However, this problem cannot be considered as fully solved. Therefore, in Sections 4.2.1 and 4.2.2 we mostly concentrate on the simpler and clear hydrodynamic description of dusty plasmas, although in Section 4.2.3, which is dedicated to wave damping and instabilities, we use some of the simplest results

from the kinetic theory of the conventional multicomponent plasmas.

4.2.1 Basic equations. Let us formulate a system of equations for describing the longitudinal waves in a uniform weakly coupled dusty plasma in the absence of external forces acting on the dust particles. For the dust component, the fluid continuity and momentum equations have the form

$$\frac{\partial n_{\mathrm{d}}}{\partial t} + \frac{\partial}{\partial x}(n_{\mathrm{d}}v_{\mathrm{d}}) = 0, \tag{87}$$

$$\frac{\partial v_{\mathrm{d}}}{\partial t} + v_{\mathrm{d}}\frac{\partial v_{\mathrm{d}}}{\partial t} = -\frac{eZ_{\mathrm{d}}}{m_{\mathrm{d}}}\frac{\partial \phi}{\partial x} - \frac{1}{m_{\mathrm{d}}n_{\mathrm{d}}}\frac{\partial p_{\mathrm{d}}}{\partial x} - \sum_{j=\mathrm{e,i,n}} v_{\mathrm{d}j}(v_{\mathrm{d}} - v_j), \tag{88}$$

The electric force in the field of the wave, the pressure of the dust component, and the momentum transfer in dust–electron, dust–ion, and dust–neutral collisions characterized by the effective frequencies v_{de}, v_{di}, and v_{dn}, respectively, are taken into account on the right-hand side of Eqn (88). It should also be taken into account that, in contrast to v_{dn}, the frequencies v_{de} and v_{di} characterize both direct collisions (collection) of electrons and ions with dust particles and their elastic (Coulomb) scattering by the particle potential. The equations for electrons and ions take the form

$$\frac{\partial n_{\alpha}}{\partial t} + \frac{\partial}{\partial x}(n_{\alpha}v_{\alpha}) = Q_{I\alpha} - Q_{L\alpha}, \tag{89}$$

$$\frac{\partial v_{\alpha}}{\partial t} + v_{\alpha}\frac{\partial v_{\alpha}}{\partial x} = -\frac{e_{\alpha}}{m_{\alpha}}\frac{\partial \phi}{\partial x} - \frac{1}{m_{\alpha}n_{\alpha}}\frac{\partial p_{\alpha}}{\partial x} - \frac{v_{\alpha}}{n_{\alpha}}\tilde{Q}_{L\alpha}$$

$$- \sum_{j\neq\alpha(j=\mathrm{e,i,d,n})} v_{\alpha j}(v_{\alpha} - v_j), \tag{90}$$

where the subscript $\alpha = \mathrm{e, i}$ for electrons and ions, respectively, and $e_{\mathrm{e}} = -e$, $e_{\mathrm{i}} = e$. On the right-hand side of equation (89), the terms $Q_{I\alpha}$ and $Q_{L\alpha}$ describe the production and the loss of electrons and ions. Production can be associated with plasma ionization and, sometimes, with processes on the dust particle surface, i.e., thermionic, photoelectric, and secondary electron emission. The losses can be due to volume recombination, losses to the walls of a discharge chamber, collection by the dust particles, etc. In the unperturbed state $Q_{I\alpha 0} = Q_{L\alpha 0}$. The first two terms on the right-hand side of Eqn (90) describe the action of the electric field of the wave and the pressure of the corresponding component. The third one describes only the momentum loss due to 'external' processes (recombination in plasma, losses to the walls), assuming that newly created particles (due to ionization) are initially at rest — the losses to the dust particles are accounted for by the next term. Finally, the fourth term describes the momentum transfer in collisions between different components, including absorbing collisions of electrons and ions with the dust particle. We note that from the momentum conservation law it follows that $n_{\alpha}m_{\alpha}v_{\alpha\beta} = n_{\beta}m_{\beta}v_{\beta\alpha}$.

Equations (87) – (90) should be supplemented by an equation of state, which in the simplest case can be written down as

$$p_j = \mathrm{const} \cdot n_j^{\gamma_j}. \tag{91}$$

Power index $\gamma_j = 1$ corresponds to isothermal perturbations of the jth component, while $\gamma_j = 5/3$ for adiabatic perturba-

tions. In the general case, equation (91) can be considered as an equation of state of the polytrophic type.

A characteristic peculiarity of waves in dusty plasmas is that the dust particle charge is not fixed. The particle charge is determined by the local parameters of the surrounding plasma (ion and electron concentrations and velocities, plasma potential) and hence follows their perturbed behavior when waves are propagating. Therefore, the system of equations (87)–(91) should be supplemented with the charge equation. Similar to kinetic equation (27), we have for the moving particles:

$$\frac{\partial Z_{\mathrm{d}}}{\partial t} + v_{\mathrm{d}}\frac{\partial Z_{\mathrm{d}}}{\partial x} = \sum_j I_j. \tag{92}$$

The system is closed by the Poisson equation

$$\frac{\partial^2 \phi}{\partial x^2} = -4\pi e[n_{\mathrm{i}} - n_{\mathrm{e}} + Z_{\mathrm{d}}n_{\mathrm{d}}]. \tag{93}$$

The system of equations (87)–(93) can be used for investigating waves in a weakly coupled dusty plasma within hydrodynamic approximation. As can be seen from the derived equations, dusty plasmas are characterized by a wider diversity of processes than the usual multicomponent plasma. A detailed analysis of the equations is rather complicated. Moreover, it is necessary to make certain assumptions about the nature of electron and ion sources and losses, depending on the problem under consideration. Some theoretical results on waves in dusty plasmas and their instability (stability) were obtained in original works [66, 128, 231–235]. The input equations in these works are similar to the system (87)–(93). However, various assumptions about dominant processes of electron and ion production and loss, elastic and inelastic collision frequencies, etc. were made. In Sections 4.2.2 and 4.2.3, we consider only several important limiting cases of linear waves in dusty plasmas, as well as their instability and damping in the simplest interpretation.

4.2.2 Ion-acoustic and dust-acoustic waves. As we have already mentioned, the presence of the dust component not only modifies the charge composition of a plasma, but also introduces new characteristic spatial and temporal scales in the system of interest. Hence, it is natural to expect not only modifications to the wave modes that exist without the dust, but also the appearance of new ones. Below, we will consider a modification of the dispersion relation for ion-acoustic waves and the appearance of the new low-frequency mode — the dust-acoustic wave. The latter is especially important from the point of view of experimental investigations into dusty plasmas because its characteristic frequency range, $\omega \sim 1 - 100\ \mathrm{s}^{-1}$, is easily accessible for processing and analysis.

Let us linearize the system of equations (87)–(93), assuming small perturbations of plasma parameters $n_j = n_{j0} + n_{j1}$, $v_j = v_{j0} + v_{j1}$ ($j = \mathrm{e, i, d}$), and $\phi = \phi_1$ proportional to $\exp(-i\omega t + ikx)$. For simplicity, we also ignore all collisions, which is only possible for short wavelengths, when characteristic free paths are longer than the characteristic scale of the problem (wavelength). In this case, we should, strictly speaking, assume the constant charge on the dust particles, because charge variations are associated with inelastic collisions of electrons and ions with the dust particles, which are being ignored.

This idealized model is extremely simplified, compared to the conditions which are realized in most experiments

and, therefore, it is inapplicable for their description. Nevertheless, it is useful to consider such a model because it can serve as the basis for investigating the effect of different processes which often determine qualitatively the final result.

The quasi-neutrality condition in the unperturbed state has the form (15). The Poisson equation (93) can be rewritten then as

$$-k^2 \phi_1 = -4\pi e[n_{i1} - n_{e1} + Z_d n_{d1}] . \tag{94}$$

Expressing, with the help of Eqns (87)–(91), the perturbations of different component densities through the wave potential ϕ_1, we get the dispersion relation

$$\varepsilon(k, \omega) = 1 + \chi_e + \chi_i + \chi_d = 0 , \tag{95}$$

where

$$\chi_e = \frac{4\pi e n_{e1}}{k^2 \phi_1} , \qquad \chi_i = -\frac{4\pi e n_{i1}}{k^2 \phi_1} , \qquad \chi_d = -\frac{4\pi Z_d e n_{d1}}{k^2 \phi_1}$$

are the susceptibilities of the corresponding components. More generally, when the dust-particle charge variations are taken into account, χ_d should be written in the form

$$\chi_d = -\frac{4\pi e}{k^2 \phi_1} (Z_{d0} n_{d1} + Z_{d1} n_{d0}) .$$

In the simplest approximation considered we have

$$\chi_j = -\frac{\omega_{pj}^2}{(\omega - k v_{0j})^2 - \gamma_j k^2 v_{Tj}^2} , \tag{96}$$

where $j = e, i, d$, i.e., the same dispersion relation as for a multicomponent collisionless plasma in the hydrodynamic approximation. A peculiarity of dusty plasmas in this simple approach only reduces to the strong asymmetry of the charge-to-mass ratios for different components:

$$\frac{e}{m_e} : \frac{e}{m_i} : \frac{|Z_d| e}{m_d} \sim 1 : 10^{-5} : 10^{-13} .$$

In this case, the inequalities $\omega_{pe} \gg \omega_{pi} \gg \omega_{pd}$ are well satisfied.

In the absence of directed drifts of plasma components ($v_{j0} = 0$), and for high frequencies $\omega \gg k v_{Te} \gg k v_{Ti} \gg k v_{Td}$, the dispersion relation takes the form

$$1 - \sum_{j=e,i,d} \frac{\omega_{pj}^2}{\omega^2} = 0 . \tag{97}$$

According to the previous consideration, the presence of dust does not practically affect the spectrum of high-frequency Langmuir waves; in this case, $\omega \approx \omega_{pe}$.

At lower frequencies $k v_{Te} \gg \omega \gg k v_{Ti} \gg k v_{Td}$, we have $\chi_e \approx 1/(k^2 \lambda_{De}^2)$ ($\gamma_e = 1$) and $\chi_i \approx -\omega_{pi}^2/\omega^2$, so that the dispersion relation acquires the form

$$\omega^2 \approx \frac{\omega_{pi}^2 k^2 \lambda_{De}^2}{1 + k^2 \lambda_{De}^2} , \tag{98}$$

implying that $\omega \approx \omega_{pi}$ for $k \lambda_{De} \gg 1$. In the opposite limiting case, $k \lambda_{De} \ll 1$, the ion-acoustic waves are initiated:

$\omega \approx k C_{IA}$, with the velocity of sound

$$C_{IA} = \left(\frac{T_e}{m_i} \frac{n_{i0}}{n_{e0}} \right)^{1/2} . \tag{99}$$

This expression differs from the standard expression for the ion-acoustic wave velocity in a nonequilibrium plasma, $T_e \gg T_i$ (see, e.g., Ref. [89]), by the factor $\sqrt{n_{i0}/n_{e0}}$. The condition for the ion-acoustic wave existence, $T_e \gg T_i$, following from $C_{IA} \gg v_{Ti}$ is weaker in this case because the existence of the negatively charged dust component implies $n_i/n_e > 1$. Therefore, the influence of charged dust particles on the ion-acoustic wave spectrum reduces to the appearance of the dependence of the velocity of wave propagation on the dust particle charge and density. The influence of the dust component on the ion-acoustic wave dispersion was first considered by Shukla and Silin [236].

For even lower frequencies

$$k v_{Te} \gg k v_{Ti} \gg \omega \gg k v_{Td} ,$$

we have $\chi_{e(i)} \approx 1/(k^2 \lambda_{De(i)}^2)$ ($\gamma_e = 1$, $\gamma_i = 1$), $\chi_d = -\omega_{pd}^2/\omega^2$, and using the notation $\lambda_D^{-2} = \lambda_{De}^{-2} + \lambda_{Di}^{-2}$ we arrive at the dispersion relation in the form

$$\omega^2 \approx \frac{\omega_{pd}^2 k^2 \lambda_D^2}{1 + k^2 \lambda_D^2} . \tag{100}$$

In the limit $k \lambda_D \gg 1$, equation (100) gives $\omega \approx \omega_{pd}$; in the opposite limit, $\omega \approx k C_{DA}$. This mode, being nonexistent in the absence of the dust particles, is called the dust-acoustic wave (DAW) and was first considered by Rao et al. [237]. The dust-acoustic wave velocity is given by

$$C_{DA} = \omega_{pd} \lambda_D = \sqrt{\frac{|Z_d| T_i}{m_d}} \sqrt{\frac{P\tau}{1 + \tau + P\tau}} . \tag{101}$$

The condition $C_{DA} \gg v_{Td}$ of the dust-acoustic wave existence can be fulfilled even when $T_d > T_i$, due to the large value (Z_d) of charge (for not too small P). Thus, the dust-acoustic wave is considerably different from the ion-acoustic wave in usual electron–ion plasmas, which can only exist when the temperature of the light component considerably exceeds the temperature of the heavy component: $T_e \gg T_i$. It will be recalled that in deriving the dispersion relations the collisions were ignored. For this reason, the dust-acoustic wave (101) is sometimes called the short-wavelength DAW [3].

4.2.3 Damping and instabilities of waves in dusty plasmas. Let us briefly consider several mechanisms of damping and instability of electrostatic waves in plasmas, caused by the presence of the dust component. We mostly limit ourselves to the low-frequency mode — the dust-acoustic wave. If the time evolution of waves is of interest, then the wave frequency can be presented in the form $\omega = \omega_r + i\gamma$, where $\omega_r = \mathrm{Re}\,\omega$ and $\gamma = \mathrm{Im}\,\omega$ are the real and imaginary parts of the frequency, respectively. In our designations $\gamma < 0$ corresponds to wave damping, and $\gamma > 0$ to wave growth (instability). In the case of weak damping (growth), the following expression for the damping decrement (instability increment) can be applied [89]:

$$\gamma = -\frac{\mathrm{Im}\,\varepsilon(\omega, k)}{\partial \mathrm{Re}\,\varepsilon(\omega, k)/\partial \omega} . \tag{102}$$

This relation will be utilized below.

One of the mechanisms leading to wave energy dissipation corresponds to collisions. The collisions with neutrals dominate in a weakly ionized plasma. Inclusion of these collisions leads to the following modification of dispersion relation (100):

$$\omega(\omega + \mathrm{i} v_{\mathrm{dn}}) \approx \frac{\omega_{\mathrm{pd}}^2 k^2 \lambda_{\mathrm{D}}^2}{1 + k^2 \lambda_{\mathrm{D}}^2} \,. \tag{103}$$

The damping decrement in the case $\omega \gg v_{\mathrm{dn}}$ is given by

$$\gamma = -\frac{v_{\mathrm{dn}}}{2} \,. \tag{104}$$

Another source of wave damping is, similarly to the common electron–ion plasma, the Landau damping mechanism which follows from the kinetic description of waves in plasma. The use of the simplest approach employing the solution of Vlasov equations for electrons, ions, and dust particles with a fixed charge in collisionless plasma leads to the following expression for the susceptibilities of the corresponding components:

$$\chi_j = \frac{1}{k^2 \lambda_{\mathrm{D}j}^2} \left[1 + F\left(\frac{\omega}{\sqrt{2}\, k v_{Tj}} \right) \right] , \tag{105}$$

where $F(x)$ is the so-called plasma dispersion function having the asymptotes (see, e.g., Ref. [110])

$$F(x) = \begin{cases} -1 - \dfrac{1}{2} x^2 - \dfrac{3}{4} x^4 + \mathrm{i} \sqrt{\pi}\, x \exp\left(-x^2\right), & x \gg 1, \\ -2x^2 + \mathrm{i} \sqrt{\pi}\, x, & x \ll 1, \end{cases} \tag{106}$$

where x is a real argument. For the dust-acoustic waves under conditions $k v_{Td} \ll \omega \ll k v_{Ti}, k v_{Te}$, it follows from formulas (105) and (106) that

$$\chi_{\mathrm{e(i)}} \approx \frac{1}{k^2 \lambda_{\mathrm{De(i)}}^2} \left[1 + \mathrm{i} \sqrt{\frac{\pi}{2}} \frac{\omega}{k v_{Te(i)}} \right] ,$$

$$\chi_{\mathrm{d}} \approx -\frac{\omega_{\mathrm{pd}}^2}{\omega^2} \left[1 - \mathrm{i} \sqrt{\frac{\pi}{2}} \left(\frac{\omega}{k v_{Td}} \right)^3 \exp\left(-\frac{\omega^2}{2 k^2 v_{Td}^2} \right) \right] .$$

The dispersion relation is arrived at by substituting these expressions into Eqn (95). Let us consider the contribution to damping, which arises due to different components. The damping on dust particles yields

$$\gamma = -\omega \sqrt{\frac{\pi}{8}} \left(\frac{\omega}{k v_{Td}} \right)^3 \exp\left(-\frac{\omega^2}{2 k^2 v_{Td}^2} \right) . \tag{107}$$

The condition of weak damping requires a large exponential factor: $\omega^2 / 2 k^2 v_{Td}^2 \gg 1$, which is almost identical to the condition $C_{\mathrm{DA}} \gg v_{Td}$, and, as could be expected, determines the validity range of the hydrodynamic approach to dust-acoustic waves. Damping decrement of the dust-acoustic wave due to ions is described by the following expression

$$\gamma = -\omega \sqrt{\frac{\pi}{8}} \left(\frac{\omega_{\mathrm{pi}}}{\omega_{\mathrm{pd}}} \right)^2 \left(\frac{C_{\mathrm{DA}}}{v_{Ti}} \right)^3 . \tag{108}$$

It is usually small because

$$\left| \frac{\gamma}{\omega_{\mathrm{r}}} \right| \sim \sqrt{\frac{|Z_{\mathrm{d}}| m_{\mathrm{i}}}{m_{\mathrm{d}}} \frac{P}{P+1}}$$

for $\tau \gg 1$ and by virtue of the condition $|Z_{\mathrm{d}}| m_{\mathrm{i}} / m_{\mathrm{d}} \ll 1$. The contribution from electrons to damping can always be ignored because $\mathrm{Im}\, \chi_{\mathrm{e}} / \mathrm{Im}\, \chi_{\mathrm{i}} = \sqrt{\mu}\, \tau^{-3/2} n_{\mathrm{e}} / n_{\mathrm{i}} \ll 1$.

A similar analysis can be performed when the plasma components possess directed velocities. In this case, the substitution $\omega \to \omega - k u_0$ should be made in the argument of the dispersion function F. Some particular cases will be considered below. The inclusion of collisions leads to the substitution of $\omega + \mathrm{i} v_j$ for ω, where v_j is the effective collision frequency of the jth component. In a weakly ionized plasma, v_j is often determined by collisions with neutrals. It should also be taken into account that inclusion of collisions will change Eqn (105) (see, e.g., Ref. [89]). Moreover, the asymptotes of the dispersion function F for an imaginary argument are in some cases different from formula (106) [238]. However, we will not discuss this situation in detail here.

Let us now examine an effect specific to dusty plasmas — that is, dust particle charge variations. It was noted above that the dust particle charge shows itself as a new degree of freedom of the dust component, and its variations should be taken into account when describing waves. For the sake of definiteness, let us consider a plasma in which the charging is determined by only electron and ion collection, which in turn can be described within the OML approach. Assuming $n_{\mathrm{e(i)}} = n_{\mathrm{e(i)}0} + n_{\mathrm{e(i)}1}$, $Z_{\mathrm{d}} = Z_{\mathrm{d}0} + Z_{\mathrm{d}1}$, and $v_{j0} = 0$ ($j = \mathrm{i}, \mathrm{e}, \mathrm{d}$) (isotropic plasma) we derive from Eqn (92), using the expressions (7) and (8) for electron and ion fluxes, the following equation for the particle charge perturbations:

$$\frac{\partial Z_{\mathrm{d}1}}{\partial t} + \Omega_{\mathrm{ch}} Z_{\mathrm{d}1} = I_{\mathrm{e}0} \left(\frac{n_{\mathrm{i}1}}{n_{\mathrm{i}0}} - \frac{n_{\mathrm{e}1}}{n_{\mathrm{e}0}} \right) , \tag{109}$$

where $I_{\mathrm{e}0} = I_{\mathrm{i}0}$ is the unperturbed flux of electrons or ions to the dust particle surface, and the charging frequency is defined by expression (30). Equation (109) is also applicable for $v_{j0} \ll v_{Tj}$ ($j = \mathrm{e}, \mathrm{i}$), because the corrections to the fluxes are on the order of $O\left[(v_{j0}/v_{Tj})^2 \right]$, as was noted in Section 2.2. For low-frequency dust-acoustic waves we have $n_{\mathrm{i}1}/n_{\mathrm{i}0} = -e\phi_1/T_{\mathrm{i}}$, $n_{\mathrm{e}1}/n_{\mathrm{e}0} = e\phi_1/T_{\mathrm{e}}$, so that linearization of Eqn (109) yields

$$Z_{\mathrm{d}1} = -\mathrm{i} \frac{I_{\mathrm{e}0}(1 + T_{\mathrm{e}}/T_{\mathrm{i}})}{\omega + \mathrm{i} \Omega_{\mathrm{ch}}} \frac{e\phi_1}{T_{\mathrm{e}}} , \tag{110}$$

and the dispersion relation accounting for charge variations acquires the form

$$1 + \frac{1}{k^2 \lambda_{\mathrm{D}}^2} - \frac{\omega_{\mathrm{pd}}^2}{\omega^2} + \frac{\Phi}{k^2 \lambda_{\mathrm{De}}^2} = 0 , \tag{111}$$

where the last term is connected to charge variations, and

$$\Phi = \mathrm{i} \frac{I_{\mathrm{e}0}(1 + T_{\mathrm{e}}/T_{\mathrm{i}})}{\omega + \mathrm{i} \Omega_{\mathrm{ch}}} \frac{n_{\mathrm{d}0}}{n_{\mathrm{e}0}} \,.$$

Typically, the condition $\Omega_{\mathrm{ch}} \gg \omega$ is satisfied and therefore the effect considered mostly contributes to the real part of the dispersion relation. In this case, the expression for Φ is considerably simplified:

$$\Phi = \frac{P(1 + \tau)(1 + z\tau)}{z(1 + \tau + z\tau)} ,$$

and the dispersion relation (111) can be rewritten in the form

$$1 + \frac{1}{k^2 \lambda_D^2} \left[1 + \frac{P(1+\tau)(1+z\tau)}{z(1+\tau+z\tau)(1+\tau+P\tau)} \right] - \frac{\omega_{pd}^2}{\omega^2} = 0 . \quad (112)$$

As follows from this expression, the effect of particle charge variations reduces the phase velocity of the dust-acoustic wave. However, for reasonable dusty plasma parameters this effect is relatively weak. Charge variations also affect the imaginary part of the dispersion relation. From equation (111) and the expression for Φ it follows that they lead to wave damping. An expression for the damping decrement can be found, for example, in Ref. [18]. However, two circumstances have to be taken into account. First, to self-consistently determine the imaginary part γ, it is necessary to account for at least the collisions leading to the dust particle charging. One needs to keep the corresponding terms in the continuity and momentum equations for the electron and ion components, and in the momentum equation for the dust component. Moreover, in the continuity equations for electrons and ions it is necessary to take into account processes which compensate for the ion and electron recombination losses on dust particles. We will not consider details here, but instead give some references to original works in which the effect of charge variations on different wave mode propagations is considered using certain assumptions [3, 18, 66, 233, 235, 239–247]. Second, in most of the laboratory facilities the main effect which influences the imaginary part of the dispersion relation is connected to collisions of dust particles (or ions for high-frequency modes, e.g., ion-acoustic waves) with neutrals.

An important example of wave instability in dusty plasmas is the streaming instability which appears due to relative drift between the ions and the stationary (on the average) dust component. This situation is common for most of the experiments on dusty plasmas, although the ion drift velocity u_0 may differ substantially depending on the concrete conditions — from $u_0 \ll v_{Ti}$ in the bulk quasi-neutral plasma to $u_0 \sim C_{AI} \gg v_{Ti}$ in the collisionless sheath near an electrode. Electrons can also possess a directed velocity but their motion can usually be ignored. This type of instability was analyzed in Refs [225, 248–253].

Let us consider some of the results obtained for the low-frequency limit, when $kv_{Td} \ll \omega \ll kv_{Ti}, kv_{Te}$. Within the framework of the simplest kinetic treatment for collisionless plasma we have $\chi_e = 1/k^2 \lambda_{De}^2$ and $\chi_d = -\omega_{pd}^2/\omega^2$. The ion susceptibility can be calculated using formula (105) by substituting $\omega \to \omega - ku_0$. In the limit $|\omega - ku_0| \ll kv_{Ti}$, this yields

$$\chi_i = \frac{1}{k^2 \lambda_{Di}^2} \left[1 + i \sqrt{\frac{\pi}{2}} \frac{\omega - ku_0}{kv_{Ti}} \right] . \quad (113)$$

From the dispersion relation (95) it follows that the waves are unstable when $u_0 > \omega/k$. The instability increment of the considered dust-acoustic mode can be written for $u_0 \gg \omega/k$ in the form

$$\gamma = \omega_{pd} \sqrt{\frac{\pi}{8}} \frac{u_0}{v_{Ti}} \left(\frac{\lambda_D}{\lambda_{Di}} \right)^2 \frac{k\lambda_D}{(1 + k^2 \lambda_D^2)^{3/2}} . \quad (114)$$

As a function of the wave number k, it reaches a maximum at $k\lambda_D = 1/\sqrt{2}$. Here, $\omega_r = \omega_{pd}/\sqrt{3}$ and

$$\gamma_{max} = \frac{\omega_{pd}}{3} \sqrt{\frac{\pi}{6}} \left(\frac{\lambda_D}{\lambda_{Di}} \right)^2 \frac{u_0}{v_{Ti}}$$

determine the frequency characteristics of the most unstable mode [18]. We note that the condition $|\omega - ku_0| \ll kv_{Ti}$ used above implies subthermal ion drift, $u_0 \ll v_{Ti}$, which does not contradict the instability condition $u_0 > C_{DA}$ for dust sound, because $C_{DA} \sim v_{Ti}\sqrt{|Z_d|m_i/m_d} \ll v_{Ti}$.

In the case of suprathermal ion drift, $u_0 \gg v_{Ti}$, ignoring the exponentially small term we get from expressions (105) and (106): $\chi_i \approx -\omega_{pi}^2(\omega - ku_0)^{-2}$. Notice that the same expression for the ion susceptibility follows from formula (96). For low-frequency ($\omega \ll ku_0$) long-wave ($k\lambda_{De} \ll 1$) oscillations, the dispersion relation (95) allows for unstable solutions. Thus, for the ion drift velocity close to the ion-sound wave velocity $u_0 \sim \omega_{pi}\lambda_{De} = C_{IA}$, the wave frequency is given by

$$\omega \approx \frac{1 + i\sqrt{3}}{2} \left(\frac{\omega_{pd}}{2\omega_{pi}} \right)^{2/3} ku_0 . \quad (115)$$

For smaller but still suprathermal drift velocities, there are two purely imaginary solutions, one of which is unstable, viz.

$$\omega \approx \pm i \left(\frac{\omega_{pd}}{\omega_{pi}} \right) ku_0 . \quad (116)$$

Taking into account ion–neutral collisions one can use the hydrodynamic approach, which yields for the ion susceptibility

$$\chi_i = -\frac{\omega_{pi}^2}{(\omega - ku_0)(\omega - ku_0 + iv_{in}) - k^2 v_{Ti}^2} . \quad (117)$$

The ion susceptibility for $(\omega - ku_0)^2, v_{in}|\omega - ku_0| \ll k^2 v_{Ti}^2$ has the form [250]

$$\chi_i = \frac{1}{k^2 \lambda_{Di}^2} \left[1 + iv_{in} \frac{\omega - ku_0}{k^2 v_{Ti}^2} \right] .$$

The instability condition is, as previously, $u_0 > \omega/k$, while the instability increment for $u_0 \gg \omega/k$ is determined by the expression

$$\gamma = \frac{1}{2} \omega_{pd} \left(\frac{\lambda_D}{\lambda_{Di}} \right)^3 \left(\frac{v_{in}}{\omega_{pi}} \right) (1 + k^2 \lambda_D^2)^{-3/2} \frac{u_0}{v_{Ti}} \quad (118)$$

and passes a maximum for $k\lambda_D \ll 1$. We note, however, that in the case $\gamma_{in} \ll kv_{Ti}$, the hydrodynamic approach ignores the dominant term associated with the Landau damping — that is, the second term in brackets in Eqn (113). The case of $u_0 \gg v_{Ti}$, with the ion–neutral and dust–neutral collisions (which always stabilize the instabilities considered) taken into account in a way similar to relation (103), was studied by Joyce et al. [185]. It is shown that low-frequency waves can be stable or unstable depending on the relation between v_{in}/ω_{pi} and v_{dn}/ω_{pd} for a fixed drift velocity u_0. The authors of Ref. [185] assumed that this instability could be a reason for the dust component 'heating' examined experimentally when lowering the neutral gas pressure.

4.3 Waves in strongly coupled dusty plasmas

As already noted in Section 3.1, in dusty plasmas it is relatively easy to achieve the situation in which the dust component is in a (strongly) nonideal state. In this case, the interaction and correlations between the dust particles can significantly influence the wave spectrum. Different theoretical approaches have been proposed to describe waves in strongly coupled dusty plasmas. We will dwell on some of them below.

The system of dust particles in the regime $1 \ll \Gamma_d \ll \Gamma_M$ is in a 'liquid-like' state, and its wave properties are similar to those of a viscous liquid. For a theoretical description of these waves, the method of 'generalized hydrodynamics' was employed in Refs [254–256]. In works [257, 258], the kinetic approach accounting for correlations between dust particles was applied. In Refs [259, 260], the dispersion relation was obtained using the quasi-localized charge approximation, originally developed to describe systems with long-range Coulomb interaction [261]. Numerical modeling of dusty plasmas can serve as the criterion of applicability of different theoretical models. Usually, advantage is taken of MD simulations within the framework of the Debye–Hückel model [262, 263].

We point out the main properties of waves in strongly coupled dusty plasmas, which are reproduced in most of the models. First, in addition to the longitudinal mode, the transverse mode also appears, which exhibits an acoustic-like dispersion $\omega \sim k$ (the group velocity is constant) and can exist for not too long wavelengths, $k > k_{cr}$ [255, 263, 264]. Longitudinal waves have an acoustic-like dispersion in the long-wavelength limit: $k\Delta \ll 1$. For short enough wavelengths, however, the acoustic character of the dispersion is violated and the group velocity can change even its sign, $\partial\omega/\partial k < 0$, i.e., the dependence $\omega(k)$ has a maximum, ω_{max}, the value of which can be significantly smaller than ω_{pd} and typically decreases with increasing $\varkappa = \Delta/\lambda_D$. An example of the dispersion relation is shown in Fig. 14 which presents the results of numerical modeling along with their comparison with analytical results obtained using different theoretical models [263]. Notice that the dust–neutral collisions can reduce the effect of strong coupling in the dust system. The difference between strongly and weakly coupled dusty plasmas practically disappears if $v_{dn}/\omega_{pd} \sim 1$ [255, 259].

For stronger interparticle interactions, when $\Gamma > \Gamma_M$, the particles form a crystalline structure, and the wave spectrum becomes similar to that in solids. There exist one longitudinal and two transverse modes which are usually called dust lattice waves (DLW). To describe waves in dust crystals, the screened Coulomb potential of interaction between particles is usually employed. The electrons and ions are included in this model in an indirect way: they provide screening of the Coulomb interaction. The simplest one-dimensional model — a chain of equidistant particles — was first considered in Ref. [265] in connection with longitudinal waves. For linear waves, when the particle displacements from equilibrium positions are much smaller than the mean interparticle distance, the dispersion relation assumes the form

$$\omega^2 = \frac{2}{\pi}\,\omega_{pd}^2 \sum_{n=1}^{\infty} \frac{\exp\left(-\varkappa n\right)}{n^3}\left(1 + \varkappa n + \frac{\varkappa^2 n^2}{2}\right)\sin^2\frac{nk\Delta}{2},$$
(119)

where the summation is taken over all particles in the chain. In the limit of large values of $\varkappa$ ($\Delta \gg \lambda_D$), it is sufficient to take
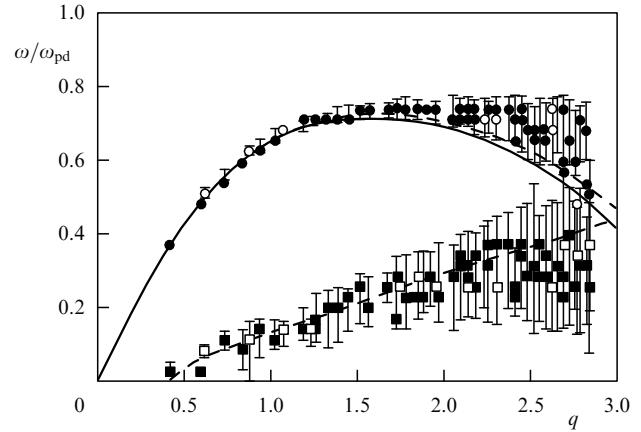
Figure 14. The dispersion relation for the longitudinal and transverse waves in a strongly coupled Debye–Hückel system at $\Gamma_d \approx 130$ and $\varkappa \approx 1.6$ [263]. The frequency is normalized to the plasma–dust frequency ω_{pd}, the wavelength is normalized to the characteristic interparticle distance $q = ka_{WS}$, where $a_{WS} = (4\pi n_d/3)^{-1/3}$ is the Wigner–Seitz radius. Symbols correspond to MD simulations. Circles stand for the longitudinal mode, squares for the transverse mode (solid for $N = 800$ particles, and open for $N = 250$ particles). The curves correspond to comparison of the simulation results with theoretical models. The upper solid (dashed) curve fits the dispersion relation for the longitudinal mode, based on quasi-localized charge approximation (generalized hydrodynamics). The lower dashed curve depicts the dispersion of the transverse mode in the approximation of generalized hydrodynamics (obtained by adjusting the parameters of the model to get better agreement with the numerical results). (The figure is kindly provided by S Hamaguchi.)

into consideration only the first term, yielding

$$\omega \approx \sqrt{\frac{2}{\pi}}\,\omega_{pd}\left(1 + \varkappa + \frac{\varkappa^2}{2}\right)^{1/2}\exp\left(-\frac{\varkappa}{2}\right)\sin\frac{k\Delta}{2}.\quad(120)$$

Acoustic-like dispersion takes place at $k\Delta \ll 1$: $\omega = C_{DL}k$. Expression (120) plays an important role in the physics of dusty plasmas because oscillations in the one-dimensional chain of strongly interacting particles can be relatively easily realized in experiments. Moreover, relation (120) is convenient for simple estimations of the characteristic wave frequency in ordered dusty plasma structures (see Section 3). Accounting for dust particle collisions with neutral particles reduces, as ever, to the substitution of $\omega(\omega + iv_{dn})$ for ω^2 in the left-hand side of dispersion relation (119).

In a similar way, dispersion relations for longitudinal waves in two-dimensional dust crystals can be obtained [266]. Dispersion relations for longitudinal and transverse waves in two-dimensional hexagonal lattices of dust particles and three-dimensional bcc and fcc lattices were derived in Ref. [267].

Vertical oscillations in a horizontal chain of strongly interacting dust particles (transverse oscillations) in a sheath were considered in Ref. [268]. The dispersion relation for this mode, assuming the screened Coulomb interaction potential and taking into account only the interaction between neighboring particles, takes the form

$$\omega^2 = \Omega_v^2 - \frac{\omega_{pd}^2}{\pi}\exp\left(-\varkappa\right)(1 + \varkappa)\sin^2\frac{k\Delta}{2}.\quad(121)$$

Replacement of the characteristic frequency Ω_v of vertical confinement by the horizontal one Ω_h gives the dispersion relation for the second transverse (horizontal) mode. Mod-

ifications of the dispersion relations (120) and (121) for longitudinal and transverse modes in a one-dimensional chain of dust particles due to ion focusing downstream from the particles (in the ion flow directed to an electrode) were considered in Ref. [269].

4.4 Experimental investigation
## of wave phenomena in dusty plasmas

4.4.1 Dust-acoustic waves. Low-frequency fluctuations of the dust-component density were first observed in an experiment on dusty plasma crystallization [223]. The experiment was performed in an rf magnetron discharge. At pressures of a few hundred mTorr, dust particles formed highly-ordered structures. When lowering the pressure, self-excited fluctuations of plasma and dust density at a frequency $f \sim 12$ Hz were observed if the particle density exceeded some critical value. Later on, this phenomenon was interpreted as the first observation of dust-acoustic waves in the laboratory [270]. In addition, low-frequency modes and possible mechanisms corresponding to these modes (including dust-acoustic waves) in an rf discharge were considered in Ref. [271].

A spontaneous excitation of low-frequency perturbations of the dust density was observed in the plasma of a Q-machine in Ref. [224]. The waves propagated with velocities $v_{ph} \sim 9$ cm s^{-1}, wavelengths $\lambda \sim 0.6$ cm, and, hence, frequencies $f \sim 15$ Hz. The excitation of these waves was interpreted to be the result of the streaming instability of the dust-acoustic waves, associated with the presence of a constant electric field $E \sim 1$ V cm^{-1} in the plasma, leading to ion drift relative to the dust component.

In experimental investigations of dust-acoustic waves, a dc discharge is often used. For example, the facility shown schematically in Fig. 15a was employed in experiments [272, 273]. A discharge was formed in nitrogen gas at a pressure $p \sim 100$ mTorr by applying a potential to an anode disk 3 cm in diameter located in the center of the discharge chamber. A longitudinal magnetic field of about 100 G provided radial plasma confinement. If the discharge current was sufficiently high (> 1 mA), dust-acoustic waves appeared spontaneously, similar to earlier experiments [224]. To investigate the properties of the waves in more detail, a low-frequency sinusoidal modulation with frequencies in the range $6-30$ Hz was applied to the anode. An example of the observed waves is shown in Fig. 15b for three different excitation frequencies. Assuming that the wave frequency is determined by the external excitation frequency, the dispersion relation — the $k(\omega)$ dependence in this case — can be obtained by measuring the wavelength. The results are shown in Fig. 15c. The observed waves exhibit linear dispersion $\omega \propto k$ and propagate with a velocity $v_{ph} \sim 12$ cm s^{-1}. This value is in reasonable agreement with the theoretical expression (101) for the dust-acoustic wave velocity [272]. One can conclude, therefore, that the observed waves correspond to the dust-acoustic waves.

A spontaneous excitation of low-frequency dust-acoustic waves was also observed in the positive column of a dc
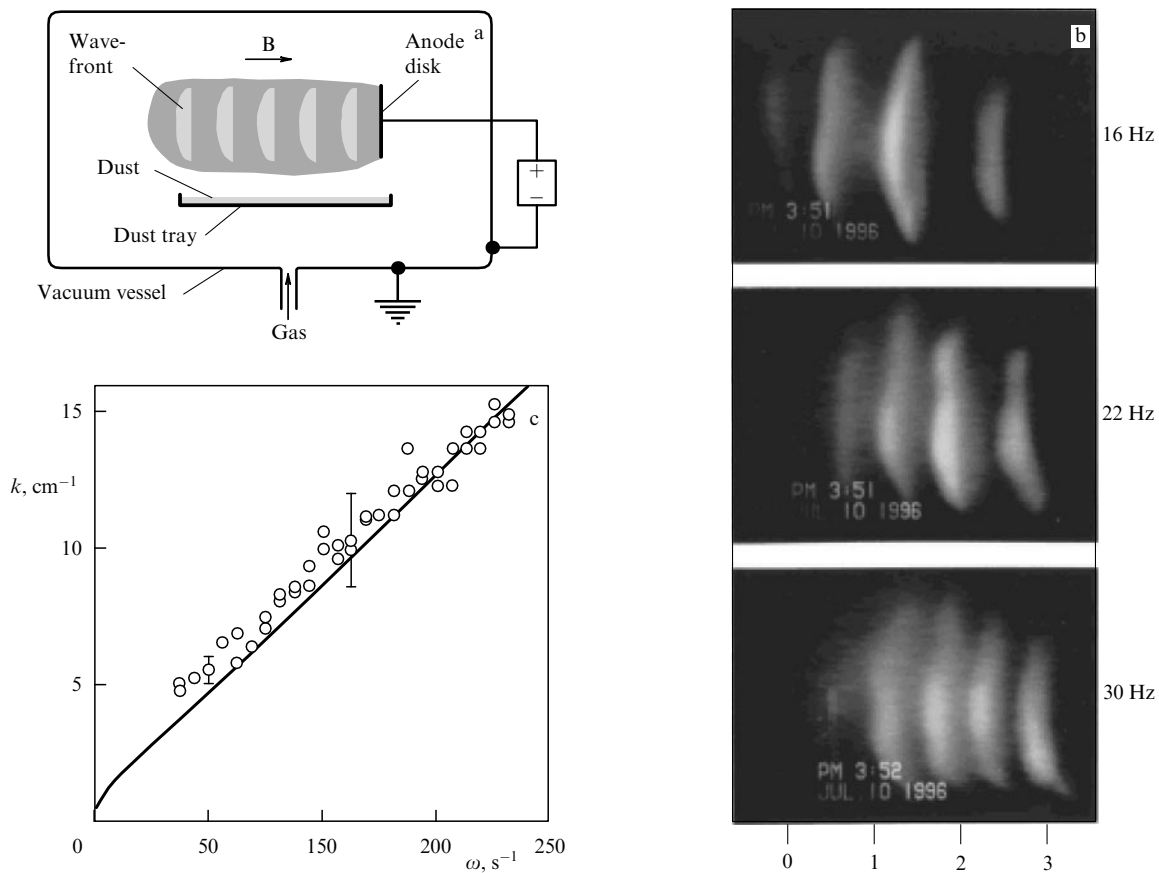
Figure 15. (a) Schematic diagram of the experimental facility used to investigate dust-acoustic waves in a dc gas discharge [273]. (b) Video images of typical wave structures in dusty plasma for three different values of the external excitation frequency (shown to the right of the images). (c) Experimentally obtained dust-acoustic wave dispersion relation (circles). The solid curve is computed from the theoretical dispersion relation which accounts for the dust–neutral collisions [see Eqn (103)]. (The figure is kindly provided by R Merlino.)
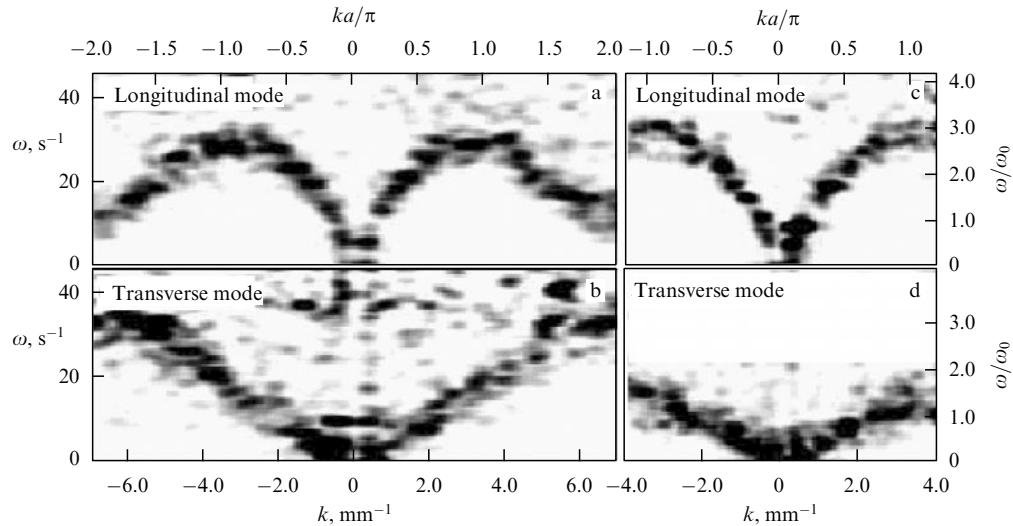
Figure 16. Spectrum of fluctuation energy density in $(\mathbf{k}, \omega)$-space in the absence of any intentional wave excitation [281]. Darker grays correspond to higher wave energy. Energy is concentrated along a curve corresponding to a dispersion relation. Figures (a) and (c) are for the longitudinal mode, while (b) and (d) are for the transverse mode. Vector $\mathbf{k}$ is directed parallel (a and b) and perpendicular (c and d) to a prinitive translation lattice vector $\mathbf{a}$. Here, $\omega_0 = 11.6$ s^{-1} is the plasma – dust frequency. (The figure is kindly provided by S Nunomura.)

discharge [18, 225] in the experimental apparatus shown schematically in Fig. 9. By reducing the neutral gas pressure and/or the discharge current, as well as by adding new particles to the discharge, a longitudinal dust-density wave propagating in the direction of the electric field (downward) was excited. A typical wave pattern is shown in Fig. 1c. The characteristic parameters of waves are: frequency $\omega \sim 60$ s^{-1}, wave number $k \sim 60$ cm^{-1}, and velocity of wave propagation $v_{ph} \sim 1$ cm s^{-1}. As shown in Ref. [18], the ion – dust streaming instability alone cannot be responsible for exciting the waves observed because damping effects should stabilize the dust-acoustic waves. In the same work, a new instability mechanism was proposed, the combination of which with the streaming instability allows us to describe the linear stage of spontaneous wave excitation. The proposed new mechanism can be qualitatively explained in the following way. The dust particles levitate in the plasma due to the balance of electric and gravity forces. When waves propagate, the dust charge experiences variations in response to electron and ion density perturbations. When there is a certain correlation between the dust charge phases and velocity perturbations, the dust particles can gain energy from the discharge electric field, which leads to wave amplification. The quantitative results obtained in Ref. [18] are in reasonable agreement with experimental observations. A similar mechanism was used for explaining wave instability in an inductively coupled rf discharge [274].

We note that when analyzing experimental findings the theory of dust-acoustic waves in weakly coupled plasmas is often used, while in experiments the dust particles can interact strongly. As already noted in Section 4.3, this can be relevant in the case of strongly dissipative systems, when $v_{dn} \sim \omega_{pd}$ (see, e.g., Ref. [275]). In addition, density perturbations of the dust component often have large enough amplitudes, i.e., the waves are essentially nonlinear. Nevertheless, in most of the works the linear theory is used, which may also be relevant in some cases, for instance, when describing instability threshold.

4.4.2 Waves in dust crystals. Excitation of waves in strongly ordered structures of dust particles (dust crystals) is often employed as a diagnostic tool in studying dusty plasmas. The main parameters entering into the dispersion relation (within the Debye – Hückel model) are the particle charge Z_d, and the ratio of the interparticle distance to the screening length — the lattice parameter $\varkappa$. Other parameters are either known in advance (e.g., particle mass) or can be easily determined in the experiment (e.g., mean interparticle distance). Hence, Z_d and $\varkappa$ can be estimated by comparing an experimental dispersion relation with a relevant theoretical model.

The excitation of waves in a one-dimensional chain of particles, formed in the sheath of an rf discharge, is described in Ref. [276]. The excitation was effected by applying a periodic potential on a small probe placed near one of the chain ends. In a modified experiment [277], the edge particle was excited by a modulated laser beam focused on it. In this experiment, the lattice parameter is determined as $\varkappa \approx 1.6 \pm 0.6$; the charge was measured independently by the vertical resonance method. We also note experiment [278] in which the instability of the vertical oscillations in a horizontal chain of dust particles (transverse mode) in the electrode sheath of a dc discharge was developed. The instability observed was attributed in this work to the charge delay mechanism considered in Section 4.1.

Laser excitation of waves was employed for an analysis of the longitudinal mode in a two-dimensional dust crystal [266]. The experiments were performed at different pressures. With increasing pressure, the lattice parameter $\varkappa$ estimated from the experiment slightly decreased. However, similar to most of the experiments in the sheath of an rf discharge, it was in the range $\varkappa \sim 0.5 - 2$. Transverse modes in a two-dimensional dust crystal, excited by laser radiation, were analyzed in Ref. [279]. Finally, an analysis of laser-excited longitudinal and transverse waves in a two-dimensional crystal was made in Ref. [280]. The experimental results are in qualitative agreement with the theory [267], which allows us to use them for an estimation of Z_d and $\varkappa$.

It is not necessary to excite the waves externally when studying the dispersion relations: this information is already contained in the random (thermal) motion of dust particles. In work [281], the dispersion relations for the longitudinal and transverse modes were measured in the absence of any external excitation. Using a Fourier transform of the particle velocity, the wave amplitude $V_{\mathbf{k}, \omega}$ and energy density $\sim V_{\mathbf{k}, \omega}^2$ were computed. As follows from Fig. 16, the highest values of the energy density are concentrated in proximity to distinct curves in $(\mathbf{k}, \omega)$-space; these curves are identified as dispersion curves. We note that in the experiment considered, the dust component was not in thermal equilibrium with the neutral component. The particle velocity distribution was close to Maxwellian one, with the mean kinetic energy several times larger than the temperature of the neutrals. This indicates the existence of a source of (stochastic) energy for the dust particles, which is mainly dissipated in dust – neutral collisions.

In work [282], solitary waves in a hexagonal monolayer dust crystal were investigated. The crystal was made from monodispersed particles levitating in the electrode sheath of a capacitively coupled rf discharge. To excite the waves, a short potential pulse (-30 V, 100 ms) was applied to a thin filament situated below the crystal, which led to the appearance of a one-dimensional disturbance (compression) propagating perpendicular to the filament. It was found that the excited wave possessed the main features of solitons, in particular, the product of its amplitude and width squared remained constant during propagation. A theory developed in Ref. [282] describes well the experiment and is based on the equation of motion for the one-dimensional chain of dust particles, the equation which takes into account dispersion, nonlinearity, and damping.

In conclusion, let us briefly discuss another effect associated with the wave processes in dusty plasmas. The so-called Mach cones with an opening angle μ determined by the ratio of the wave propagation velocity (sound velocity) in a medium to a (supersonic) disturbance velocity, $\sin \mu = c_{\mathrm{s}}/V$, can form in dusty plasmas due to acoustic dispersion and can be used for dusty plasma diagnostics [283]. In laboratory conditions they were observed in Refs [284, 285] and their excitation was attributed to the presence of fast (supersonic) particles beneath the lattice of a two-dimensional dust crystal in the sheath of an rf discharge, whereas the origin of such fast particles was not fully understood. In work [286], the focused spot of a laser beam propagating with a supersonic velocity through a plasma crystal was utilized as the supersonic object.

5. New directions in experimental research

In this section, some new directions in the laboratory investigation of dusty plasmas are considered. The term 'new' is of course conditional here, because the field itself is very recent — active investigations began only ten years ago. In this review we mainly focus on the following new directions of dusty plasma research: investigations under microgravity conditions, external perturbations, and the use of nonspherical particles. In conclusion, we briefly mention potential applications of dusty plasmas.

5.1 Investigations of dusty plasmas under microgravity conditions

In many cases, the force of gravity considerably limits the possibilities of laboratory experiments in ground-based conditions. For example, it prevents the formation of extended three-dimensional structures. To support particles against gravity, strong electric fields are required, which only exist in plasma sheaths or striations. These regions are characterized by a high degree of anisotropy and suprathermal ion flows. In these conditions, external forces are comparable with the interparticle forces. Hence, most dusty plasmas investigated on earth are essentially two-dimensional, strongly inhomogeneous, and anisotropic in the vertical direction. Most of these complications can be avoided by performing experiments under microgravity conditions [14]. Such experiments were recently carried out in several types of plasmas. In Sections 5.1.1 – 5.1.3, we briefly discuss each of them separately.

5.1.1 Experiments on dusty plasma induced by UV radiation. The behavior of an ensemble of particles charged by solar radiation was studied in a microgravity experiment on-board the 'Mir' space station [59]. The main elements of the experimental setup (see Fig. 17a) comprised: glass ampoules with bronze particles of radius $25 - 50$ μm coated with a monolayer of cesium; an illumination source — a semiconductor laser with an operating wavelength 0.67 μm and power 30 mW, and a recording system — a video camera and videomodule. Since in the initial state the particles were deposited on the ampoule walls, the experiment was performed employing the following scheme: dynamic effect (impact) on the system; relaxation for a period $3 - 4$ s in order to reduce the random particle velocities acquired from the initial impulse (impact); illumination of the system by solar
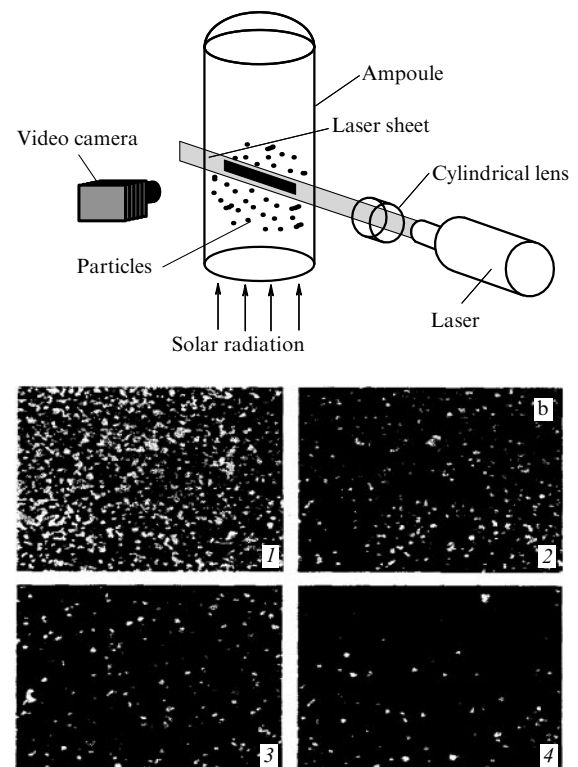
Figure 17. (a) Schematic representation of the experimental setup for studying the behavior of dust particles charged by solar radiation under microgravity conditions. (b) Sequence of states of the dust particle system within 2 s (*1*), 20 s (*2*), 50 s (*3*), and 110 s (*4*) after shaking the ampoule in experiments on the investigation of the behavior of dust particles charged by solar radiation in microgravity conditions.

radiation for a period of several minutes with subsequent relaxation to the initial state — particle deposition on the walls. Figure 17b illustrates the evolution of the particle system in an ampoule at a buffer gas pressure of 40 Torr. The particle charge was determined from a comparison of the experimentally established time dependence of dust density in the ampoule with numerical modeling or with results of particle trajectory analysis [59, 287]. The charges determined in this way fell in the range $(5-10) \times 10^4$ elementary charges. No strong correlation of interparticle distances was observed. The pair correlation functions obtained indicate that non-ideal short-range-ordered structures were formed in this experiment.

5.1.2 Experiments in a dc gas discharge. The experimental investigation of dusty plasmas in a dc gas discharge was performed on-board the 'Mir' space station [288]. The major difference between this experimental apparatus and a similar one used in ground-based experiments (see Fig. 9) was the presence of a two-grid electrode placed between the cathode and the anode. During the experiments, the electrode was at a floating potential and prevented negatively charged particles from escaping to the anode.

In the experiments, neon gas at a pressure $p = 1$ Torr was utilized. The discharge current was varied in the range from 0.1 to 1 mA. Nonmonodispersed bronze spheres with a mean radius $\bar{a} \approx 65$ μm were used. The electron temperature and the plasma number density were estimated as $T_e \sim 3-7$ eV and $n_e \sim n_i \sim 10^8 - 3 \times 10^9$ cm^{-3}, respectively.

The experiment was performed using the following procedure. The particles were initially deposited on the tube walls. For this reason, the system was subjected to dynamic action after initiating a discharge with a given current I. In a plasma volume, the particles were charged by collecting electrons and ions and moved toward the anode. In the vicinity of the grid electrode a part of the particles trapped in this region formed a stationary three-dimensional structure (cloud). A typical image of such a structure recorded by a video camera is shown in Fig. 18. When the discharge was switched off, the particles went back to the tube walls. The experiment was repeated at a new discharge current value.

An analysis of video images of the stationary dust structure formed near the grid electrode allowed the measurement of the static (pair correlation function) and dynamic (diffusion coefficient) characteristics of the dust particle system. Comparison with numerical simulations of dissipative Debye – Hückel systems (see Section 3.1) was employed for dusty plasma diagnostics [289, 290]. In addition, an analysis of the particle's drift motion to the grid electrode at the initial stage of the experiment was used to estimate the particle charge. Below we summarize the main experimental findings.

Measured pair correlation functions revealed the formation of ordered structures of dust particles of a liquid-like type (short-range order). This is in agreement with the estimate of the modified coupling parameter Γ^* (made on the basis of measuring the diffusion coefficient) which decreases from ~ 75 to ~ 25 with an increase in the discharge current. The kinetic energy of chaotic particle motion was estimated as $T_d \sim 10^5$ eV. Finally, the charge was estimated as $Z_d \sim -2 \times 10^6$, which corresponds to the surface potential of about -40 V and is considerably larger than the magnitude predicted by the OML theory. Note that the physics of charging and interaction of large particles $(a \geqslant \lambda_{Di}, l_i)$ has
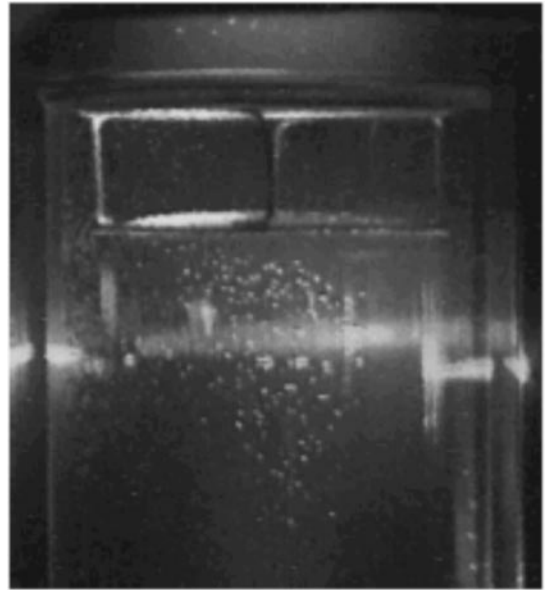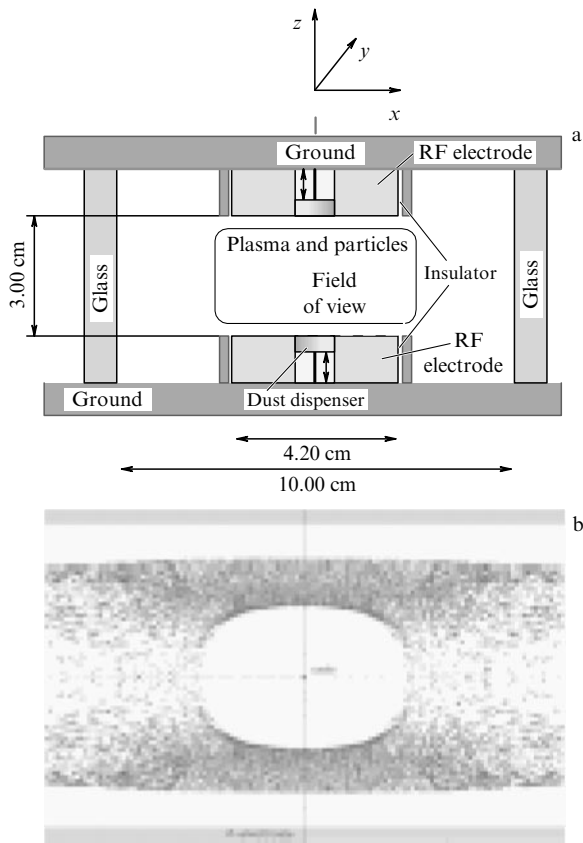

Figure 18. Video image of a typical structure of a dust cloud formed in the vicinity of a grid electrode in a dc discharge under microgravity conditions. The characteristic size of the cloud is about 2 cm in the radial direction.

been relatively poorly studied, mainly because ground-based experiments with such large particles are typically impossible. For this reason, the above-described experiments in microgravity conditions are of obvious interest.

5.1.3 Experiments in an rf discharge. Dusty plasmas formed in an rf discharge have been intensively investigated under microgravity conditions. A typical scheme of an experimental setup is shown in Fig. 19a. The results of the first rocket experiments (within ~ 6 min of microgravity) and their qualitative analysis were reported in Ref. [130].

Currently, the 'Plasma Crystal' laboratory, created within the framework of the Russian – German scientific cooperation program and operating on-board the International Space Station (ISS), is actively functioning. Its main tasks include investigations of dusty plasma crystals, phase transitions, wave phenomena, properties of boundaries between different plasma regions, etc. in a three-dimensional isotropic dusty plasma at the kinetic level. The first 'basic' experiments designed to study the behavior of the dust component over a broad range of dusty plasma parameters were performed at the beginning of March 2001. Monodispersed systems and binary mixtures of particles of different size ($a = 1.7$ and 3.4 μm) were investigated at different argon pressures and rf powers. At present, most of the investigations are in the active phase or in the stage of data analysis. Thus, we first discuss several important phenomena which were observed in rocket experiments [130, 291], and then briefly mention some of the published results achieved on-board ISS.

The typical structure of the dust particle system in an rf discharge under microgravity conditions is shown in Fig. 19b. As can be seen from the figure, the dust component does not fill the whole volume: the central part of the discharge (void) is free of dust particles, as are the regions adjacent to the electrodes and walls. The boundary between dusty plasma and the usual electron – ion plasma is sharp both in the region of the void and at the periphery. At the periphery, far from the central axis of the discharge, the particles exhibit convective

Figure 19. (a) Schematic of the experimental setup for investigating the dust structures in an rf gas discharge under microgravity conditions. The main dimensions are indicated in the figure. (b) Typical video image of the dust cloud in an rf discharge under microgravity conditions. The central part of the discharge is free of dust particles — a so-called void is formed.

motions. Close to the axis, the structure is stable and does not support convective motion. Here, the dust cloud reveals the highest ordering. The particles form layers parallel to the electrode in the vicinity of the outer cloud boundary, but this symmetry is broken considerably toward the internal part of the cloud.

One of the main problems connected with the structure of dust clouds in an rf discharge under microgravity conditions is the void formation. It is common to assume that the electric field in the discharge is directed from the center to the periphery, and hence the electrostatic force F_e acting on negatively charged dust particles is pointed to the center. The formation of a void implies the occurrence of some effect which not only compensates for the action of the electric force, but also leads to the repulsion of dust particles from the central region of the discharge. It is established that the void forms at a relatively small number of particles in the discharge too, i.e., its formation is not an essentially collective effect. This can correspond to an internal property of the discharge — the existence of some force directed from the center to the periphery and exceeding the electrostatic force. In work [130], it was assumed that the void could be caused by the thermophoretic force. This assumption has not been confirmed so far. Moreover, the results of numerical simulation of the system considered [292] raise some doubts about this assumption. In works [131, 132, 293], it was suggested that the ion drag force F_I is responsible for the void formation. The necessary condition for the void

formation is $|F_I/F_e| > 1$, at least in the vicinity of the discharge center. This condition was verified in Ref. [133] using new results for the ion drag force acting on an individual particle in a collisionless regime (for ion scattering from a dust particle). Below, we present details of this estimation. In a weak electric field, $E \ll T_i/el_i$, the ions drift with a subthermal velocity — this situation wittingly takes place in the vicinity of the center (the electric field is zero in the center). The ion drift velocity equals $u = \mu_i E$, where μ_i is the ion mobility defined as $\mu_i = el_i v_{Ti}/T_i$. Using expressions (51) and (61) for F_e and F_I, and taking into account that both the forces are proportional to the electric field we get $|F_I/F_e| \approx \delta l_i/\lambda_D$, where δ is a weak function of dusty plasma parameters: $\delta \sim 0.5$ for typical experimental conditions. Therefore, in the collisionless regime when $l_i \gg \lambda_D$ at least should be satisfied, the condition $|F_I/F_e| > 1$ is always fulfilled. For this reason, it is quite natural to assume that the void formation is caused primarily by the ion drag force.

Reverting to the experiments performed on-board ISS we mention work [294] describing basic experiments on dust component crystallization. Under certain conditions, the coexistence of domains of fcc, bcc, and hcp structures has been observed in the mostly ordered dusty plasma region — that is, the lower central part of the dust cloud. At the same time, string-like structures (when particles are aligned in vertical chains) which are typical for ground-based experiments in an rf discharge have not been observed. The results of the structure observation were compared with theoretical predictions of the Debye–Hückel model. A comparison of static (structure) and dynamic characteristics of the dust particle system with those obtained from numerical modeling within the framework of Debye–Hückel systems (see Section 3.1) and from dc-discharge research was performed in Refs [289, 290]. This comparison can be used to estimate the coupling strength in dusty plasmas, which is mostly determined by the particle charge and plasma screening length. In work [295], the longitudinal oscillations excited by applying a low-frequency modulation voltage to the electrodes were analyzed. Comparison of the experimental dispersion relation with the theoretical prediction was used to estimate the dust particle charge. Excitation of shock waves in the dust component by a gas flow was described in Ref. [296]. Investigation of the boundaries between the conventional electron–ion plasma and dusty plasma, as well as between two different dusty plasmas composed of particles of different sizes, was reported in Ref. [297]. The 'decharging' of dusty plasmas by switching off the rf voltage was studied in work [298].

5.2 External perturbations
Investigation of different external perturbations of dusty plasma structures is of substantial interest for several reasons. First, the perturbations which affect the background plasma insignificantly can be employed as diagnostic tools. External perturbations can also be used to control the spatial location and ordering of dusty plasma structures, and to input additional energy in order to investigate their behavior in extreme conditions.

The action of laser radiation finds wide use. As discussed above, it is employed to manipulate particles when measuring the interparticle potential (see Section 2.4), excite the dust cluster rotation (see Section 3.3), excite vertical oscillations of individual particles (see Section 4.1) and low-frequency waves in dusty plasma structures (crystals) (see Section 4.4), and
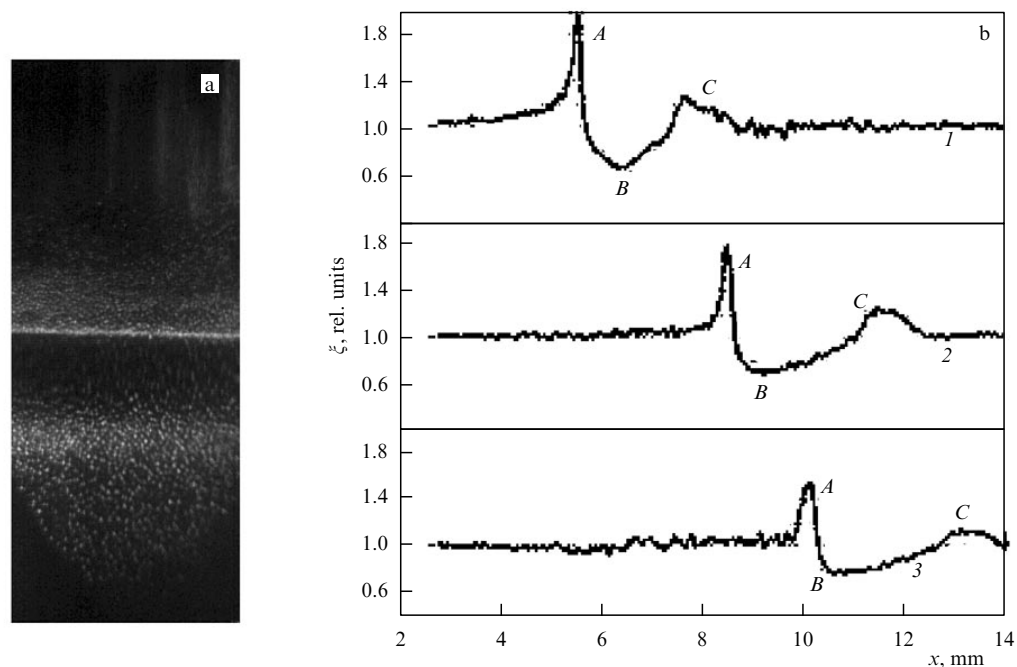
Figure 20. Video image of a solitary wave (a) and compression factor ξ in the wave at different moments in time (b). The time interval between curves *1* and *2* is 120 ms, and between curves *2* and *3* 60 ms. The wave is excited by a gas-dynamic impact in the dc gas-discharge setup. The symbols *A* and *C* correspond to the compression regions, and symbol *B* corresponds to the rarefaction region.

form Mach cones (see Section 4.4). The application of laser radiation is still expanding. In this context, we note recent works where laser radiation was utilized for manipulating dust particles in a dc discharge in order to determine the particle charges [83] and forming a localized 'point' source to investigate the waves emitted by this source in a two-dimensional dusty plasma crystal in an rf discharge [299].

'Electrostatic' action on dusty plasma structures is also employed as an external perturbation. Typically, an additional low-frequency voltage is applied either to the electrode(s) or to a small object (probe) situated near the dust particle structure. This method is widely used to excite waves in dusty plasma structures. In addition, in work [300] it was used to analyze the long-range interaction between the dust particles levitating near the sheath edge of an rf discharge and a macroscopic object — a thin wire. It is shown that for a negative potential of the wire the nearest particles experience electrostatic repulsion, while at sufficiently long distances an attraction takes place. The ion drag force was taken to be a mechanism responsible for long-range attraction. Finally, the influence of a probe situated near the sheath edge of an rf discharge on the structure and the properties of dust crystals formed in this region was analyzed in Ref. [301].

A magnetic field can also serve as a source of external perturbation. As noted in Section 3.3, the vertical magnetic field can lead to rotation of dust crystals in a horizontal plane. The effect is associated with the tangential component of the ion drag force which appears due to distortion of ion trajectories in a magnetic field. This issue was discussed in detail in Ref. [125].

Finally, a 'gas-dynamic' action on a dusty plasma structure can also be employed. As an example, we consider the excitation of nonlinear waves in a dc discharge [302]. The main difference from the experimental setup described in Section 3.2 was the following. Below the hollow cylindrical

cathode, a plunger was set which could move with the aid of a permanent magnet. The plunger could be moved at a speed of about $30-40$ cm s^{-1} (for a distance of $4-5$ cm). A grid kept at a floating potential was inserted 7 cm above the cathode. When the plunger was moving downward, the particles were also moving downward to a region of stronger electric field, and the dust structure became unstable. It was possible to excite solitary waves as well as instabilities that appeared in the whole volume of dusty plasma. The image of a solitary wave and profiles of the compression factors at different moments in time are shown in Fig. 20. As follows from the figure, the perturbation consists of two compression regions separated by a region of rarefaction. Both compression regions move downward with velocities of $1.5-3$ cm s^{-1} (on the order of the dust-acoustic wave velocity), but the lower compression moves slightly faster. The minimum of the rarefaction region initially moves with the lower compression and then acquires the speed of the upper compression. In this way, an increase in the front steepness of the upper compression region is observed. In the rarefaction region, the upward motion of dust grains is observed with velocities up to 15 cm s^{-1}, which is several times larger than the dust-acoustic wave velocity. Theoretical interpretation of the phenomenon observed constitutes an intriguing problem.

5.3 Dusty plasma of strongly asymmetric particles
Most of the experimental and theoretical works dealing with investigation of dusty plasmas were performed with spherical particles. Only recently has dusty plasma with asymmetric particles been investigated experimentally and theoretically [303–308]. Note that in Ref. [303] the geometrical aspect ratio was $\alpha \sim 3$, and the first experiments with strongly asymmetric particles [$\alpha = (40-80) \gg 1$] were carried out in Ref. [304].

It is well known that colloidal solutions, which have much in common with dusty plasmas, show a much broader
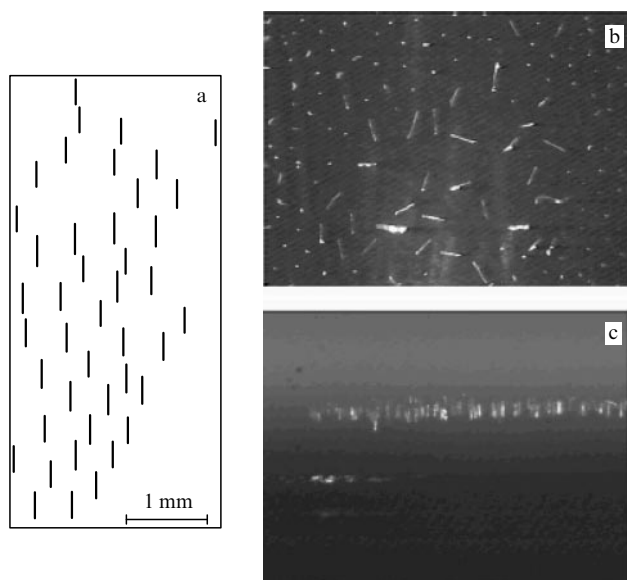
Figure 21. (a) Digitized image of a part of a horizontal section of a structure involving cylindrical macroparticles of length 300 μm and diameter 15 μm levitating in a striation of a dc discharge in a neon/hydrogen mixture (1:1) at a pressure of 0.9 Torr and discharge current of 3.8 mA. (b, c) Typical video images of structures formed by cylindrical particles levitating near the sheath edge of an rf discharge. The discharge was initiated in krypton at a pressure of 52 Pa and discharge power of 80 W. Figure (b) shows a top view; dots correspond to vertically oriented particles. Figure (c) gives a side view.

spectrum of possible states in the case of strongly asymmetric cylindrical or disk particles. In such solutions, liquid phase and several liquid–crystal and crystal phases with different degrees of orientational and positional ordering can be observed. It is also well known that the employment of cylindrical probes (in addition to spherical) considerably broaden the possibilities of low-temperature plasma diagnostics. It is obvious that the use of cylindrical (in addition to spherical) particles can considerably broaden the potentialities of *noninvasive* plasma diagnostics.

In work [304], in which an experimental setup analogous to that described in Section 3.2.2 was adapted, the nylon particles ($\rho = 1.1\,\mathrm{g\,cm^{-3}}$) of length 300 μm and diameters 7.5 and 15 μm, as well as particles of lengths 300 and 600 μm and diameter 10 μm, were introduced into the plasma of a dc discharge. The discharge was initiated in neon or a neon/hydrogen mixture at a pressure of $0.1-2$ Torr. The discharge current was varied from 0.1 to 10 mA. In this parameter range, standing striations were formed in the discharge, which made possible particle levitation. A neon/hydrogen mixture was used to levitate heavier particles of larger diameter (15 μm) or larger length (600 μm). In this case, the particles formed structures consisting of $3-4$ horizontal layers. Lighter particles levitated in pure neon and formed much more extended structures in the vertical direction. In Fig. 21a, a part of a horizontal section of an ordered structure levitating in a striation of a dc discharge excited in a neon/hydrogen mixture (1:1) at a pressure of 0.9 Torr and discharge current of 3.8 mA is shown.

The observation of structures formed by microcylinders revealed clear ordering. All particles lay in the horizontal plane and were oriented in a certain direction. It could be expected that their orientation was determined by the cylindrical symmetry of the discharge. However, no correlation between the particle orientation and discharge tube symmetry was found. Nor could the preferential orientation of the particles be explained by the interparticle interaction, because individual particles were oriented in the same direction. Presumably, the preferential orientation was related to an insignificant asymmetry in the discharge tube. This was confirmed by the fact that the orientation could be changed by introducing an artificial perturbation into the discharge.

In later experiments [306], nylon particles of lengths 300 and 600 μm and diameter 10 μm coated by a thin layer of conducting polymer were utilized. In a dc discharge they formed structures identical to those formed by uncoated particles of the same size.

Levitation of cylindrical particles was also observed near the sheath edge of a capacitively coupled rf discharge [305]. In this experiment, the cylindrical particles of length 300 μm and diameters 7.5 and 15 μm were used, and a small fraction of very long particles (up to 800 μm) 7.5 μm in diameter was also present. A typical picture of a structure formed by these particles is shown in Fig. 21b. Longer particles are oriented horizontally and mainly located in the central part limited by a ring placed on the electrode, while shorter particles are oriented vertically along the electric field. Levitation and ordering of the cylindrical particles occurred only for pressures higher than 5 Pa and a discharge power above 20 W. An increase in the discharge power did not significantly affect particle levitation. The average distance between vertically oriented particles varied from 1 to 0.3 mm. An increase in particle density leads to quasi-crystalline structure degradation and an increase in particle kinetic energies. A further increase in density is impossible because the particles 'fall down' from the structure. Levitation of particles coated by a conducting polymer was not observed in an rf discharge for the conditions at which the dielectric particles of the same size and mass could levitate. Instead, the conducting particles stuck to the electrode, preserving vertical orientation, and some stuck to each other forming multiparticle fractal complexes with up to 10 particles.

The preferential orientation of cylindrical particles is determined by an interplay between the interaction of non-uniform electric fields in striations or sheaths with a particle charge and induced dipole and quadrupole moments. In a dc discharge, the particle charge is typically larger than in an rf discharge, allowing particle levitation in weaker electric fields. In this case, the dipole moment, which is proportional to the electric field strength squared, is much smaller than in an rf discharge. This can explain the different orientations of similar-sized particles: horizontal in a dc discharge, and vertical in an rf discharge. Theoretical investigations into the charging of horizontally and vertically oriented particles, their equilibrium positions (levitation height and angle), and the energy of electrostatic interaction between cylindrical particles depending on their orientation can be found in Ref. [309].

5.4 Dusty plasma at cryogenic temperatures
The coupling in the dust component increases as the temperature of a gas discharge decreases. This is connected both with a direct fall in dust particle kinetic energy and a diminution in the screening length due to a decrease in the ion temperature. The first experiments with dusty plasmas in a cryogenic gas discharge under a liquid-nitrogen temperature

of 77 K were performed in work [310]. Both glow dc discharge and capacitively coupled rf discharge were used. Ordered dust structures in the glow cryogenic discharge were similar to the structures observed at room temperatures. However, a much stronger influence of the thermophoretic force on the dynamics and stability of dust structures was observed. Very extensive (about 30 cm) ordered structures consisting of long chains and occupying practically the whole volume of the positive column of a dc gas discharge were for the first time observed in a dc discharge as well.

In experiments with an rf discharge it was found that at cryogenic temperatures the density of dust particles in the main volume of the ordered structures can increase considerably, while at the periphery it is similar to that in common rf discharges. In the lower part of dust structures, the propagation of traveling density waves was observed. The dust-acoustic wave velocity in cryogenic conditions was several times larger than in normal conditions. With decreasing pressure, instabilities led to structure separation into transverse layers with clear boundaries. The authors of Ref. [310] explain the formation of much more dense structures in cryogenic plasmas mainly by the decrease of the Debye radius, which leads to an exponential decrease in the interparticle interaction energy and allows the particles to be closer to each other.

5.5 Possible applications of dusty plasmas
Dusty plasmas have already been applied in industry for many decades, for example, in such technologies as precipitation of aerosol particles in combustion products of electric power stations, plasma spraying, and electrostatic painting, as well as in a number of other areas. In the beginning of the 1990s it was understood that a large part of the contamination on the surface of silicon wafers during manufacturing of semiconductor elements for electronics was not coming from insufficient cleaning of the production area of dust, but was an unavoidable consequence of plasma etching and deposition technologies. In widespread capacitively coupled rf discharge reactors, all particles are charged negatively and levitate close to one of the electrodes. After switching off the discharge they deposit on the surface of the silicon wafer. Submicron-sized particles deposited on the surface of processable wafers can reduce the working surface, cause dislocations and voids, and reduce adhesion of thin films. Great efforts focused on reduction of the number of undesirable dust particles in industrial plasma reactors have given positive results [36, 37, 311], and this problem can be considered as practically solved.

For the power supply of space vehicles, automatic weather stations, antisubmarine buoys, etc., compact autonomous power-supply sources with a power about $1 - 10$ kW and with working resources of several years are necessary. At present, solar power photoelectric converters, thermoelectric sources with thermoemissive elements on ^{90}Sr, ^{238}Pu, or ^{210}Po, and thermoemissive converters (TEC), where a nuclear reactor on ^{235}U is used as the heat source, are widely applied. All these sources have disadvantages, in particular, very low efficiency. Moreover, a nuclear reactor is very complicated to produce.

Recently, in work [312], the conversion of nuclear into electric energy by the photovoltaic effect in wide bandgap semiconductors based on diamond films obtained by precipitation of the carbon from the gas phase (CVD diamond) and boron nitride was suggested. Creation of such sources has

become possible due to the investigation of diamond-film synthesis, resulting in the production of semiconducting structures, and the investigation of the physics of low-temperature dusty plasmas.

The principle of the action of the sources, which convert the energy of radioactive isotopes into electricity by the photovoltaic effect, is the following. Under the influence of ionizing radiation a specially selected gaseous mixture is excited and radiates in the UV range. The ultraviolet radiation due to the photovoltaic effect induces the electro-motive force in the wide bandgap semiconductor. For this purpose, semiconductors based on diamond structures are the most convenient because they have high radiation resistance and high conversion efficiency (up to 70%). As a radioactive isotope it is possible to utilize β-active isotopes having a comparatively high half-life period ($10 - 30$ years), for example, ^{90}Sr or similar solid isotopes, e.g., α-active ^{238}Pu.

To use solid isotopes in the photovoltaic converters, it is necessary to have the isotope surface area as large as possible. A homogeneous mixture of gas and isotope dust, which has a maximum possible surface-to-volume ratio, is the most attractive. Excitation of the gas mixture is accomplished by β- or α-radiation from the radioactive dust. Estimates show that at a dust size of $1 - 20$ μm and dust number density in the gas of $10^5 - 10^9$ cm^{-3} it is possible to obtain the power density of ~ 1 W dm^{-3}. The gas pressure has to be on the order of $1 - 10$ atm for effective energy conversion of β- or α-radiation into UV radiation.

The main physical problem arising during the creation of such a battery consists in the necessity of having the homogeneous gas – dust medium at pressures of several atmospheres. Results received recently in investigations of dusty plasmas and their condensation and crystallization [313, 314] demonstrate such a possibility. Self-consistent processes in such plasmas result in the establishment of an ordered stationary state which is necessary for the transport of the radiation from the volume of the exited gas to photo-converters.

In recent years it has become obvious that the presence of dust in plasmas does not always result in undesirable consequences. Powders produced employing plasma technologies can have interesting and useful properties: very small sizes (from a nanometer to the micrometer range), mono-dispersity, and high chemical activity. The size, structure and composition of the powder can be varied easily in compliance with the specific requirements of a certain technology. In this connection, two trends can be distinguished in applied research of dusty plasmas [37]. The first one represents a development of the well-established technologies of surface modification, except that in this case the surface of dust particles is the subject of treatment. With the aim of creating particles with specific properties, sputtering, surface activation, etching, or separation of clustered grains in plasmas can be adapted. The second important trend in applied dusty plasma research is the creation of new nanostructured materials, like thin films with an inclusion of nanometer-sized particles.

The typical size of the elements of integrated circuits in microelectronics is reduced every year and in the nearest future it will likely reach 10 nm. Furthermore, there is a tendency to replace the capacitively coupled rf discharge by the inductively coupled one. These plasmas are characterized by higher electron density and lower sheath potential. Altogether, this results in a reduced particle trapping

capacity and leads to the main part of the particles dropping on the surface of the silicon wafer during plasma processing. This implies that the solution introduced in the 1990s, which was mostly based on dust particle confinement in special traps, will not work anymore. This poses a serious problem to producers of integrated circuits of the next generation, which demands further applied research of the properties of dusty plasmas.

6. Conclusions

Despite a history spanning nearly a century, the investigation of dusty plasmas has acquired particular attention only during the last decade, after the experimental discovery of the crystallization of the dust component. Due to their unique properties dusty plasmas are successfully used in solving fundamental and applied problems. The simplicity of visualization permits measurements (of the dust component) at the kinetic level. In this case, a detailed analysis of thermodynamic and kinetic properties of dislocations and other defects of the dust lattices becomes possible. The latter have much in common with the usual crystalline lattice of solid bodies. Much attention is attracted to studies of easily excited linear and nonlinear low-frequency waves and their instabilities. Investigation of phase transitions in systems of symmetric and asymmetric dust particles provides useful information about critical phenomena and self-organization processes, in particular, about the possibilities of natural formation of ordered dusty-plasma structures in the universe. The first space experiments under microgravity conditions were performed on-board the space stations 'Mir' and ISS. A number of important and sometimes unexpected results have been obtained. The understanding of the observed effects is impossible without a detailed investigation of elementary processes in dusty plasmas, such as particle charging, interaction between the particles, the main forces acting on the particles, etc.

One of the most important application problems is the removal of dust particles when manufacturing computer chips by plasma-aided technologies. To solve this problem, a deep understanding of physical processes in a gas-discharge dusty plasma is necessary. Moreover, the unique possibility to confine and control physical and chemical properties of dust particles makes dusty plasma a perfect tool for creating powders with prescribed properties and for modifying them.

In this review, the authors tried not only to discuss the most significant experimental and theoretical results obtained recently, but also to mention problems which are as yet unsolved. The field of dusty plasmas is one of the most rapidly growing fields in physics — over the last few years more than one publication per day, on average, has appeared. There is no doubt, therefore, that many intriguing and important results will be obtained in the future.

The authors wish to express their sincere gratitude to V N Tsytovich for valuable discussions and useful comments made when reading the manuscript.

References

1. Goertz C K *Rev. Geophys.* **27** 271 (1989)
2. Northrop T G *Phys. Scripta* **45** 475 (1992)
3. Tsytovich V N *Usp. Fiz. Nauk* **167** 57 (1997) [*Phys. Usp.* **40** 53 (1997)]
4. Bliokh P, Sinitsin V, Yaroshenko V *Dusty and Self-Gravitational Plasmas in Space* (Dordrecht: Kluwer Acad. Publ., 1995)
5. Whipple E C *Rep. Prog. Phys.* **44** 1197 (1981)
6. Robinson P A, Coakley P *IEEE Trans. Electr. Insul.* **27** 944 (1992)
7. Tsytovich V N, Winter J *Usp. Fiz. Nauk* **168** 899 (1998) [*Phys. Usp.* **41** 815 (1998)]
8. Winter J, Gebauer G *J. Nucl. Mater.* **266–269** 228 (1999)
9. Winter J *Phys. Plasmas* **7** 3862 (2000)
10. Wuerker R F, Shelton H, Langmuir R V *J. Appl. Phys.* **30** 342 (1959)
11. Paul W, Raether M *Z. Phys.* **140** 262 (1955)
12. Ikezi H *Phys. Fluids* **29** 1764 (1986)
13. Chu J H, I L *Phys. Rev. Lett.* **72** 4009 (1994)
14. Thomas H et al. *Phys. Rev. Lett.* **73** 652 (1994)
15. Hayashi Y, Tachibana K *Jpn. J. Appl. Phys.* **33** L804 (1994)
16. Melzer A, Trottenberg T, Piel A *Phys. Lett. A* **191** 301 (1994)
17. Morfill G E, Thomas H *J. Vac. Sci. Technol. A* **14** 490 (1996)
18. Fortov V E et al. *Phys. Plasmas* **7** 1374 (2000)
19. Fortov V E et al. *Pis'ma Zh. Eksp. Teor. Fiz.* **63** 176 (1996) [*JETP Lett.* **63** 187 (1996)]
20. Fortov V E et al. *Phys. Lett. A* **219** 89 (1996)
21. Nefedov A P, Petrov O F, Fortov V E *Usp. Fiz. Nauk* **167** 1215 (1997) [*Phys. Usp.* **40** 1163 (1997)]
22. Fortov V E et al. *Pis'ma Zh. Eksp. Teor. Fiz.* **64** 86 (1996) [*JETP Lett.* **64** 92 (1996)]
23. Nefedov A P et al. *Pis'ma Zh. Eksp. Teor. Fiz.* **72** 313 (2000) [*JETP Lett.* **72** 218 (2000)]
24. Fortov V E et al. *Phys. Lett. A* **258** 305 (1999)
25. Fortov V E et al. *Phys. Lett. A* **284** 118 (2001)
26. Fortov V E et al. *Phys. Plasmas* **6** 1759 (1999)
27. Langmuir I, Found G, Dittmer A F *Science* **60** 392 (1924)
28. Zhukhovitskiĭ D I, Khrapak A G, Yakubov I T, in *Khimiya Plazmy* (Plasma Chemistry) Vol. 11 (Ed. B M Smirnov) (Moscow: Energoatomizdat, 1984) p. 130
29. Yakubov I T, Khrapak A G *Sov. Tech. Rev. B: Therm. Phys.* **2** 269 (1989)
30. Sodha M S, Guha S *Adv. Plasma Phys.* **4** 219 (1971)
31. Soo S L *Multiphase Fluid Dynamics* (Brookfield: Gower Technical, 1990)
32. Havnes O et al. *J. Geophys. Res.* **92** 2281 (1987)
33. Pilipp W et al. *Astrophys. J.* **314** 341 (1987)
34. Selwyn G S, Haller K L, Patterson E F *J. Vac. Sci. Technol. A* **11** 1132 (1993)
35. Selwyn G S, in *Proc. of the 6th Workshop on the Physics of Dusty Plasmas, La Jolla, Calif., USA, 22–25 March 1995* (Eds P K Shukla, D A Mendis, V W Chow) (Singapore: World Scientific, 1996) p. 177
36. Bouchoule A, in *Dusty Plasmas: Physics, Chemistry and Technological Impacts in Plasma Processing* (Ed. A Bouchoule) (Chichester: Wiley, 1999) p. 305
37. Kersten H et al. *Contrib. Plasma Phys.* **41** 598 (2001)
38. Dubin D H E, O'Neil T M *Rev. Mod. Phys.* **71** 87 (1999)
39. Shikin V B *Usp. Fiz. Nauk* **158** 127 (1989) [*Sov. Phys. Usp.* **32** 452 (1989)]
40. Tsytovich V N, Whipple E C, Thomas H *Fiz. Plazmy* **28** 675 (2002) [*Plasma Phys. Rep.* **28** 623 (2002)]
41. Morfill G E, Tsytovich V N, Thomas H *Fiz. Plazmy* **29** 3 (2003) [*Plasma Phys. Rep.* **29** 1 (2003)]
42. Chung P M, Talbot L, Touryan K J *Electric Probes in Stationary and Flowing Plasmas: Theory and Application* (New York: Springer-Verlag, 1975)
43. Allen J E *Phys. Scripta* **45** 497 (1992)
44. Goree J *Plasma Sources Sci. Technol.* **3** 400 (1994)
45. Uglov A A, Gnedovets A G *Plasma Chem. Plasma Proc.* **11** 251 (1991)
46. Kilgore M D et al. *J. Vac. Sci. Technol. B* **12** 486 (1994)
47. Lapenta G *Phys. Plasmas* **6** 1442 (1999)
48. Allen J E, Annaratone B M, de Angelis U *J. Plasma Phys.* **63** 299 (2000)
49. Khrapak S A et al. *Phys. Rev. Lett.* **90** 225002 (2003)
50. Kilgore M D et al. *J. Appl. Phys.* **73** 7195 (1993)
51. Zobnin A V et al. *Zh. Eksp. Teor. Fiz.* **118** 554 (2000) [*JETP* **91** 483 (2000)]
52. Goree J *Phys. Rev. Lett.* **69** 277 (1992)
53. Lampe M et al. *Phys. Rev. Lett.* **86** 5278 (2001)
54. Su C H, Lam S H *Phys. Fluids* **6** 1479 (1963)
55. Pal' A F et al. *Fiz. Plazmy* **28** 32 (2002) [*Plasma Phys. Rep.* **28** 28 (2002)]

56. Smirnov B M *Aerozoli v Gaze i Plazme* (Aerosols in Gases and Plasmas) (Moscow: IVTAN, 1990)

57. Raĭzer Yu P *Fizika Gazovogo Razryada* (Gas Discharge Physics) (Moscow: Nauka, 1987) [Translated into English (Berlin: Springer-Verlag, 1991)]

58. Mendis D A *Plasma Sources Sci. Technol.* **11** A219 (2002)

59. Fortov V E et al. *Zh. Eksp. Teor. Fiz.* **114** 2004 (1998) [*JETP* **87** 1087 (1998)]

60. Sickafoose A A et al. *Phys. Rev. Lett.* **84** 6034 (2000)

61. Walch B, Horányi M, Robertson S *Phys. Rev. Lett.* **75** 838 (1995)

62. Khrapak S A et al. *Phys. Rev. E* **59** 6017 (1999); Erratum: **60** 3450 (1999)

63. Rosenberg M, Mendis D A *IEEE Trans. Plasma Sci.* **PS-23** 177 (1995)

64. Rosenberg M, Mendis D A, Sheehan D P *IEEE Trans. Plasma Sci.* **PS-24** 1422 (1996)

65. Rosenberg M, Mendis D A, Sheehan D P *IEEE Trans. Plasma Sci.* **PS-27** 239 (1999)

66. Khrapak S A, Morfill G *Phys. Plasmas* **8** 2629 (2001)

67. Lipaev A M et al. *Zh. Eksp. Teor. Fiz.* **112** 2030 (1997) [*JETP* **85** 1110 (1997)]

68. Cui C, Goree J *IEEE Trans. Plasma Sci.* **PS-22** 151 (1994)

69. Matsoukas T, Russell M *J. Appl. Phys.* **77** 4285 (1995)

70. Matsoukas T, Russell M, Smith M *J. Vac. Sci. Technol. A* **14** 624 (1996)

71. Matsoukas T, Russell M *Phys. Rev. E* **55** 991 (1997)

72. Vaulina O S et al. *Zh. Eksp. Teor. Fiz.* **115** 2067 (1999) [*JETP* **88** 1130 (1999)]

73. Uhlenbeck G E, Ornstein L S *Phys. Rev.* **36** 823 (1930)

74. Vaulina S et al. *Phys. Rev. E* **60** 5959 (1999)

75. Vaulina O S et al. *Phys. Scripta* **T84** 229 (2000)

76. Quinn R A, Goree J *Phys. Rev. E* **61** 3033 (2000)

77. Morfill G, Ivlev A V, Jokipii J R *Phys. Rev. Lett.* **83** 971 (1999)

78. Ivlev A V, Konopka U, Morfill G *Phys. Rev. E* **62** 2739 (2000)

79. Khrapak S A, Morfill G E *Phys. Plasmas* **9** 619 (2002)

80. Fortov V E et al. *Phys. Lett. A* **229** 317 (1997)

81. Nefedov A P et al. *Pis'ma Zh. Eksp. Teor. Fiz.* **72** 313 (2000) [*JETP Lett.* **72** 218 (2000)]

82. Barkan A, D'Angelo N, Merlino R *Phys. Rev. Lett.* **73** 3093 (1994)

83. Fortov V E et al. *Phys. Rev. Lett.* **87** 205002 (2001)

84. Dubin D H E, in *Proc. of the 6th Workshop on the Physics of Dusty Plasmas, La Jolla, Calif., USA, 22–25 March 1995* (Eds P K Shukla, D A Mendis, V W Chow) (Singapore: World Scientific, 1996)

85. Nefedov A P, Petrov O F, Khrapak S A *Fiz. Plazmy* **24** 1109 (1998) [*Plasma Phys. Rep.* **24** 1037 (1998)]

86. Al'pert Ya L, Gurevich A V, Pitaevskiĭ L P *Iskusstvennye Sputniki v Razrezhennoĭ Plazme* (Artificial Satellites in Rarefied Plasma) (Moscow: Nauka, 1964) [Translated into English: Al'pert Ya L, Gurevich A V, Pitaevsky L P *Space Physics with Artificial Satellites* (New York: Consultants Bureau, 1965)]

87. Khrapak S A, Ivlev A V, Morfill G *Phys. Rev. E* **64** 046403 (2001)

88. Daugherty J E et al. *J. Appl. Phys.* **72** 3934 (1992)

89. Aleksandrov A F, Bogdankevich L S, Rukhadze A A *Osnovy Elektrodinamiki Plazmy* (Principles of Plasma Electrodynamics) (Moscow: Vysshaya Shkola, 1978) [Translated into English (New York: Springer-Verlag, 1984)]

90. Nambu M, Vladimirov S V, Shukla P K *Phys. Lett. A* **203** 40 (1995)

91. Vladimirov S V, Nambu M *Phys. Rev. E* **52** R2172 (1995)

92. Vladimirov S V, Ishihara O *Phys. Plasmas* **3** 444 (1996)

93. Ishihara O, Vladimirov S V *Phys. Plasmas* **4** 69 (1997)

94. Xie B, He K, Huang Z *Phys. Lett. A* **253** 83 (1999)

95. Lemons D S et al. *Phys. Plasmas* **7** 2306 (2000)

96. Lapenta G *Phys. Rev. E* **62** 1175 (2000)

97. Melandsø F, Goree J *Phys. Rev. E* **52** 5312 (1995)

98. Lampe M et al. *Phys. Plasmas* **7** 3851 (2000)

99. Maiorov S A, Vladimirov S V, Cramer N F *Phys. Rev. E* **63** 017401 (2001)

100. Winske D *IEEE Trans. Plasma Sci.* **PS-29** 191 (2001)

101. Lapenta G *Phys. Rev. E* **66** 026409 (2002)

102. Vladimirov S V, Maiorov S A, Ishihara O *Phys. Plasmas* **10** 3867 (2003)

103. Bolotovskiĭ B M, Stolyarov S N *Usp. Fiz. Nauk* **162** (2) 177 (1992) [*Sov. Phys. Usp.* **35** 143 (1992)]

104. Ginzburg V L *Usp. Fiz. Nauk* **166** 1033 (1996) [*Phys. Usp.* **39** 973 (1996)]

105. Hou L-J, Wang Y-N, Mišković Z L *Phys. Rev. E* **68** 016410 (2003)

106. Lampe M, Joyce G, Ganguli G *Phys. Scripta* **T89** 106 (2001)

107. Hou L-J, Wang Y-N, Mišković Z L *Phys. Rev. E* **64** 046406 (2001)

108. Ishihara O, Vladimirov S V, Cramer N F *Phys. Rev. E* **61** 7246 (2000)

109. Landau L D, Lifshitz E M *Gidrodinamika* (Fluid Mechanics) (Moscow: Nauka, 1988) [Translated into English (Oxford: Pergamon Press, 1987)]

110. Lifshitz E M, Pitaevskiĭ L P *Fizicheskaya Kinetika* (Physical Kinetics) (Moscow: Nauka, 1979) [Translated into English (Oxford: Pergamon Press, 1981)]

111. Epstein P S *Phys. Rev.* **23** 710 (1924)

112. Draine B T, Salpeter E E *Astrophys. J.* **231** 77 (1979)

113. Nitter T *Plasma Sources Sci. Technol.* **5** 93 (1996)

114. Talbot L et al. *J. Fluid Mech.* **101** 737 (1980)

115. Havnes O et al. *Plasma Sources Sci. Technol.* **3** 448 (1994)

116. Jellum G M, Daugherty J E, Graves D B *J. Appl. Phys.* **69** 6923 (1991)

117. Balabanov V V et al. *Zh. Eksp. Teor. Fiz.* **119** 99 (2001) [*JETP* **92** 86 (2001)]

118. Rothermel H et al. *Phys. Rev. Lett.* **89** 175001 (2002)

119. Daugherty J E, Porteous R K, Graves D B *J. Appl. Phys.* **73** 1617 (1993)

120. Hamaguchi S, Farouki R T *Phys. Rev. E* **49** 4430 (1994)

121. Hamaguchi S, Farouki R T *Phys. Plasmas* **1** 2110 (1994)

122. Morfill G E, Grün E *Planet. Space Sci.* **27** 1269 (1979)

123. Northrop T G, Birmingham T J *Planet. Space Sci.* **38** 319 (1990)

124. Barnes M S et al. *Phys. Rev. Lett.* **68** 313 (1992)

125. Konopka U et al. *Phys. Rev. E* **61** 1890 (2000)

126. Kaw P K, Nishikawa K, Sato N *Phys. Plasmas* **9** 387 (2002)

127. Ishihara O et al. *Phys. Rev. E* **66** 046406 (2002)

128. D'Angelo N *Phys. Plasmas* **5** 3155 (1998)

129. Khrapak S A, Yaroshenko V V *Phys. Plasmas* **10** 4616 (2003)

130. Morfill G E et al. *Phys. Rev. Lett.* **83** 1598 (1999)

131. Goree J et al. *Phys. Rev. E* **59** 7055 (1999)

132. Tsytovich V N et al. *Phys. Rev. E* **63** 056609 (2001)

133. Khrapak S A et al. *Phys. Rev. E* **66** 046414 (2002)

134. Tsytovich V *Phys. Scripta* **T89** 89 (2001)

135. Trigger S A *Phys. Rev. E* **67** 046403 (2003)

136. Trigger S A et al. *Contrib. Plasma Phys.* **43** 377 (2003)

137. Landau L D, Lifshitz E M *Mekhanika* (Mechanics) (Moscow: Nauka, 1988) [Translated into English (Oxford: Pergamon Press, 1976)]

138. Hahn H-S, Mason E A, Smith F J *Phys. Fluids* **14** 278 (1971)

139. Khrapak S et al. *IEEE Trans. Plasma Sci.* **32** 555 (2004)

140. Liboff R L *Phys. Fluids* **2** 40 (1959)

141. Zafiu C, Melzer A, Piel A *Phys. Plasmas* **9** 4794 (2002)

142. Zafiu C, Melzer A, Piel A *Phys. Plasmas* **10** 1278 (2003)

143. Khrapak S A et al. *Phys. Plasmas* **10** 4579 (2003)

144. Tsytovich V N *Comments Plasma Phys. Control. Fusion* **15** 349 (1994)

145. Hamaguchi S *Comments Plasma Phys. Control. Fusion* **18** 95 (1997)

146. Ignatov A M *Fiz. Plazmy* **22** 648 (1996) [*Plasma Phys. Rep.* **22** 585 (1996)]

147. Tsytovich V N, Khodataev Y K, Bingham R *Comments Plasma Phys. Control. Fusion* **17** 249 (1996)

148. Daugherty J E, Graves D B *J. Vac. Sci. Technol. A* **11** 1126 (1993)

149. Tsytovich V N et al. *Comments Plasma Phys. Control. Fusion* **18** 281 (1998)

150. Konopka U, Ratke L, Thomas H M *Phys. Rev. Lett.* **79** 1269 (1997)

151. Konopka U, Morfill G E, Ratke L *Phys. Rev. Lett.* **84** 891 (2000)

152. Takahashi K et al. *Phys. Rev. E* **58** 7805 (1998)

153. Melzer A, Schweigert V A, Piel A *Phys. Rev. Lett.* **83** 3194 (1999)

154. Morfill G E et al. *Phys. Plasmas* **6** 1769 (1999)

155. Perrin J, Hollenstein C, in *Dusty Plasmas: Physics, Chemistry and Technological Impacts in Plasma Processing* (Ed. A Bouchoule) (Chichester: Wiley, 1999) p. 77

156. Kremer K, Robbins M O, Grest G S *Phys. Rev. Lett.* **57** 2694 (1986)

157. Robbins M O, Kremer K, Grest G S *J. Chem. Phys.* **88** 3286 (1988)

158. Stevens M J, Robbins M O *J. Chem. Phys.* **98** 2319 (1993)

159. Hamaguchi S, Farouki R T, Dubin D H E *Phys. Rev. E* **56** 4671 (1997)

160. Ichimaru S *Rev. Mod. Phys.* **54** 1017 (1982)

161. Ichimaru S *Statistical Plasma Physics* Vol. 1 *Basic Principles* (Redwood City, Calif.: Addison-Wesley, 1992)

162. Zamalin V M, Norman G E, Filinov V S *Metod Monte-Karlo v Statisticheskoĭ Termodinamike* (Monte Carlo Method in Statistical Thermodynamics) (Moscow: Nauka, 1977)

163. Ohta H, Hamaguchi S *Phys. Plasmas* **7** 4506 (2000)

164. Meijer E J, Frenkel D *J. Chem. Phys.* **94** 2269 (1991)

165. Vaulina O S, Khrapak S A *Zh. Eksp. Teor. Fiz.* **119** 264 (2001) [*JETP* **92** 228 (2001)]

166. Vaulina O, Khrapak S, Morfill G *Phys. Rev. E* **66** 016404 (2002)

167. Vaulina O S, Khrapak S A *Zh. Eksp. Teor. Fiz.* **117** 326 (2000) [*JETP* **90** 287 (2000)]

168. Dubin D H E *Phys. Rev. A* **42** 4972 (1990)

169. Farouki R T, Hamaguchi S *Phys. Rev. E* **47** 4330 (1993)

170. Lindemann F A *Z. Phys.* **11** 609 (1910)

171. Hansen J-P, Verlet L *Phys. Rev.* **184** 151 (1969)

172. Löwen H, Palberg T, Simon R *Phys. Rev. Lett.* **70** 1557 (1993)

173. Löwen H *Phys. Rev. E* **53** R29 (1996)

174. Rosenberg R O, Thirumalai D *Phys. Rev. A* **33** 4473 (1986)

175. Kremer K, Grest G S, Robbins M O *J. Phys. A: Math. Gen.* **20** L181 (1987)

176. Vaulina O S, Vladimirov S V *Phys. Plasmas* **9** 835 (2002)

177. Zuzic M et al. *Phys. Rev. Lett.* **85** 4064 (2000)

178. Quinn R A et al. *Phys. Rev. E* **53** R2049 (1996)

179. Hayashi Y *Phys. Rev. Lett.* **83** 4764 (1999)

180. Thomas H M, Morfill G E *Nature* **379** 806 (1996)

181. Melzer A, Homann A, Piel A *Phys. Rev. E* **53** 2757 (1996)

182. Thomas H M, Morfill G E *J. Vac. Sci. Technol. A* **14** 501 (1996)

183. Schweigert V A et al. *Phys. Rev. Lett.* **80** 5345 (1998)

184. Zhakhovskiĭ V V et al. *Pis'ma Zh. Eksp. Teor. Fiz.* **66** 392 (1997) [*JETP Lett.* **66** 419 (1997)]

185. Joyce G, Lampe M, Ganguli G *Phys. Rev. Lett.* **88** 095006 (2002)

186. Fortov V E et al. *Phys. Lett. A* **229** 317 (1997)

187. Golubovskiĭ Yu B, Nisimov S U, Suleĭmenov I É *Zh. Tekh. Fiz.* **64** (10) 54 (1994) [*Tech. Phys.* **39** 1005 (1994)]

188. Golubovskiĭ Yu B, Nisimov S U *Zh. Tekh. Fiz.* **65** (1) 46 (1995) [*Tech. Phys.* **40** 24 (1995)]

189. Golubovskiĭ Yu B, Nisimov S U *Zh. Tekh. Fiz.* **66** (7) 20 (1996) [*Tech. Phys.* **41** 645 (1996)]

190. Fortov V E et al. *Phys. Rev. E* **54** R2236 (1996)

191. Fortov V E et al. *Zh. Eksp. Teor. Fiz.* **111** 467 (1997) [*JETP* **84** 256 (1997)]

192. Fortov V E et al. *Zh. Eksp. Teor. Fiz.* **111** 889 (1997) [*JETP* **84** 489 (1997)]

193. Khodataev Y K et al. *Phys. Rev. E* **57** 7086 (1998)

194. Nefedov A P et al. *Zh. Eksp. Teor. Fiz.* **115** 837 (1999) [*JETP* **88** 460 (1999)]

195. Samaryan A A et al. *Zh. Eksp. Teor. Fiz.* **117** 939 (2000) [*JETP* **90** 817 (2000)]

196. Fortov V E et al. *Dokl. Ross. Akad. Nauk* **366** 184 (1999) [*Dokl. Phys.* **44** 279 (1999)]

197. Vladimirov V I et al. *Fiz. Plazmy* **27** 37 (2001) [*Plasma Phys. Rep.* **27** 36 (2001)]

198. Vladimirov V I et al. *Zh. Eksp. Teor. Fiz.* **120** 353 (2001) [*JETP* **93** 313 (2001)]

199. Gilbert S L, Bollinger J J, Wineland D J *Phys. Rev. Lett.* **60** 2022 (1988)

200. Grier D G, Murray C A *J. Chem. Phys.* **100** 9088 (1994)

201. Cândido L et al. *J. Phys.: Condens. Matter* **10** 11627 (1998)

202. Lai Y-J, I L *Phys. Rev. E* **60** 4743 (1999)

203. Totsuji H *Phys. Plasmas* **8** 1856 (2001)

204. Totsuji H, Totsuji C, Tsuruta K *Phys. Rev. E* **64** 066402 (2001)

205. Astrakharchik G E, Belousov A I, Lozovik Yu E *Phys. Lett. A* **258** 123 (1999)

206. Astrakharchik G E, Belousov A I, Lozovik Yu E *Zh. Eksp. Teor. Fiz.* **116** 1300 (1999) [*JETP* **89** 696 (1999)]

207. Juan W-T et al. *Phys. Rev. E* **58** R6947 (1998)

208. Klindworth M et al. *Phys. Rev. B* **61** 8404 (2000)

209. Melzer A, Klindworth M, Piel A *Phys. Rev. Lett.* **87** 115002 (2001)

210. Amiranashvili Sh G, Gusein-zade N G, Tsytovich V N *Phys. Rev. E* **64** 016407 (2001)

211. Tomme E B et al. *Phys. Rev. Lett.* **85** 2518 (2000)

212. Piel A *J. Phys. B: At. Mol. Phys.* **36** 533 (2003)

213. Homann A, Melzer A, Piel A *Phys. Rev. E* **59** R3835 (1999)

214. Trottenberg T, Melzer A, Piel A *Plasma Sources Sci. Technol.* **4** 450 (1995)

215. Zuzic M, Thomas H M, Morfill G E *J. Vac. Sci. Technol. A* **14** 496 (1996)

216. Piel A, Melzer A *Plasma Phys. Control. Fusion* **44** R1 (2002)

217. Ivlev A V et al. *Phys. Rev. Lett.* **85** 4060 (2000)

218. Zafiu C, Melzer A, Piel A *Phys. Rev. E* **63** 066403 (2001)

219. Wang Y-N, Hou L-J, Wang X *Phys. Rev. Lett.* **89** 155001 (2002)

220. Nunomura S et al. *Phys. Rev. Lett.* **83** 1970 (1999)

221. Samarian A A et al. *Phys. Rev. E* **64** 025402(R) (2001)

222. Sorasio G, Resendes D P, Shukla P K *Phys. Lett. A* **293** 67 (2002)

223. Chu J H, Du J-B, I L *J. Phys. D: Appl. Phys.* **27** 296 (1994)

224. Barkan A, Merlino R L, D'Angelo N *Phys. Plasmas* **2** 3563 (1995)

225. Molotkov V I et al. *Zh. Eksp. Teor. Fiz.* **116** 902 (1999) [*JETP* **89** 477 (1999)]

226. Tsytovich V N, de Angelis U *Phys. Plasmas* **6** 1093 (1999)

227. Tsytovich V N, de Angelis U *Phys. Plasmas* **7** 554 (2000)

228. Tsytovich V N, de Angelis U *Phys. Plasmas* **8** 1141 (2001)

229. Tsytovich V N, de Angelis U *Phys. Plasmas* **9** 2497 (2002)

230. Tsytovich V N, de Angelis U, Bingham R *Phys. Rev. Lett.* **87** 185003 (2001)

231. D'Angelo N *Phys. Plasmas* **4** 3422 (1997)

232. Ivlev A V et al. *Phys. Plasmas* **6** 741 (1999)

233. Ivlev A V, Morfill G *Phys. Plasmas* **7** 1094 (2000)

234. Ostrikov K N et al. *Phys. Rev. E* **61** 4315 (2000)

235. Wang X et al. *Phys. Plasmas* **8** 5018 (2001)

236. Shukla P K, Silin V P *Phys. Scripta* **45** 508 (1992)

237. Rao N N, Shukla P K, Yu M Y *Planet. Space Sci.* **38** 543 (1990)

238. Fried B D, Conte S D *The Plasma Dispersion Function; the Hilbert Transform of the Gaussian* (New York: Academic Press, 1961)

239. Melandsø F, Aslaksen T, Havnes O *Planet. Space Sci.* **41** 321 (1993)

240. Varma R K, Shukla P K, Krishan V *Phys. Rev. E* **47** 3612 (1993)

241. Jana M R, Sen A, Kaw P K *Phys. Rev. E* **48** 3930 (1993)

242. Bhatt J R, Pandey B P *Phys. Rev. E* **50** 3980 (1994)

243. Vladimirov S V *Phys. Plasmas* **1** 2762 (1994)

244. Bhatt J R *Phys. Rev. E* **55** 1166 (1997)

245. Annou R *Phys. Plasmas* **5** 2813 (1998)

246. Vladimirov S V et al. *Phys. Rev. E* **58** 8046 (1998)

247. Ostrikov K N et al. *Phys. Plasmas* **7** 461 (2000)

248. Rosenberg M *Planet. Space Sci.* **41** 229 (1993)

249. Rosenberg M *J. Vac. Sci. Technol. A* **14** 631 (1996)

250. D'Angelo N, Merlino R L *Planet. Space Sci.* **44** 1593 (1996)

251. Kaw P, Singh R *Phys. Rev. Lett.* **79** 423 (1997)

252. Mamun A A, Shukla P K *Phys. Plasmas* **7** 4412 (2000)

253. Rosenberg M *J. Plasma Phys.* **67** 235 (2002)

254. Kaw P K, Sen A *Phys. Plasmas* **5** 3552 (1998)

255. Kaw P K *Phys. Plasmas* **8** 1870 (2001)

256. Xie B S, Yu M Y *Phys. Rev. E* **62** 8501 (2000)

257. Murillo M S *Phys. Plasmas* **5** 3116 (1998)

258. Murillo M S *Phys. Plasmas* **7** 33 (2000)

259. Rosenberg M, Kalman G *Phys. Rev. E* **56** 7166 (1997)

260. Kalman G, Rosenberg M, DeWitt H E *Phys. Rev. Lett.* **84** 6030 (2000)

261. Kalman G, Golden K I *Phys. Rev. A* **41** 5516 (1990)

262. Winske D, Murillo M S, Rosenberg M *Phys. Rev. E* **59** 2263 (1999)

263. Ohta H, Hamaguchi S *Phys. Rev. Lett.* **84** 6026 (2000)

264. Murillo M S *Phys. Rev. Lett.* **85** 2514 (2000)

265. Melandsø F *Phys. Plasmas* **3** 3890 (1996)

266. Homann A et al. *Phys. Lett. A* **242** 173 (1998)

267. Wang X, Bhattacharjee A, Hu S *Phys. Rev. Lett.* **86** 2569 (2001)

268. Vladimirov S V, Shevchenko P V, Cramer N F *Phys. Rev. E* **56** R74 (1997)

269. Ivlev A V, Morfill G *Phys. Rev. E* **63** 016409 (2001)

270. D'Angelo N *J. Phys. D: Appl. Phys.* **28** 1009 (1995)

271. Praburam G, Goree J *Phys. Plasmas* **3** 1212 (1996)

272. Thompson C et al. *Phys. Plasmas* **4** 2331 (1997)

273. Merlino R L et al. *Phys. Plasmas* **5** 1607 (1998)

doi> 274. Zobnin A V et al. *Zh. Eksp. Teor. Fiz.* **122** 500 (2002) [*JETP* **95** 429 (2002)]
doi> 275. Pieper J B, Goree J *Phys. Rev. Lett.* **77** 3137 (1996)
doi> 276. Peters S et al. *Phys. Lett. A* **223** 389 (1996)
doi> 277. Homann A et al. *Phys. Rev. E* **56** 7138 (1997)
doi> 278. Misawa T et al. *Phys. Rev. Lett.* **86** 1219 (2001)
doi> 279. Nunomura S, Samsonov D, Goree J *Phys. Rev. Lett.* **84** 5141 (2000)
doi> 280. Nunomura S et al. *Phys. Rev. E* **65** 066402 (2002)
doi> 281. Nunomura S et al. *Phys. Rev. Lett.* **89** 035001 (2002)
doi> 282. Samsonov D et al. *Phys. Rev. Lett.* **88** 095004 (2002)
doi> 283. Havnes O et al. *J. Geophys. Res.* **100** 1731 (1995)
doi> 284. Samsonov D et al. *Phys. Rev. Lett.* **83** 3649 (1999)
doi> 285. Samsonov D et al. *Phys. Rev. E* **61** 5557 (2000)
doi> 286. Melzer A et al. *Phys. Rev. E* **62** 4162 (2000)
doi> 287. Vaulina O S et al. *Zh. Eksp. Teor. Fiz.* **119** 1129 (2001) [*JETP* **92** 979 (2001)]
doi> 288. Nefedov A P et al. *Zh. Eksp. Teor. Fiz.* **122** 778 (2002) [*JETP* **95** 673 (2002)]
doi> 289. Fortov V E et al. *Phys. Rev. Lett.* **90** 245005 (2003)
doi> 290. Fortov V E et al. *Zh. Eksp. Teor. Fiz.* **123** 798 (2003) [*JETP* **96** 704 (2003)]
doi> 291. Thomas H M, Morfill G E *Contrib. Plasma Phys.* **41** 255 (2001)
292. Akdim M R, Goedheer W J *Phys. Rev. E* **65** 015401(R) (2002)
doi> 293. Samsonov D, Goree J *Phys. Rev. E* **59** 1047 (1999)
doi> 294. Nefedov A P et al. *New J. Phys.* **5** 33 (2003)
doi> 295. Khrapak S et al. *Phys. Plasmas* **10** 1 (2003)
doi> 296. Samsonov D et al. *Phys. Rev. E* **67** 036404 (2003)
doi> 297. Annaratone B M et al. *Phys. Rev. E* **66** 056411 (2002)
doi> 298. Ivlev A V et al. *Phys. Rev. Lett.* **90** 055003 (2003)
doi> 299. Piel A, Nosenko V, Goree J *Phys. Rev. Lett.* **89** 085004 (2002)
300. Samsonov D et al. *Phys. Rev. E* **63** 025401(R) (2001)
doi> 301. Law D A et al. *Phys. Rev. Lett.* **80** 4189 (1998)
doi> 302. Fortov V E et al. *Phys. Rev. E* **69** 016402 (2004)
doi> 303. Mohideen U et al. *Phys. Rev. Lett.* **81** 349 (1998)
doi> 304. Molotkov V I et al. *Pis'ma Zh. Eksp. Teor. Fiz.* **71** 152 (2000) [*JETP Lett.* **71** 102 (2000)]
doi> 305. Annaratone B M et al. *Phys. Rev. E* **63** 036406 (2001)
306. Fortov V E et al., in *Proc. of the XXV Intern. Conf. on Phenomena in Ionized Gases: ICPIG, Nagoya, Japan, 17 – 22 July 2001* Vol. 3 (Ed. T Goto) (Nagoya: Nagoya Univ., 2001) p. 35
doi> 307. Vladimirov S V, Nambu M *Phys. Rev. E* **64** 026403 (2001)
308. Shukla P K, Mamun A A *Introduction to Dusty Plasma Physics* (Bristol: IOP Publ., 2001)
309. Ivlev A V et al. *Phys. Rev. E* **68** 026403 (2003)
doi> 310. Fortov V E et al. *Dokl. Ross. Akad. Nauk* **382** 50 (2002) [*Dokl. Phys.* **47** 367 (2002)]
doi> 311. Selwyn G S, Singh J, Bennett R S *J. Vac. Sci. Technol. A* **7** 2758 (1989)
312. Baranov V Yu et al., in *Izotopy: Svoĭstva, Poluchenie, Primenenie* (Isotopes: Properties, Production, and Applications) (Ed. V Yu Baranov) (Moscow: IzdAT, 2000) p. 626
doi> 313. Pal' A F, Starostin A N, Filippov A V *Fiz. Plazmy* **27** 155 (2001) [*Plasma Phys. Rep.* **27** 143 (2001)]
doi> 314. Pal' A F et al. *Zh. Eksp. Teor. Fiz.* **119** 272 (2001) [*JETP* **92** 235 (2001)]